Triboelectric Nanogenerators for Energy Harvesting, Self-Powered Sensing, and High Voltage Applications

A Dissertation
Presented to
The Academic Faculty

By

Steven Linchao Zhang

In Partial Fulfillment
of the Requirements for the Degree
Doctor of Philosophy in the
School of Materials Science and Engineering

Georgia Institute of Technology
August 2020

Triboelectric Nanogenerators for Energy Harvesting, Self-Powered Sensing, and High Voltage Applications

Approved by:

Dr. Zhong Lin Wang, Advisor
School of Materials Science and Engineering
Georgia Institute of Technology

Dr. Preet Singh
School of Materials Science and Engineering
Georgia Institute of Technology

Dr. Zhiqun Lin
School of Materials Science and Engineering
Georgia Institute of Technology

Dr. Meilin Liu
School of Materials Science and Engineering
Georgia Institute of Technology

Dr. Husam N. Alshareef
Physical Science & Engineering Division
King Abdullah University of Science and Technology

Date Approved: 06/24/2020

Dedicated To my beloved family

ACKNOWLEDGEMENTS

First of all, I would like to express my sincere gratitude to my research advisor, Professor Zhong Lin Wang, for his continuous support of Ph.D. study and for providing invaluable guidance for my path to become an independent scholar and researcher. He had always asked thought provoking questions, and abundantly supplied the resources to facilitate effective and high impact research. Without his help during research, I would not be able to have the many achievements. It is a great honor to have him as my advisor and learning from him in the past five years. I would also like to acknowledge the rest of my committee members, Prof. Husam N. Alshareef, Prof. Zhiqun Lin, Prof. Meilin Liu, and Prof. Preet Singh for willing to spend their valuable time to serve on my dissertation committee, and in giving me insightful advice on my doctoral research and dissertation.

Also, I would like to thank the many talented scholars that I have worked with in this research group. I had received a lot of help from them, especially through the many helpful discussions. In particular, I would like to thank Dr. Ying-Chih Lai and Dr. Minyi Xu. For Dr. Ying Chih Lai, I especially would like to thank him for being the leader in the same subgroup as me when I had first joined the lab. I would not have been able to start my research so smoothly without his mentorship. For Dr, Minyi Xu, I would like to thank him for sharing much of his experimental and theoretical knowledge and being patient even when I approach him with many questions. Finally, I would like to thank all the colleagues in Professor Wang's lab whom I had spent various satisfying and memorable moments during the time in Georgia Tech. Also, I would like to thank the many friends that I have met here in Atlanta.

Lastly, but most importantly, I would like to thank my family for their selfless love and endless support. My parents unconditionally supported me in my Ph.D. journey. Without their support, I would not be able to achieve what I am able to achieve today.

TABLE OF CONTENTS

LIST OF TABLES

LIST OF FIGURES

LIST OF SYMBOLS AND ABBREVIATIONS

AC	Alternating Current
AF-TENG	Aeroelastic Flutter based TENG
Au	Gold
CV	Cyclic voltammetry
DC-TENG	Direct Current TENG
DIW	Direct Ink Write
EMG	Electromagnetic Generator
EMP	Electromagnetic Pulse
EMP-TENG	EMP-TENG
FEP	Fluorinated Ethylene Propylene
FFT	Fast Fourier Transform
HV	High Voltage
ICP	Inductive coupled plasma
IOTs	Internet of Things
IR	Infrared
LED	Light Emitting Diode
PDMS	Polydimethylsiloxane
PENG	Piezoelectric Nanogenerator
PET	Polyethylene Terephthalate
PETG	Polyethylene Terephthalate Glycol
PI	Polyimide (Kapton)
Pt	Platinum
PTFE	Polytetrafluorethylene
PVD	Physical Vapor Deposition

PVDF	Polyvinylidene Fluoride
PU	Polyurethane
RuO_2	Ruthenium Dioxide
SEM	Scanning Electron Microscopy
SS-TENG	Sea Snake Triboelectric Nanogenerator
T-TENG	Tower-like Triboelectric Nanogenerator
TENG	Triboelectric Nanogenerator

SUMMARY

As we are currently entering into a fourth industrial revolution, an era of ubiquitous, mobile supercomputing, intelligent robots, self-driving cars, neuro-technological brain enhancements, finding reliable sources of energy are of utmost importance. The collective world generation of power in 2018 was calculated to be 24000 terawatt hours, and renewable energy sources have been on the rise, doubling in contribution to U.S. electricity generation since 2008. In order to support demands of entering the age of Internet of Things(IOTs), a portable, cost-effective, renewable source of energy is required to power different IOT sensors. Triboelectric nanogenerators (TENGs), which were based on the triboelectric effect, were first invented in Professor Wang's group in 2012, and it could harness ambient mechanical energy, such as from wind, rain, ocean waves,[1] and human body movements, into electricity by the coupling of contact electrification and electrostatic inductions. TENG has been shown to be one of the best choices in harvesting mechanical vibrational energy, due to triboelectrification is an ubiquitous effect with an abundant choice of materials. Also, not only the TENG could be used as an energy harvester, it could also be utilized as a self-powered active sensor, which is able to sense characteristics of different mechanical motions, expanding its ability to operate as a sensing network. Furthermore, TENGs due to their high voltage characteristics, have been utilized in various high voltage applications recently. In this dissertation, three main research area relating TENGs are focused. The first is to use TENG as a more selective and sensitive self-powered active sensor and transforming paper into self-powered active sensors. Furthermore, self-powered fluid sensors are also discussed, and these sensors could aid users in sensing environmental conditions, such as wave height and wind speed. The second is to expand the use of TENGs in energy harvesting. One objective is to harvest

more effectively in harsh environments. This is done by investigating new theory of electrostatic screening effect in different harsh environment, and also investigating the electrostatic screening effect in different materials. Another objective is to lower the impedance of triboelectric nanogenerators. This was done by constructing multi-layer-based device, and its circuit model was used to show that multi-layer based nanogenerator device could achieve higher output power density at a lower impedance. Furthermore, it is necessary to store the harvested energy; thus, a hybrid EMG-TENG (electromagnetic generator-triboelectric nanogenerator) energy harvester was integrated with a microsupercapacitor. The third is to investigate triboelectric nanogenerators as a high voltage source on electronic components, such as capacitors and resistors, for novel applications, such as a high instantaneous power TENG and a fully self-powered sensing system and a self-powered personal security device.

CHAPTER 1. INTRODUCTION

1.1 Mechanism of Triboelectric Nanogenerator

Triboelectric Nanogenerators (TENGs) are energy harvesters that could effectively harvest mechanical energy into electricity by the coupling of two phenomenon: contact electrification and electrostatic induction. Contact electrification, a phenomenon that have been recorded from Greek times, occurs when two different materials contact each other. After contact, one of the materials' surface would become positively charged, whereas the other material's surface would become negatively charged. For example, when rubbing a silk cloth with a glass rod, the silk cloth would become negatively charged after contact, while the glass rod would become positively charged. This has recently been shown to be caused by electrons transfer, as surface electrons would move across the material's interface to cause one of the materials to be positively charged and the other material to be negatively charged.[2] The other phenomenon, electrostatic induction, is simply a redistribution of electronic charge in an object, caused by the influence of nearby charges. When a conductive material is placed near a negatively charged object, the conductive material would develop a net positive charge on the end closer to the negatively charged object, as electrons would be repelled by the negative charges from the object. There would also be a net negatively charge on the end farther away from the negatively charged object, due to the repulsion of electrons.

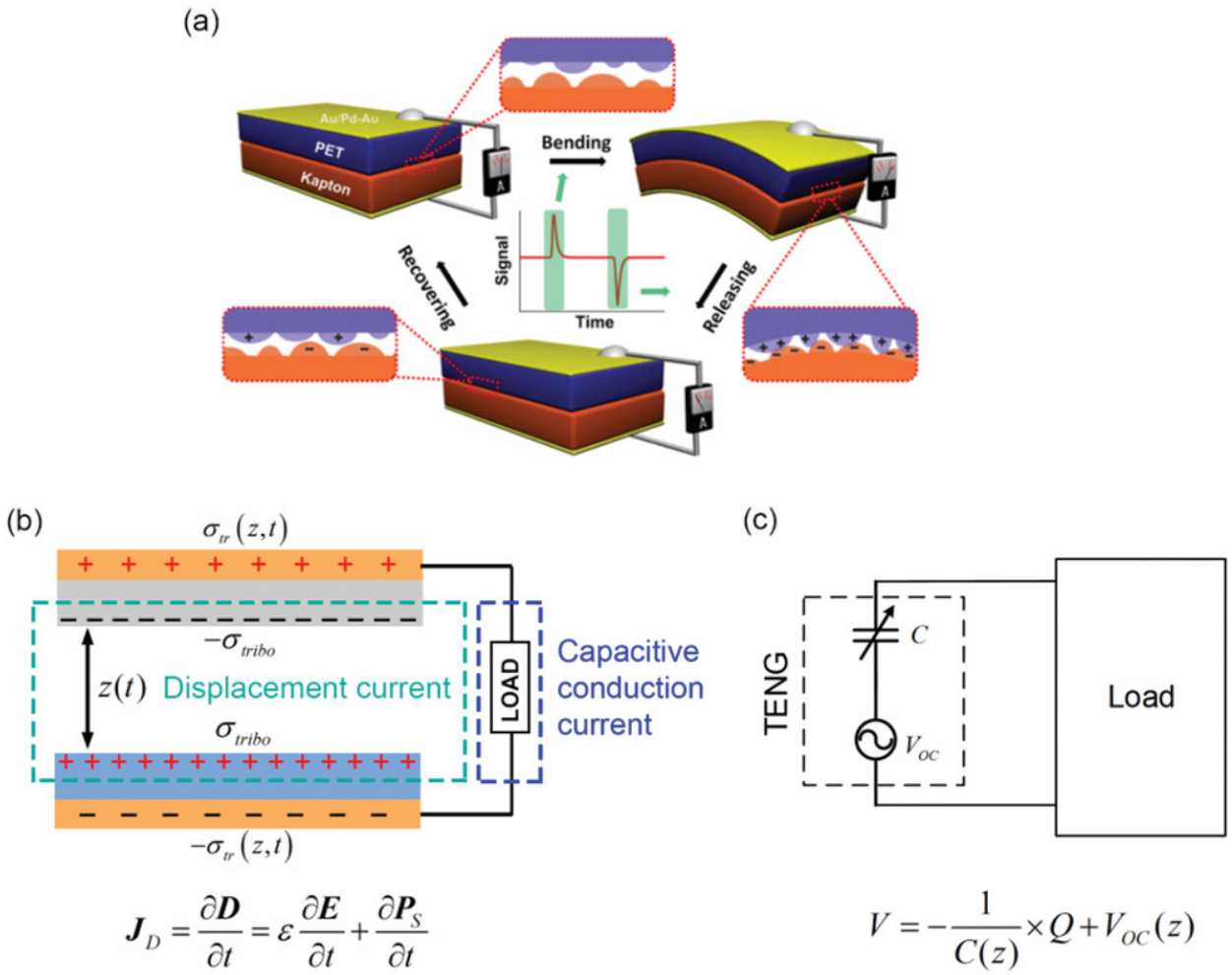

Figure 1 Theoretical Model of TENG. a) Schematic illustration of the first TENG and its operation cycle.[3] b) The displacement current model of vertical contact separation mode TENG. c) The equivalent circuit model of vertical contact separation mode of TENG.[4]

Thus, by utilizing these two principles, the first triboelectric nanogenerator is created,[3] as shown in Figure 1a. This triboelectric nanogenerator is made of two thin-film dielectric materials, Kapton film and polyethylene terephthalate (PET) film with back electrodes of gold (Au)/ platinum (Pt)-Au coated by sputtering on them. When the device undergoes cyclic pressing or bending, the contact status between the materials would change, and when the two materials are in full contact, the PET film would become positively charged, whereas the Kapton film would become negatively charged by contact electrification. Since both materials, the PET and the Kapton film, are dielectric, the charges would remain on the surface of the material for a long time, dependent on

the material properties of the dielectric. After the external force that pushed the materials into full contact is released, the opposite charges on the materials would be separated, and the back electrode on the PET would have a net negative charge close to the PET, and the back electrode on the Kapton would have a net positive charge close to the Kapton. This would cause a high potential difference between the two electrodes. If the electrodes are connected through an external load, current would be able to flow across the wire connecting the two electrodes. As the two dielectrics are brought towards full contact again, the current would flow in the opposite direction due to the change in the potential difference, as the charges on the conductive surface would be screened by the charges of the dielectric layer. This would result a continuous alternating current (AC) output by repeating the contact-separation cycle.

1.2 Theoretical Origin of TENG

Even though the mechanism of the TENG has been well understood, the understanding of the fundamental physics model has been lacking until recently. In 2017, a study showed the physics behind the TENG is to be caused by Maxwell's displacement current,[5] which is defined as Equation (1) below,

$$J_D = \frac{\partial D}{\partial t} = \varepsilon \frac{\partial E}{\partial t} + \frac{\partial P}{\partial t} \tag{1}$$

where J_D is the free electric current density, D is the displacement field, ε is the permittivity of the dielectrics, E is the electric field, and P is the polarization field. The first term, $\varepsilon \frac{\partial E}{\partial t}$, represents electromagnetic induction, so that it represents the existence of electromagnetic wave and the theory of light. As a result, this term has been the foundation of antenna, TV, radio, and wireless communication technology. The last term in Equation 1, $\frac{\partial P}{\partial t}$, called polarization current density,

comes from change in polarization of individual molecules of the dielectric material, which could be caused by either piezoelectric or triboelectric effect.

In piezoelectric nanogenerators (PENG), due to the structure of the piezoelectric material, a vertical mechanical deformation results in a generation of piezoelectric polarization charges at the two ends of the material, which would cause a change in the polarization, leading to a displacement current produced. For TENG, surface electrostatic charges on the dielectric would cause a time-changing electric field when the dielectric materials are separated. Figure 1b shows the basic model of a contact separation mode TENG. The charges on the dielectric surfaces are oppositely charged after contact electrification, with the charge density of $\pm\sigma_{tribo}$, which would become saturated after multiple cycles of contact separation. When the materials are in full contact, the electrostatic field between the dielectric charges on the dielectrics is high, whereas once the materials are fully separated, the electrostatic field would become low, as the charges on the dielectric would be effectively shielded by the opposite charges on the conductor. Thus, during the process of separating, the change of the electric field would drive electrons to flow through the external load by a capacitive conduction current. The amount of transferred charges between the electrodes, σ_{tr}, is a function of vertical displacement z, and thus, the mechanical energy that induced the change in z is converted to electrical energy. Since J_D is equivalent to the change of transferred charge as a function of time, the displacement current could be calculated as Equation 2 below, and it is equivalent to the capacitive conduction current.

$$\frac{\partial D(z,t)}{\partial t} = J_D(z,t) = \frac{\partial \sigma_{tr}(z,t)}{\partial t} \quad (2)$$

The displacement current is the only conduction mechanism for electricity transport in capacitive conduction and leads to the output current of TENG by electromagnetic induction, rather than the flow of free charge of the capacitor.

1.3 Circuit Model of TENG

Not only is the fundamental physics important in understanding TENG, another important model to fully understand the TENG is the circuit model of the TENG. For vertical contact separation mode of the TENG, oppositely charged surfaces with a changing gap distance, z, could be regarded as a gap distance dependent capacitance, with the capacitance to be high when the dielectric surfaces are in full contact, and the capacitance to be low when the dielectrics are fully separated. Also, the TENG is also shown to be a gap distance dependent open-circuit voltage source, with the open-circuit of the TENG could be calculated by Equation 3 below, as the open-circuit voltage, V_{OC}, of the TENG is directly related to the charge density on the surface of the dielectric and the gap distance.

$$V_{OC}(z) = \frac{Q_{tribo}}{C(z)} = \frac{\sigma_{tribo} z}{\varepsilon_0} \tag{3}$$

Since TENG is both a gap distance dependent open-circuit voltage source and a gap-distance capacitance, a circuit model, as shown in Figure 1c, is then created for the TENG with an open-circuit voltage source and a variable capacitance in series. Furthermore, when the TENG is connected to a load, the voltage of the load could be calculated by Kirchhoff's circuit law by the Equation 4 below.

$$V_{Load} = -\frac{1}{C(z)} xQ + V_{OC}(z) \tag{4}$$

This circuit model of TENG would be the theoretical tool that enables the study, design, and optimization of the TENG, and would be further used in this dissertation as a tool to optimize performance of TENG in harsh environments, and illustrate the effect of dielectric layers on nanogenerator performance, as shown in Section 3.1-Section 3.2, in which electrostatic screening effect on TENG are discussed.[6-13]

1.4 Material Choices for TENG

For TENG, insulating materials are oppositely charged after physical contact, as the surface of one material will take electrons from the other material after contact. A key question to answer is which pair of insulating materials would produce the highest charge density, as the increase in charge generation have been a main strategy to improve the output power of TENG. From tests performed by Bill W. Lee, a triboelectric series, which stated the amount of charge transferred between the surface is dependent on the electron affinity of the material, was created.[14] A positive charge affinity means that the material is more likely to lose electrons, whereas a negative charge affinity means that the material is more likely to gain electrons. For example, he had values of the electron affinity in the table of two materials (polyurethane foam, +60 nC/J and Teflon (PTFE), -190 nC/J). Thus, when these two materials contact with each other, there would be about 250 nano coulombs of charge transfer per joule of frictional energy of contact. Furthermore, a new triboelectric series was performed recently from our group by testing solid-liquid contact, in which different polymers were contacted with a liquid mercury electrode, and the charge density was measured.[15] Figure 2 shows the triboelectric series of materials and their triboelectric charge density. It is important to note that materials that have the highest negative charge density are typically materials that have group 17 elements (Cl, F) or O on the periodic table, as these materials have the highest charge affinity, making it more of an electron acceptor.[16-18] Examples of these

materials include Polyterafluroethylene (PTFE), Fluorinated Ethylene Propylene (FEP) and Polyvinylidene Fluoride (PVDF). Furthermore, materials that are more positive on the triboelectric series typically contains more amine group (NH_3), as this group largely promote the charge-donating tendency.[19, 20]

There are multiple methods in improving triboelectric nanogenerators by alternating the state of materials. Functionalizing of the material surface is one of the key approaches in increasing the charge density of TENG. Surface modification could be done through methods of radical injection, plasma treatment, and ion injection.[21-23] Yun has showed that injecting oxygen radicals into polydimethylsiloxane (PDMS) surface by a sodium hydroxide treatment could enhance a 15 times increase in power when compared to the untreated PDMS.[24] The reason in the large enhancement was due to the Si-CH_3 bond was converted into a Si-O bond, which allowed for the treated PDMS to act more as an electron acceptor. Furthermore, fluorination by plasma treatment in tetrafluoromethane (CF_4) has been shown to considerably improve the output power.[22, 23] Also, another approach to change triboelectric output is by adding monolayers with electron-donating or electron-accepting functional end group on the surface.[25, 26] These methods all could greatly increase the output performance of TENG by alternating surface states of materials.

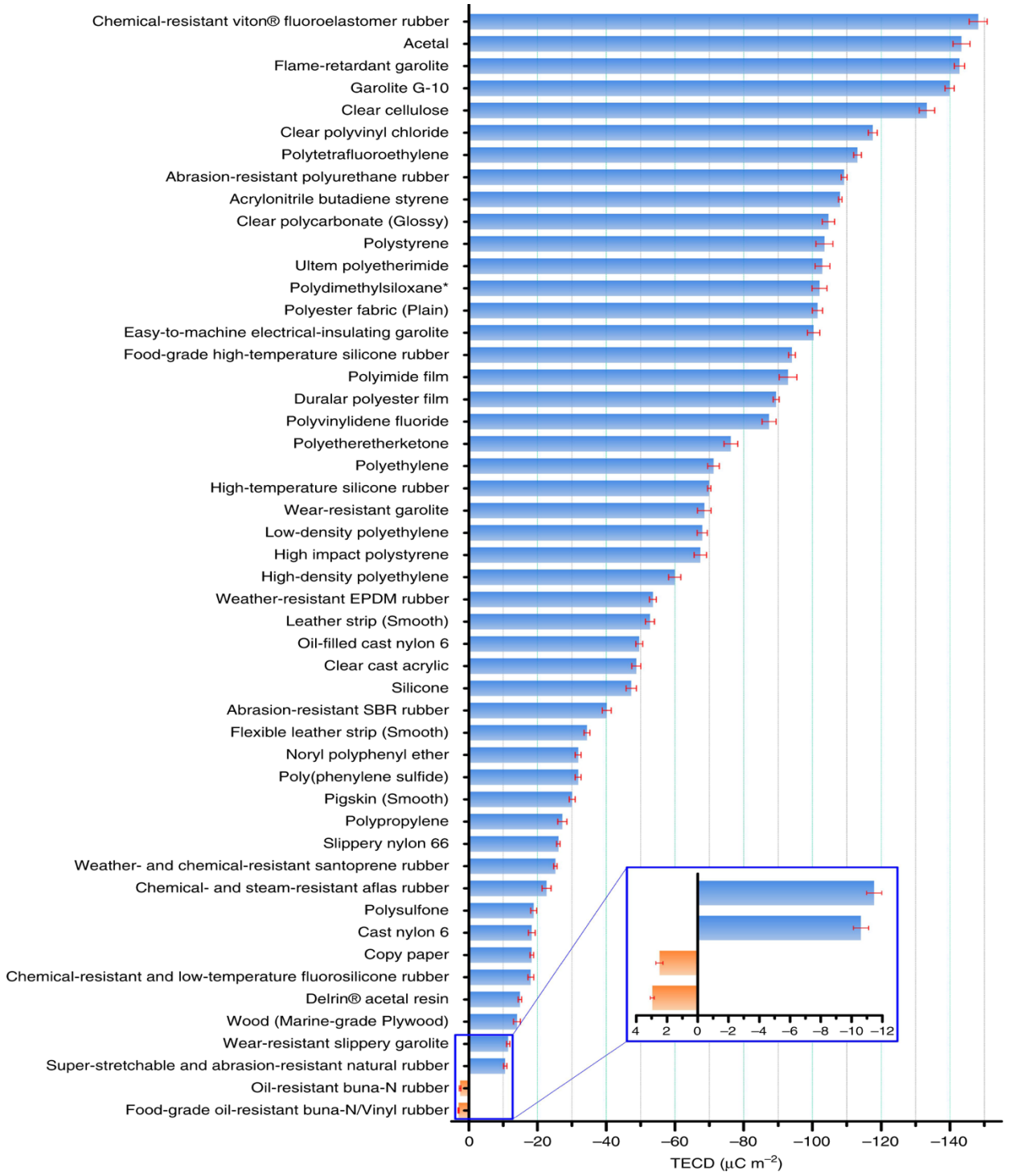

Figure 2 The Quantified Triboelectric Series. The error bar indicates the range within a standard deviation.[15]

Another method in improving TENGs performance is by increasing the contact area by fabricating microscale or nanoscale surface structure. By increasing the surface area of contact, there would be more probability for charge transfer; thus, producing a larger output voltage or current. It is important to note that when two surface make contact by mechanical force, the actual contact area is much smaller than the surface area of the two surfaces, due to the surfaces would have different degrees of surface roughness.[27] Various methods, such as force-assembled colloidal arrays,[28] soft lithography,[29] and surface nanomaterial fabrication[30] have been used to form nanoscale or microscale surface features, and it has been shown to cause a considerable increase in transferred charges. As well, for application in self-powered sensors, the added microstructure allows the TENG to be more sensitive to force applied, thus making the sensor more sensitive.[31] In my works, a typical surface reactive ion etching procedure was done to increase the roughness of PTFE by producing microstructures on the PTFE surface, causing an increase in output charge. By changing the surface roughness of the TENG, the performance could be great enhanced by increasing the contact surface area.

Another approach to increase TENG performance is by changing the dielectric constant of the material. As shown previously in Section 1.2, the output performance of the TENG is dependent on the change of electrical displacement field. Thus, one could alter the initial electrical field by adding dielectric layers, as the dielectric would be polarized in the electric field, cause a decrease in the electrical displacement field. This work is further shown and explained in Section 3.1.1, in which water could cause electrostatic screening effect on the performance of nanogenerator, and Section 3.2, in which the substrate material could be changed to maximize the output voltage of the TENG, leading to a production of a higher output power.

In this section, material choice for TENG was discussed, and the TENG that would have a high output performance from typically involve one contact electrification material with electron donating group on its surface and the other with more electron accepting group on its surface. Also, three different methods by alternating states of materials were demonstrated for improving the TENG's output performance. They are to functionalize the material's surface, to add nano or microstructures onto surfaces, and to change material's dielectric constant. In the next section, the four different structures, or working mode, of TENG are discussed.

1.5 Four Working Modes of TENG

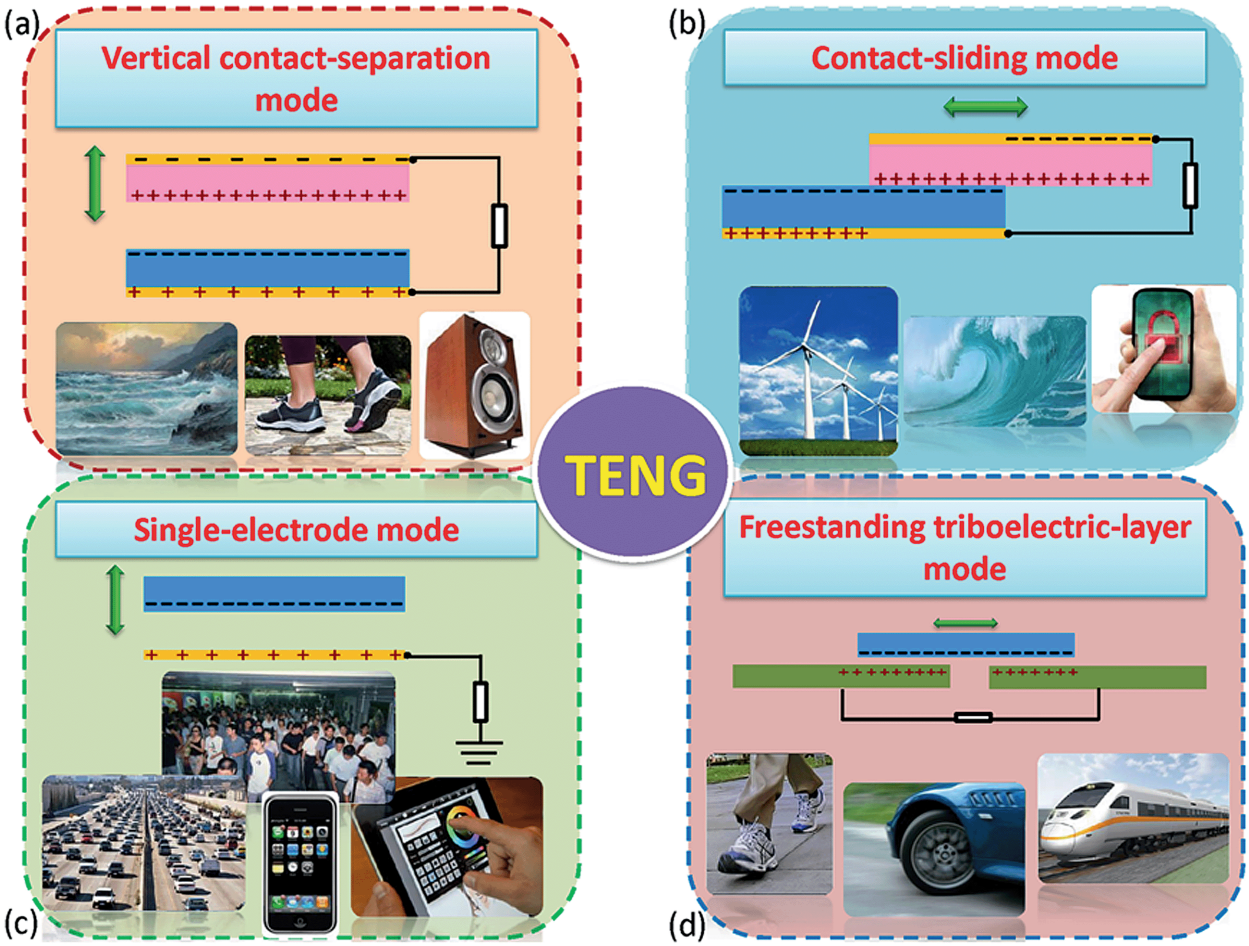

Figure 3. The Four Fundamental Modes of Triboelectric Nanogenerators: (a) vertical contact-separation mode; (b) in-plane contact-sliding mode; (c) single-electrode mode; and (d) freestanding triboelectric-layer mode.[32]

With a strong understanding of materials used in triboelectric nanogenerators, this section would cover different structures of triboelectric nanogenerators. Depending on the direction of the polarization change and electrode configurations, four different operation modes of the TENG have been proposed since its initial design in 2012. The four modes shown in Figure 3 include vertical contact-separation (CS) mode, lateral-sliding (LS) mode, single electrode (SE) mode, and freestanding triboelectric-layer (FT) mode.[32] The vertical-contact separation is the simplest design of the TENG. In this mode, the relative motion is perpendicular to the surfaces of the dielectric surfaces. Once the two surfaces are separated by a small air gap, a potential drop is created. Once the air gap is removed, due to pressing the dielectric materials together, the potential drop disappears. Thus, essentially, the periodic contact and separation between two materials creates a changing potential drop, which is able to drive electrons to move between the electrodes, producing an output current. For this device, it is important to note that the capacitance is inversely proportional to the gap of the device. Thus, at a very high separation distance, the capacitance is very small, which would cause an infinitely high voltage. The lateral-sliding mode starts off with the same structure as the vertical contact-separation mode, but instead it utilizes a relative sliding in parallel to the interface to create a potential. Similar to vertical contact separation mode, when the dielectric material is pressed together, the potential drop is zero, and when the dielectrics are separated, a potential drop is created. It is important to note for the sliding mode, the change of capacitance for the sliding mode TENG is usually smaller than that of contact separation mode TENG, which would cause a smaller output voltage.[7] The sliding between the dielectric surfaces could be done by simple planar motion, a cylindrical rotation, or disc rotation. The single-electrode mode is used when a part of the TENG could not be electrically connected to a load because the dielectric layers, electrodes, and wires are moving. Such a device configuration largely limits the

TENGs' applicability for harvesting energy from an arbitrary moving object, because the electrode of the TENG has to be interconnected to the entire system by interconnect. Thus, in single electrode mode, the bottom part of the TENG is grounded, and the moving object can induce electrons directly onto the top electrode. This mode could be used effectively to harvest energy from human body motion. The last mode, the freestanding triboelectric mode, a pair of electrodes lie underneath a moving dielectric layer. As the dielectric layer moves, an electrical output is induced from asymmetric charge distribution as the freely moving object change its position. It is proven as the best mode to investigate theory of TENG, as if the mover is a dielectric, the capacitance could be considered constant relative to the position of the mover.[9] With these four modes, different applications of TENG could be realized, as some of the modes would be more effective in different uses.

1.6 Current Applications of TENG

The major applications of TENG could be used in three main areas: self-powered active sensor, an energy harvester for self-powered systems, and for power sources for high voltage instruments.

For self-powered active sensors, since TENG can transform mechanical stimuli into electrical signals directly, it could use the electrical signals generated as a sensor to tell about the characteristics of the mechanical stimuli. Since it occurs without applying an external power unit to the device, the sensor is considered self-powered. Overall, TENGs have been used as a self-powered sensor for a range of sensing types such as finger touch,[33] motion sensing,[34] sounds,[35] and also biomedical sensing, such as measuring pulse.[36, 37]

Thanks for the merits such as light-weight, low cost, abundant material and structural choices, TENG could be used as an effective and efficient energy harvester by harvesting biomechanical energy,[37-40] blue energy (energy from ocean waves, and ocean current)[1, 41-43], vibration energy,[44-46] and wind energy.[47-50] TENG is also known to have superior performances at harvesting low frequency compared to conventional electromagnetic generators (EMGs).[51] This is effective for harvesting biomechanical energy, because human motion or even a human pulse operates at low frequencies. Furthermore, TENG has been used in harvesting energy from low-frequency ocean waves. Another set of research involves using TENG to harvest various vibrations, and energy from the wind as they are ambient in the environment. With the energy harvested, many different electronic devices could be powered.

Also, the last main application of the TENG is to use the intrinsic characteristics of high voltage and low current which allows TENG as an alternative of conventional HV power sources with unprecedented portability.[52-57] The high voltage of the TENG could be easily over 100 kV; thus, these power sources do not require sophisticated power converters, which reduce the system complexity and cost. Also, since the charge transferred from TENG is small, the HV applications of TENG should have little requirements on current, and better performance could be achieved then compared to conventional sources, as higher current could cause a higher noise in the system. Also, the lower current is demonstrated to be safer for the personnel operating and the instrument itself. Furthermore, with the high voltage application, several TENG based commercial product, such as air filters[58] and face masks[59] have been launched in China, which pioneer and pave the path towards large scale commercialization of TENG.

1.7 Dissertation Scope

With the three main applications of TENG explained, this dissertation aims on expanding each of the applications of the TENG (self-powered active sensing, energy harvesting, and high-voltage applications).

In Chapter 2, applications of TENG for self-powered active sensing are discussed. Firstly, for self-powered active sensing, there is a need for self-powered sensing of strain, especially strain from human body motion, which previous nanogenerators have not obtained with a high sensitivity and selectivity. Thus, the first auxetic-based contact mode TENG was developed to create a self-powered strain sensor that has a much higher sensitivity and selectivity. This work is shown in Section 2.1. Also, since triboelectric nanogenerator could be made with any materials, there is a vision that one could transform everyday objects, such as paper into self-powered active sensors. The use of paper in TENG is shown in Section 2.2 and 2.3. In Section 2.2, the use of paper as a self-powered acoustic sensor is shared, and in Section 2.3, the use of paper-based origami structures in creating TENG structure is shared. This shows the role of transforming paper into self-powered active sensors. Furthermore, in Section 2.4, self-powered fluid sensors are discussed. The first work involving self-powered fluid sensors is a self-powered wind speed sensor that use frequency to detect wind speed instead of utilizing current was constructed. Also, another work of self-powered fluid sensor, a self-powered wave height sensor, is discussed.

For TENG use in energy harvesting, as shown in Section 3, enhancement of the harvesting efficiency, and decreasing load impedance of TENG is a must, as the impedance of TENG is currently much higher than most commercial electronics. Thus, in this dissertation, strategies and new theories on enhancing harvesting efficiency by mitigating an electrostatic screening effect

from water for harvesting ocean wave energy and decreasing the load impedance of the TENG in ocean wave harvesting are shared in Section 3.1 and Section 3.2. Also, the electrostatic screening effect, that will be shared in Section 3.1, from water is then examined in detail by changing the substrate material of the TENG. Three different solid substrate materials with different dielectric constants were tested, and the output performance of the nanogenerators were evaluated in Section 3.3. It was found that the lower dielectric constant of the material contributes to a higher output power generated in the freestanding case, which shows the advantages of aerogel-based structure in energy harvesting. Lastly, the energy harvested from the TENG needs to be effectively stored in an energy storage device. To address this issue, Section 3.4 shows a hybrid electromagnetic triboelectric bracelet in effectively harvesting energy and storing the harvested energy in a supercapacitor with a low discharge current.

For TENG use in high voltage applications, since this is a relatively new field, understanding the effect of high voltage discharge in different electrical components, such as resistors and capacitors, is needed, as shown in Section 4. First, the high voltage discharge in resistive systems are examined in Section 4.1. It was found that TENG could short a 3D- printed fuse, changing the resistance of the fuse. With this work, applications in self-powered sensing system and personal security device are discussed and demonstrated. Then, capacitive based systems were tested, and the effect of electrostatic discharge are examined in Section 4.2. It shows that by utilizing high voltage pulses generated from TENG, and passing it through a capacitor, electrostatic discharge was examined, and this process could significantly increase instantaneous power density of TENG.

The above-mentioned goals are summarized in Table 1, and in the next chapter, the current progress to achieve these goals in TENG for self-powered active sensing would be discussed.

Table 1: Existing Challenges and Goals of This Thesis in TENG for Self-Powered Active Sensing, Energy Harvesting, and High-Power Voltage Applications

	Challenges	Goals
Self-Powered Active Sensing	❖ Proof of Concept Phase ❖ Lack of self-powered strain sensing and accurate wind speed sensing ❖ Lack of solid hardware solution	❖ Fabricate first self-powered strain sensor utilizing contact mode. ❖ Transform paper into a sensing platform ❖ Use of Frequency to Sense Wind Speed, and self-powered active sensing of wave height
Energy Harvesting	❖ Low Power Output limited by electrostatic screening effect. ❖ Low efficiency due to impact loss and high impedance of nanogenerator ❖ Lack of energy storage elements to store harvested energy	❖ Developed New theory to reduce electrostatic screen effect in harvesting ocean waves and investigate effect of different substrate material on performance of nanogenerator. ❖ Developed multi-layer TENG to reduce impedance of nanogenerator ❖ Integrate a wearable TENG/EMG with a microsupercapcitor.
High- Voltage Applications	❖ High Voltage (~kV) ❖ Low Current (~μA)	❖ Investigated effect of electrostatic discharge from high voltage of TENG. ❖ Utilized high voltage application of TENG to produce high current.

CHAPTER 2. TENG AS SELF-POWERED ACTIVE SENSOR

The rapid development of internet of things (IoTs) requires wireless, multi-functional, independent operation of sensor network. Considering the large number and small scale of sensors, the implantation of traditional power supply into powering these sensors has become a big challenge. In this regards, self-powered active sensors based on triboelectric nanogenerators (TENGs) would be an optimum solution. Since the TENG can transform mechanical stimuli into electrical signals directly, it could use the electrical signals generated as a sensor to tell about the characteristics of the mechanical stimuli, by analysis of the electrical signal's magnitude and frequency. Also, this is considered a self-powered sensing, as no external power device is needed for the sensing operation. For analyzing the magnitude of the voltage or current peak, one could obtain information on how much force or pressure is acted on a TENG element.[31, 60-62] Also, for analyzing the electrical signal's frequency, one could obtain how fast an object is moving, which allows it to be utilized as a motion sensor,[63-65] Furthermore, the TENG has been shown to be used as a self-powered chemical sensor, due to the sensed chemical can change an output impedance of a chemical sensor. The electrical performance of the TENG strongly depends on the load impedance of the device; thus, by investigating the electrical performance of the TENG integrated with an impedance based chemical sensors, different chemicals could be sensed with TENG technology.[66-69]

In this chapter, a new self-powered active sensor utilizing novel materials is designed, and it is the first active sensor for TENG component to actively detect strain motion with high selectivity and sensitivity.[70] Furthermore, self-powered sensors based on different kind of everyday materials, such as paper, have been created, and by utilizing signal processing and machine learning techniques, different kinds of vibrations or mechanical motions could be

detected. Then, a new wind speed sensor based on aeroelastic fluttering is proposed. The novelty of this sensor is the use of frequency to measure wind speed, whereas in previous reports, they had use current value to detect wind speed. Another fluid sensor was made and demonstrate, and it was used for wave height monitoring.

2.1 Auxetic Foam Based TENG as a Self-Powered Active Strain Sensor

Strain sensors that can monitor various human body motion have received great attention in recent years, due to their many applications in human-machine interfacing and medical monitoring.[71-74] Current strain sensors are driven by rigid power supplies, which would limit their usage and applications in many cases, especially when harvesting energy on and from the human body.[75, 76] Previous works from our group include a piezoelectric strain sensor, but piezoelectric nanogenerators could not provide a sustainable power supply, as the output voltage is too low, which would make this technology to be difficult in charging a battery or capacitor.[77, 78] To provide a sustainable power supply, TENG had been used previously to harvest energy from the human body and have been shown to display a change of output potential at different strains of stretching by utilizing the sliding mechanism of the TENG. [79, 80] However, for a TENG to operate as a self-powered active strain sensing component, both the selectivity and sensitivity of the sensor are important values. By utilizing the sliding mode of the TENG, when the materials are being stretched in previous reports, [79, 80] their devices could not be used as an effective strain sensor, because their sensitivity is low, due to less change of effective contact area, and a corresponding voltage could be related to two different strains, symbolizing their sensors are not selective.

To address these issues of low sensitivity and selectivity, the sliding mode mechanism in previous designs were changed to a contact-separation single electrode mode. For vertical-contact

separation single electrode mode, the output performance, especially the total charge on the material's surface, strictly depends on the contact area between two dielectric surfaces and the separation distance between the two materials.[6, 81] Thus, a design is made to have the two dielectric materials of the TENG initially to have no or very small contact area when no strain is applied, and once strain is applied, the contact area increases directly with increasing strain. The optimal material choice for this design is to use an auxetic material, [82] which are materials that have a negative Poisson's ratio, for the inner dielectric of the TENG. Once the auxetic material is stretched, the auxetic material is then able to contact the outer triboelectric layer. Furthermore, once the auxetic material is released from stretching, the auxetic material would separate from the outer triboelectric layer.

The auxetic material that was used in this work is an auxetic polyurethane (PU) foam. To fabricate this auxetic PU foam, a PU Foam was triaxially compressed inside an aluminum square tube with a side length of 1 in. The tube with the PU foam inside was then heated in the furnace at a temperature of 175 °C for 10 minutes. Compressing the foam triaxially would cause the ribs of the foam's cell to buckle, forming a re-entrant cell structure. Furthermore, heating the foam past the softening point followed by cooling would cause the material to retain the buckled structure. The foam was then removed from the aluminum tube and cooled to room temperature to produce the auxetic PU tube.

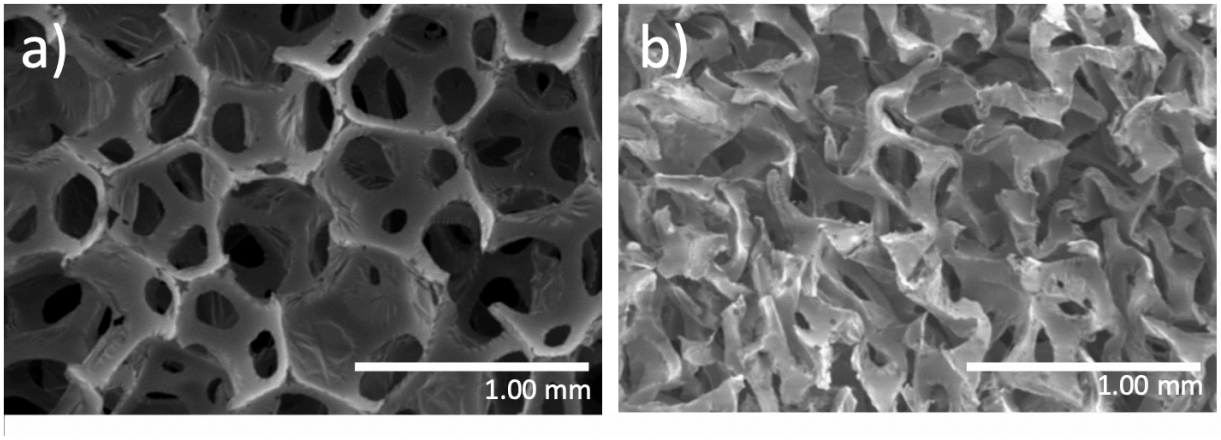

Figure 4. SEM images of Polyurethane foam. a) original PU foam. b) Auxetic polyurethane foam.[70]

After the auxetic PU foam has been cooled to room temperature, the original PU foam shown in Figure 4a and auxetic PU foam shown in Figure 4b were both compared on the microscopic level by using scanning electron microscopy (SEM). In order to be viewed in the SEM, gold was first sputtered onto the polyurethane foam. The auxetic PU foam has a buckled structure, which makes the foam stretchable, whereas the previous PU foam was not stretchable. Once the auxetic foam is stretched, the auxetic would unbuckle, which would cause an increase in volume. Also, the auxetic re-entrant foam shows a larger contact area, which would cause the charge transferred from contact electrification to be higher compared to the charge transferred by the regular PU foam. It is also important to note that the original PU has pores ranging in diameter of 200-300 microns, which because of the porous structure would cause less contact electrification, resulting in less charge transferred.

With the new auxetic foam material, the mechanical properties of the material were investigated. When a tensile force was applied on the auxetic PU in its longitudinal direction, the other two directions, the latitudinal directions, would also expand.[83] This is due to the tension would cause the buckled cell to unfold and to expand laterally. The intrinsic strain of expanding

in the *y* and *z* directions due to Poisson's relationship is compared with the strain of expanding in the *x* direction, and the relationship is shown in Figure 5a. The Poisson's ratio, the negative ratio between the transverse strain and the longitudinal strain in the elastic loading direction, was calculated to be the negative slope of the line, which is measured to be −0.62. Figure 5b and Figure 5c shows the optical images of the unstretched and the fully stretched state of the PU foam. From Figure 5b and 5c, it shows the photograph of the auxetic foam before and after stretching, respectively. It could be seen that the material expands in the latitudinal direction when stretched in the longitudinal direction.

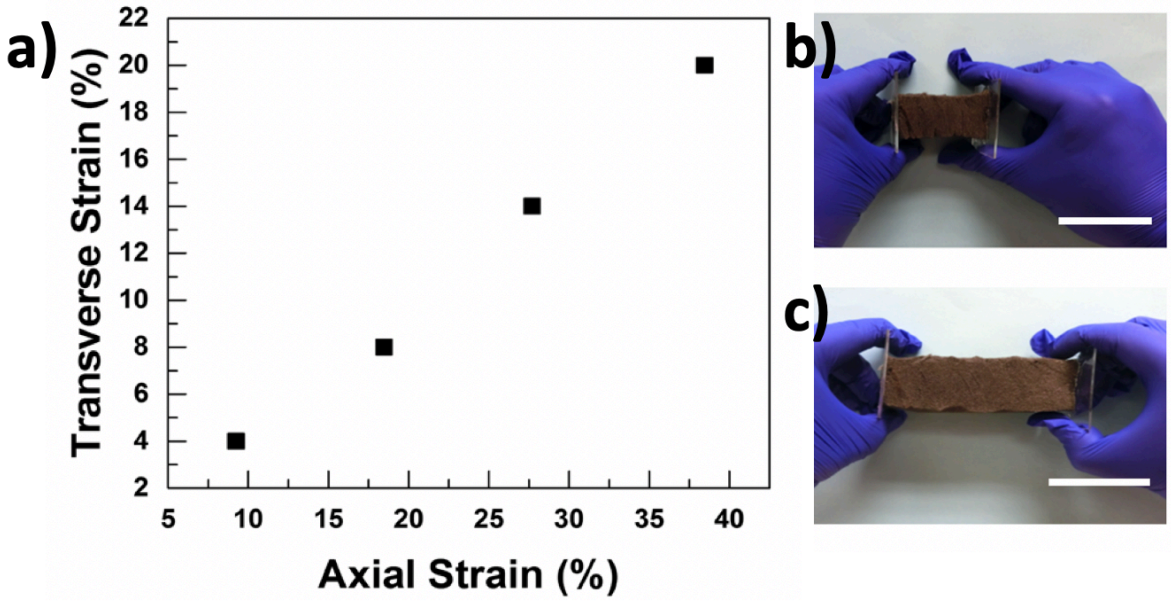

Figure 5. Mechanical properties of the Auxetic Foam Material. a) Transverse strain versus applied axial strain of auxetic PU foam. b) Photograph of as prepared auxetic PU foam (scale bar: 5 cm). c) Photograph of the auxetic foam when stretched at 40% strain (scale bar: 5 cm).[70]

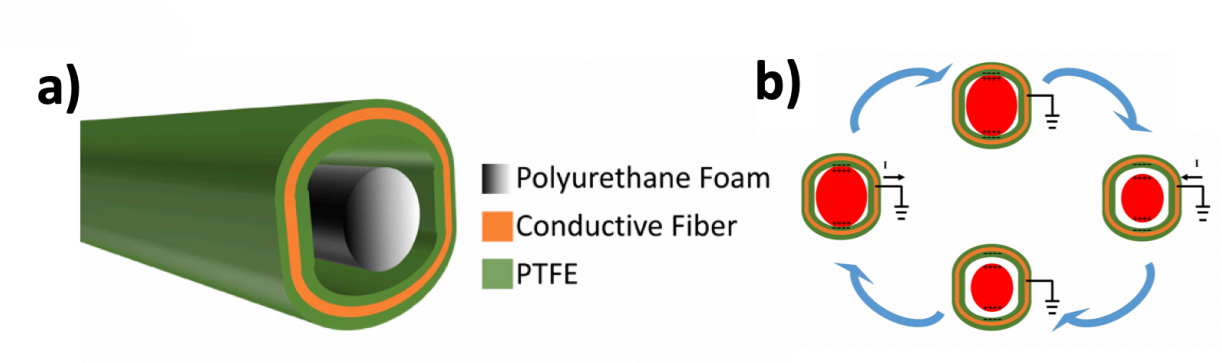

Figure 6. Structure and Mechanism of the Auxetic Foam Based TENG. a) Illustration of auxetic foam-based TENG. b) Mechanism of auxetic foam-based TENG.[70]

After evaluating the properties of the auxetic polyurethane foam, the auxetic foam based TENG, as shown in Figure 6a, is fabricated. The outside shell is a polytetrafluorethylene (PTFE) layer with a conductive fabric that has been attached on the back side. The PTFE layer was then wrapped carefully over the auxetic PU foam. The working mechanism of the TENG device is shown in Figure 6b. When the auxetic PU foam is stretched, the PU foam expanded and contacted with the PTFE friction layer, causing triboelectrification. Since PU foam and PTFE friction layer are opposite on the triboelectric series, the PU foam would generate positive charges, whereas the PTFE would generate negative charges.[15, 19] After the PU foam was released from the stretched state, the PU foam would separate from the PTFE, returning to its original position. The charge separation would cause the PTFE to induce positive charges onto the conductive fabric, which would drive electrons to flow from the reference electrode, ground, to the conductive fabric, producing a net current. Furthermore, if the PU foam is subjected to a higher strain, there would be a larger contact area between the PU foam and the PTFE friction layer, and thus there would be more charges stored in the PTFE layer after release, which would cause more induced charge on the conductive fabric. This allows the PU foam to act as a self-powered active strain sensor, as the output electric signals are strain dependent.

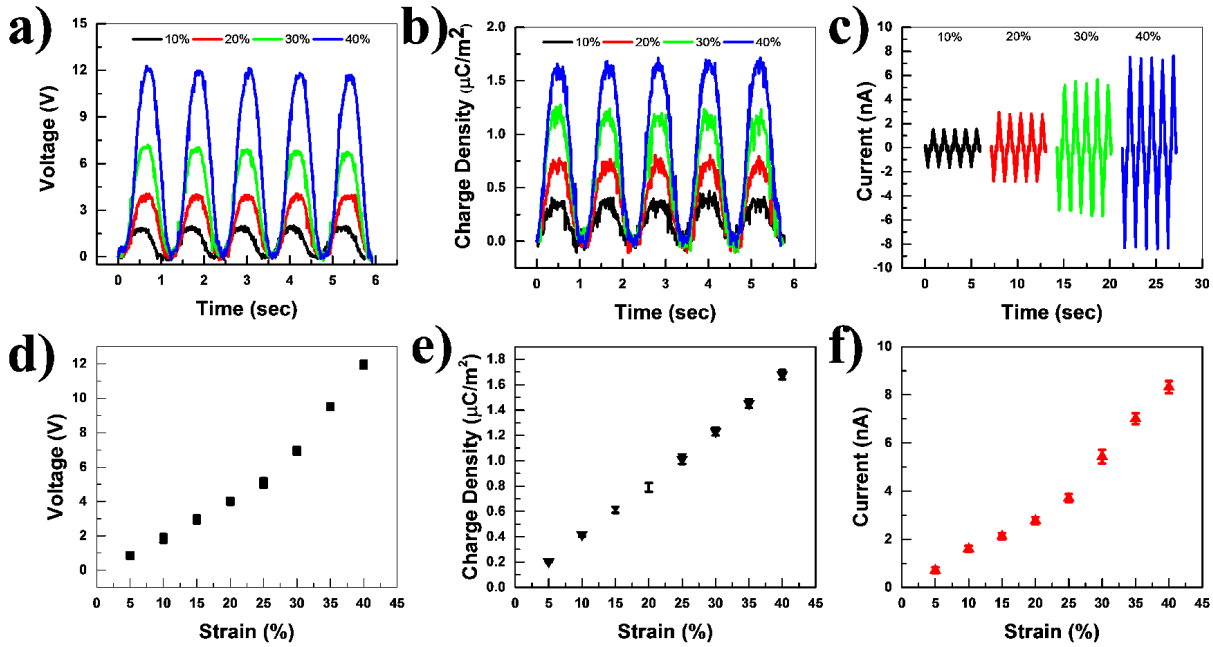

Figure 7. Electrical outputs of Auxetic Foam Based TENG at different strain. a) The open circuit voltage (V_{OC}). b) Transferred charge density (σ_{tr}). c) Short circuit current (I_{sc}). d) Sensitivity of V_{OC} with strain. e) Sensitivity of σ_{tr} with strain. f) Sensitivity of I_{sc} with strain.[70]

Afterwards, the auxetic based TENG was fixed onto a linear motor, and the linear motor was able to produce oscillatory motion, stretching the auxetic foam periodically. The output performances of the device, open-circuit voltage (V_{oc}), transferred charge density, (σ_{tr}), and short-circuit current (I_{sc}), all measured by Kiethley 6514 electrometer, were investigated by stretching the PU foam to different strains (10%, 20%, 30%, 40%) under the same frequency (1 Hz), as shown in Figure 7a-c. The resulting output open-circuit voltage reached 12 V, the resulting charging density reached 1.6 μC m^{-2}, and the resulting output short-circuit current reached 8.5 nA at 40% strain. Also, the values of open-circuit voltage, transferred charge density, and short-circuit current continue to monotonically increase with increasing strain, which unlike the previous results, showed that the voltage increased as the device approaches a fully stretched state and then showed the voltage decreased afterward with increasing strain. For the previous reports, the voltage decreased because of (1) the increase of resistance during stretching would cause the voltage and

current to decrease after further increasing the strain, which is evident in Yi et al's work[84] and (2) the overstretched state would have a decreasing and less effective contact area with increasing strain, causing a decrease in the output voltage and charge, which is evident in the work done by Wu et al.[85] This auxetic foam TENG avoids this issue due to the resistance of the conductive fiber on the PTFE does not vary as the strain increases, and the contact area would always increase with increasing strain. This further emphasizes the importance of the auxetic foam TENG as a strain sensor, as only one strain value is obtained at a specific open-circuit voltage, whereas in previous reports they could obtain two different strain value corresponding to a peak to peak voltage value.[84]

To further evaluate the output performance of the TENG, the maximum V_{oc}, Q_{tr}, and I_{sc} of the TENG is plotted as the function of strain and shown in Figure 7d–f. The sensitivity, or gauge factor, is defined as $d(\Delta V/A)/d\varepsilon$, where ΔV is the relative change in the output voltage, A is the maximum area of the device, and ε is the applied tensile strain on the device. The open circuit voltage reached 1.6 V cm^{-2}, the charge density reached 4.57 μC m^{-2}, and the obtained current reached 1.16 nA cm^{-2}. The sensitivity of the gauge factor from the generated voltage was compared to the sensitivity in previous triboelectric strain sensors. For example, the device with a gauge factor of 0.6 V cm^{-2} was obtained in Wu et al.,[79] and a gauge factor of only 0.14 V cm^{-2} was obtained in Yi et al.[84] The better sensitivity is caused by these two main reasons: (i) the increase of the contact area of the TENG due to the strain helps the triboelectric friction layer to accumulate more charges, which would cause a larger change in potential difference per unit area of device when the foam is stretched; (ii) The TENG would also have a higher separation distance when the foam is released from the stretched state at larger strains. This would further enhance the electric potential due to Equation 3, which states the voltage is proportional to the separation

distance. Thus, the auxetic-foam based TENG showed a higher sensitivity and selectivity to strain than the other TENGs.

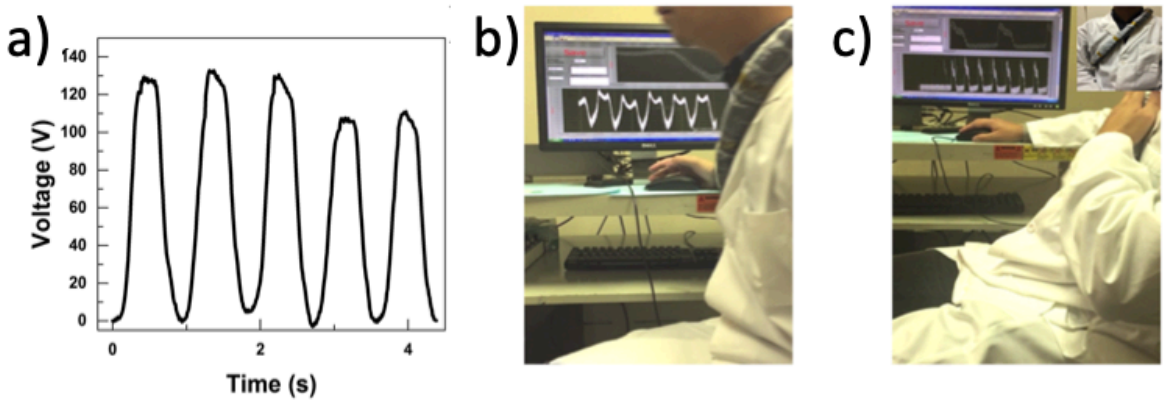

Figure 8. Application of Auxetic Foam based TENG as seat belt a) Output of the seatbelt when subjected to maximum strain applied. b) Demonstration of output by moving shoulder. c) Demonstration of output by tapping. Inset: Photograph of a person wearing the auxetic seatbelt.[70]

With the higher sensitivity and selectivity of the sensor and the superior mechanical properties, such as higher durability, and higher indentation and shear resistance of the foam, the next work is to show its use in practical application. It was found that this device could be used for application that require a long lifetime, such as a smart seatbelt and smart weight sensor. To fabricate this smart seatbelt, ten auxetic PU foams were glued onto each other, and a large-scale PTFE-conductive fabric-PTFE friction layer was wrapped carefully around the multiple auxetic PU foam structure. The device was then fixed onto both sides of the chair, as shown in inset of Figure 8c. When a user moves back and forth on a seat, the triboelectric seat belt would be stretched in the latitudinal direction, which would cause the foam to expand in the longitudinal direction and caused contact electrification. The voltage corresponding to the displacement of the moving back and forth motion was investigated and is shown in Figure 8a. The relationship between the open circuit voltage and displacement is linear, and the device has good sensing performance from 3 cm

to the maximum displacement of 15 cm. Furthermore, the sensor could easily be calibrated by utilizing this fitting line. When the user moves back and forth is revealed in Figure 8b, the output voltage was collected and displayed on the computer screen. Further application of the device includes sensing at high thrusting motion, such as if a person is involved in the car accident, and the foam could actively sense the signal, provoking an air bag in response to how high the sensed thrusting motion. The sensing of the high thrusting motion could be sensed by utilizing an Arduino Microcontroller, which is able to detect the output voltage from the TENG and compare it to a threshold voltage. When stretching with the small thrusting motion, the voltage did not pass a set threshold, so the Arduino microcontroller would not do any further processing. On the other hand, when subjected to a faster thrusting motion, the voltage exceeded a threshold voltage, and would cause the microcontroller to trigger a buzzer. This demonstrates an important role of the nanogenerator in sensing aggressive deceleration, which allows it to sense if an user is involved in a car accident. Furthermore, the TENG could detect and harvest energy from tapping motion, as revealed in Figure 8c.

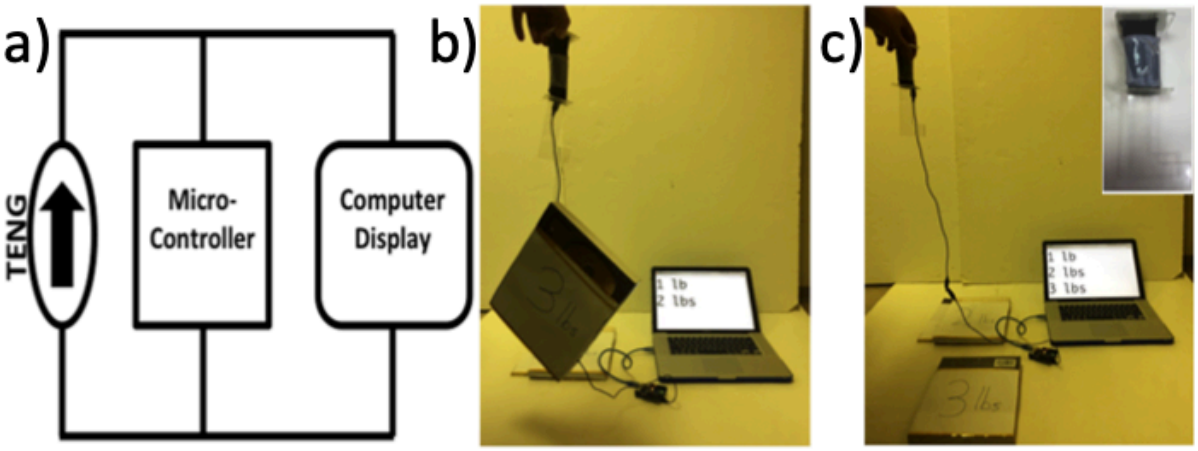

Figure 9. Applications of the Auxetic Foam Based TENG as a weight Sensor. a) Circuit diagram of connecting the TENG to Arduino microcontroller and computer display b) Demonstration of weighing the book. c) Demonstration of weighing the book after release.[70]

Also, the high strain sensitivity renders the auxetic foam based TENG to act as a self-powered weight sensor. The system is shown in the inset of Figure 9c. The lighter objects would cause a smaller deformation and strain onto the auxetic foam, which would cause a smaller change in the produced voltage. And, heavier objects would cause a larger deformation on the foam, causing a larger voltage change. Different items with different weights (1 lb., 2 lb., 3 lb.) were weighed by the auxetic weight sensors and the output V_{oc} is displayed in Figure 9b. Different weight of objects could generate different voltages; for example, 1 lb. object corresponds to 1.5 V, 2 lb. object corresponds to 7 V, and 3 lbs. object corresponding to 12 V. Thus, the voltage increased with the weight of the materials. To characterize and further sense the different outputs from the different weights, an Arduino microcontroller was connected with the weight sensor. If the output voltage exceeds a threshold voltage, the weight would be displayed on a computer screen. The circuit diagram for this integration of TENG and the Arduino Microcontroller is shown in Figure 9a. As shown in Figure 9c, the auxetic weight sensor could sense different weights accurately and could display an output on the computer screen corresponding to the exact weight of the device. After the three-pound object is dropped, the phrase '3 lbs' is displayed onto the computer screen, and this demonstrates the effectiveness of the auxetic foam TENG in its application as a weight sensor.

In this work, the first contact-mode triboelectric self-powered strain sensor has been fabricated to sense body motion was demonstrated. By utilizing a new material, auxetic polyurethane foam, the auxetic foam would expand when the foam is stretched and caused contact with a PTFE friction layer to generate electricity. This contact mode TENG exhibited a strain sensitivity of 1.6 V cm^{-2}, which had a higher sensitivity compared to TENGs that used sliding mode mechanisms. Furthermore, with the higher sensitivity, the nanogenerator could be utilized

in various self-powered sensing applications, such as monitoring human body movement, a weight sensor, and a seat belt to monitor different body motion in the car. With the application of the seat belt, it could be utilized in detecting high thrust motion and aggressive deceleration, which could prove valuable in the future of IOT in self-driving cars, as the car could detect whether the user got involved in an accident. In the next two sections, transforming paper into a self-powered active sensing unit by utilizing triboelectric nanogenerator is discussed.

2.2 Paper-Based Triboelectric Nanogenerator as an Acoustic Sensor

Paper is formed by multiple layers of cellulose fibers and it is recognized as the most environmental-friendly and renewable material.[86] It is a versatile material with many uses, such as for writing, packaging, and decorating, and it is hard to imagine living a life without paper. Recently, it has been intensively studied in the past two decades, and advancement of paper in electronics has been witnessed.[87, 88] Paper based electronics have been considered as one of the most exciting technologies in the near future due to its sustainability, low cost, and mechanical flexibility.[89] Recently, paper-based energy harvesters have been intensively developed for self-powered energy generation and self-powered sensing.[85, 90-93] In this section and the next section, transforming paper that people use every day into a smart self-powered sensing material by utilizing TENG is discussed.

The first work of utilizing paper-based nanogenerator for self-powered active sensing is for it to operate as an acoustic sensor.[94] Sound or acoustic energy is an important form of energy that exists in everyday life and has been overlooked as a green energy source that could be harvested, mainly due to it has a lower power density compared to other forms of energy.[95] However, even with a low energy that could be harvested from sound, it needs to be sensed by a

microphone, or an acoustic sensor, which outputs an electric signal based on the sound pressure variation it sense. With an acoustic sensors, various application had been studied, such as speech recognition,[96] hearing aids,[97] and structural maintenance.[98] One issue with most commercial microphone is that it requires power for operation and sound amplification.[99] Furthermore, there have been another type of acoustic sensors, called self-powered acoustic sensors, that do not consume power, but are bulky in nature or complex to manufacture and costly to scale in size.[100-102] Thus, there still remains a challenge in designing a microphone or acoustic sensor, which is passive and has a sound quality comparable to its active counterparts while still preserving a lightweight and versatile form factor. Paper would be an excellent choice in fabricating acoustic sensors, as it is able to have both the versatile form factor and being lightweight in nature. Thus, in this work, the design, fabrication, evaluation, and applications of a flexible and self-powered paper-based acoustic sensor is performed.

First, I am going to discuss how this a paper can generate electric signal by the triboelectric effect. Holes were made in the paper to create mini-resonant cavity for air when sound propagates, resulting in an enhancement of the vibrations on the paper media. Thus, this acoustic sensor would work on the principle of vibration-induced contact, as propagation of sound through air causes compression and rarefaction of the paper film, and during the compression or contact stage, when the copper contacts a PTFE surface, charges would be generated on both PTFE and copper due to contact electrification. The process is explained and shown in Figure 10. After full contact, subsequent rarefaction would separate the paper and the PTFE. This would produce an electric potential between the copper electrode on the paper and a copper electrode behind the PTFE if it is open-circuit state. For a short-circuit state, with the circuit diagram shown in Figure 10, it would create a current to flow from the copper on the paper towards the copper behind the PTFE. As the

copper layer on paper approaches the PTFE layer again, the flow of current reverses in direction, completing a cycle of electricity generation. Thus, this device is able to convert mechanical sound-based energy into electricity, which is shown by the alternating current, and this device would be referenced as a self-powered paper-based triboelectric acoustic sensor.

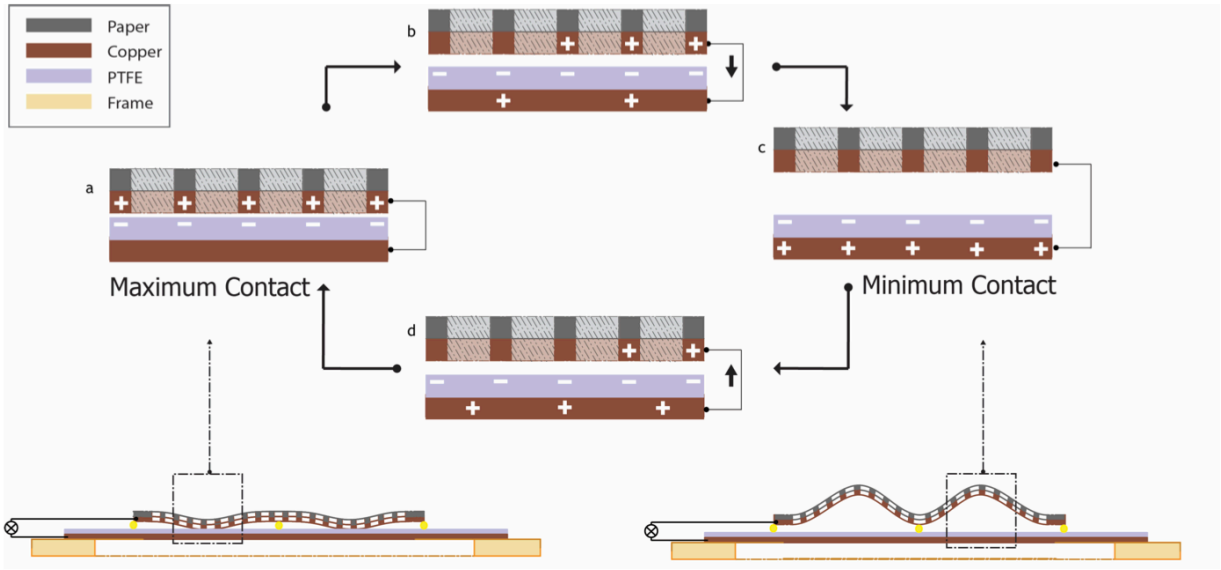

Figure 10. Working Mechanism of Electricity Generation Process of Paper-Based Self-Powered Triboelectric Acoustic Sensor.[94]

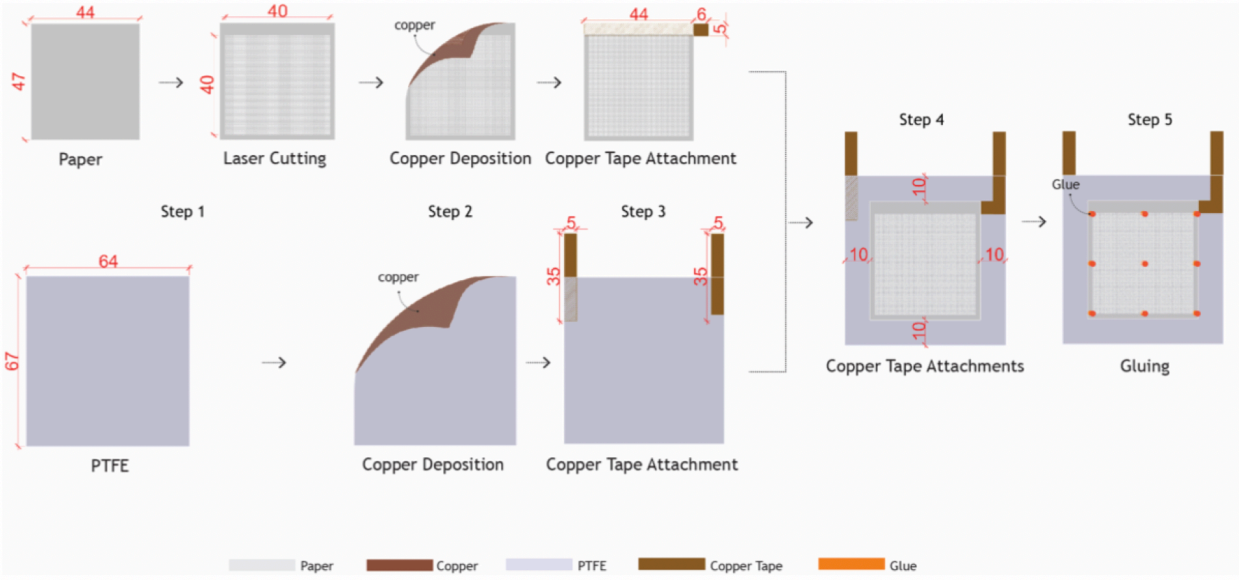

Figure 11. Fabrication Process of Paper-Based Self-Powered Triboelectric Acoustic Sensor. Step 1: Preparation of micro-hole paper. Step 2: Deposition of copper layer. Step 3: Attaching copper tape as electrodes. Step 4: Stacking PTFE and paper. Step 5: Gluing PTFE and paper. All dimensions are in mm. [94]

Next, I am going to explain on how to create and fabricate this self-powered triboelectric acoustic sensor. To fabricate this device, with the steps shown in Figure 11, firstly, 400 μm diameter holes with an even spacing of 200 μm were micromachined via laser cutter on copier paper in a grid pattern. The 400 μm holes and spacing of 200 μm spacing were maximized to produce the highest output. The hole pattern forms a 4 cm. x 4 cm. square grid. A small boarder of 5 mm on one side and 2 mm on the other side is left to be used for attachment of the PTFE layer, and is kept small to ensure the ease of reproducibility of the cavity created between copper and paper after being attached together. Then, both the paper sheet and PTFE sheet are coated on one side by Physical Vapor Deposition (PVD) a thin layer of copper that acts as electrode. Then, a conductive copper tape was attached on the copper side of the paper and the PTFE in order to extend the electrodes for measurement purposes or to connect to an external circuit. The paper and PTFE are placed on top of each other such that the copper layer of paper is on top of the non-

coated side of PTFE, which is not conductive. Then, the paper layer with the copper side facing PTFE is glued to an uncoated PTFE using glue dots at nine anchor points.

Next, the output performance of the paper-based structure needs to be measured. To test and characterize the performance of the self-powered paper-based triboelectric acoustic sensor, a frequency sweep using a JBL Flip 2 speaker was used as an input sound recording. The frequency sweep is a sine wave linearly increasing in frequency (20Hz-20kHz) with an increase of frequency defined as 1kHz per second, as shown in Figure 12b. The frequency was standardized at 1000 Hz frequency and the sound pressure level is standardized at 94 dB or 1 Pa of pressure. The power in dB re mV/Pa at 1000 Hz frequency is defined as the acoustic sensitivity of the acoustic sensor. It is used as a representative of the sound quality of the acoustic sensor. The electrical response generated by the triboelectric acoustic sensor is measured as voltage by utilizing an Analog Discovery oscilloscope, which has a 1 MΩ resistance. Please note that with a 1 MΩ resistance, the voltage is not in open-circuit state, which would result in a lower output voltage measured. Figure 12a shows the electrical response for the acoustic sensor for the chirp sound input. The maximum voltage is achieved at a resonant frequency of approximately 275 Hz. Furthermore, the power in dB is measured by utilizing the 20*log (sensitivity/Vnoise). At 1000 Hz, the acoustic sensitivity is -26.63 dB re mV/Pa, which is shown in Figure 12c.

With the measurement of output performance completed, it is necessary to show applications of this paper based triboelectric acoustic sensor. To show practical applications of the sensor, a smart tabletop with two paper-based triboelectric acoustic sensors placed on the table with two people speaking, in order to simulate a conversation. As the two people speak, the location can simply be determined by comparing the voltage output of multiple the triboelectric

acoustic sensor patches. The paper based triboelectric acoustic sensor patch placed near to a speaker will have a higher output voltage compared to the one that is placed farther away from the speaker, due to the higher amplitude that the closer patch would detect. Figure 13b shows a simple example of such localization and the setup of the two acoustic sensors and two speakers. Furthermore, to test the output signal, the acoustic sensors are hooked up to Analog Discovery oscilloscope to measure the output voltage, which is shown in Figure 13a and Figure 13c, when two speakers in different position speak directly to each other. When speaker A (yellow) speaks, the closer acoustic sensor to speaker A, microphone 1, has a higher output voltage amplitude than the other acoustic sensor, as shown in Figure 13a, and Figure 13c. Similarly, when speaker B (blue) starts speaking, the closer acoustic sensor, microphone 2, has higher output voltage amplitude than the other microphone 2, as shown in Figure 13a and Figure 13c. This demonstrate that by utilizing two triboelectric patches, an application of self-powered position sensing of the speakers could be detected. Such infrastructure can be further expanded to include multiple acoustic sensors on the table to determine position of more speakers.

Also, the triboelectric paper based acoustic sensor could be used for speech recognition. Since the triboelectric paper based acoustic sensor could be placed on almost everyday objects, the paper was placed onto a Coca-Cola bottle, as seen in Figure 14a. A person then speaks the phrase "Let's Share a Coca-Cola" to the bottle with the paper-based acoustic sensor attached on the packaging label of the bottle, as shown in the right image of Figure 14a. The output voltage is then measured, and the time series graph of live speech is shown in the time series voltage, as shown in Figure 14c, with the corresponding spectrogram shown in Figure 14d. The spectrogram shows the paper-based triboelectric acoustic sensor is able to produce sufficient detail that is enough to do spectral feature extraction for speech recognition.

In this work, the design, evaluation, and applications of the paper based triboelectric acoustic sensor is performed and shown. The triboelectric acoustic sensors' simple fabrication process and ease of deployment on a variety of surfaces enables new opportunities for audio sensing over large indoor/outdoor areas for both mobile and stationary objects. This shows that it is possible to convert a widely used material into a sensing surface that could be used to detect sound by the triboelectric effect. Furthermore, applications were demonstrated, and this paper-based triboelectric acoustic sensor could be used for both position sensing of speakers and for speech recognition, as the output signal was able to produce enough detail for spectral feature extraction. In the next section, other use of paper in fabricating self-powered sensors leveraging different design of triboelectric nanogenerator is discussed.

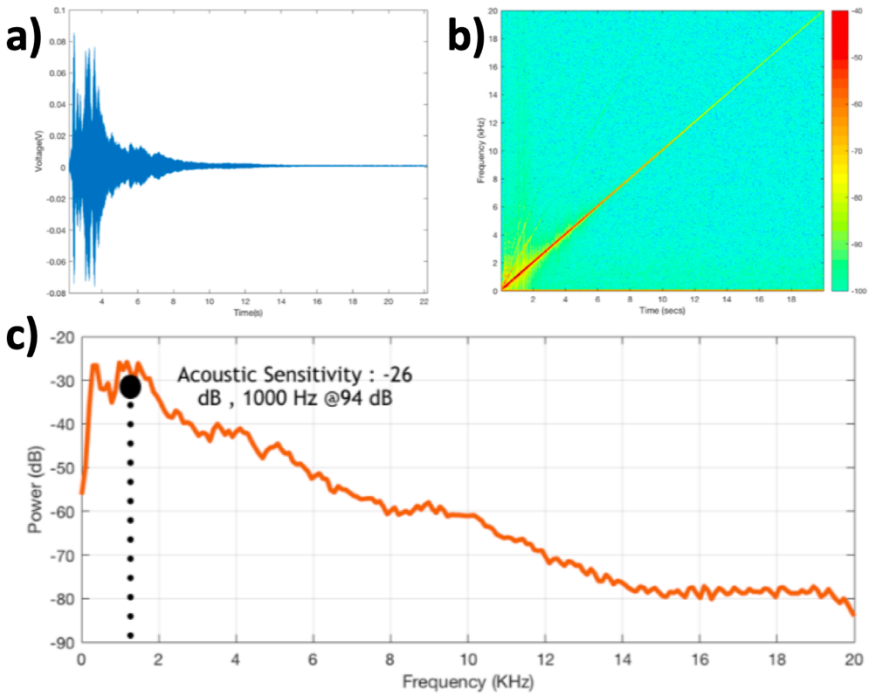

Figure 12. Electrical Response from Self-Powered Acoustic Sensor. a) Voltage vs time with increasing frequency over time. b) Spectrogram of the frequency sweep with linearly increasing frequency. c) Acoustic sensitivity variation across the audio frequency band (20Hz-20kHz). [94]

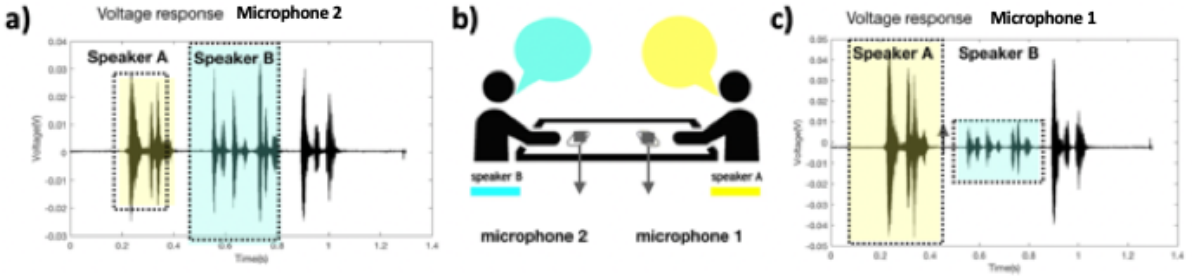

Figure 13. Application of Paper Based Acoustic Sensor as a Smart Tabletop. a) Output voltage response on paper-based triboelectric sensor 2 from Speaker A and Speaker B. b) Setup of smart tabletop with two speakers and two paper based acoustic sensor. c) Output voltage response from paper-based triboelectric acoustic sensor 1 from Speaker A and Speaker B.[94]

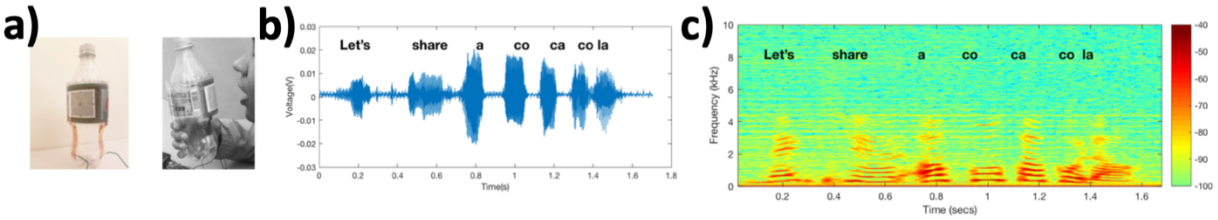

Figure 14. Application of Paper Based Acoustic Sensor as a Sound-sensitive Bottle. a) Photograph of paper based acoustic sensor embedded in a soda bottle. b) Photograph of a user speaking to the paper based acoustic sensor. c) Voltage response of the paper-based acoustic sensor when user speak "Let's share a Coca-Cola". d) Spectrogram of the paper-based acoustic sensor when user speak "Let's share a Coca-Cola". [94]

2.3 Triboelectric Nanogenerator Based on Paper-Based Origami Structures for Self-Powered Sensing Applications

Furthermore, I wanted to further expand the area of paper-based nanogenerator for self-powered active sensing. A property of paper allows it to be folded to make origami, allowing for different form factors to arise. Recently, research had been focused on embedding electronics such as printed circuit boards (PCB) into paper folds.[103] Originally, PCBs are produced as 2D shapes, but by folding PCB arrays, it is possible to create 3D objects that contain electronic functions. Similarly, utilizing the change of form factor, contact-separation mode TENG could be designed through a piece of constructing paper, whereas before, multiple layers were used to construct TENG. By folding paper, a crease, composed of two rigid faces and connecting joint, is created. Repeated folds across a single sheet generates tessellation crease patterns, which provides

mechanical properties that enable the motions of compressing and expansion. In this design, conductive copper and dielectric layer are put onto the rigid faces that are produced after a fold. During compression stages, copper and PTFE would contact, causing contact electrification. After separation, there would be charges transferred from one electrode to the other electrode on the other side of the fold, producing electricity and harvesting the compression and separation's energy. Thus, the idea of this project is to integrate the aesthetic and functional traits of paper creases with a triboelectric nanogenerator to harvest energy for self-powered active sensing.[104]

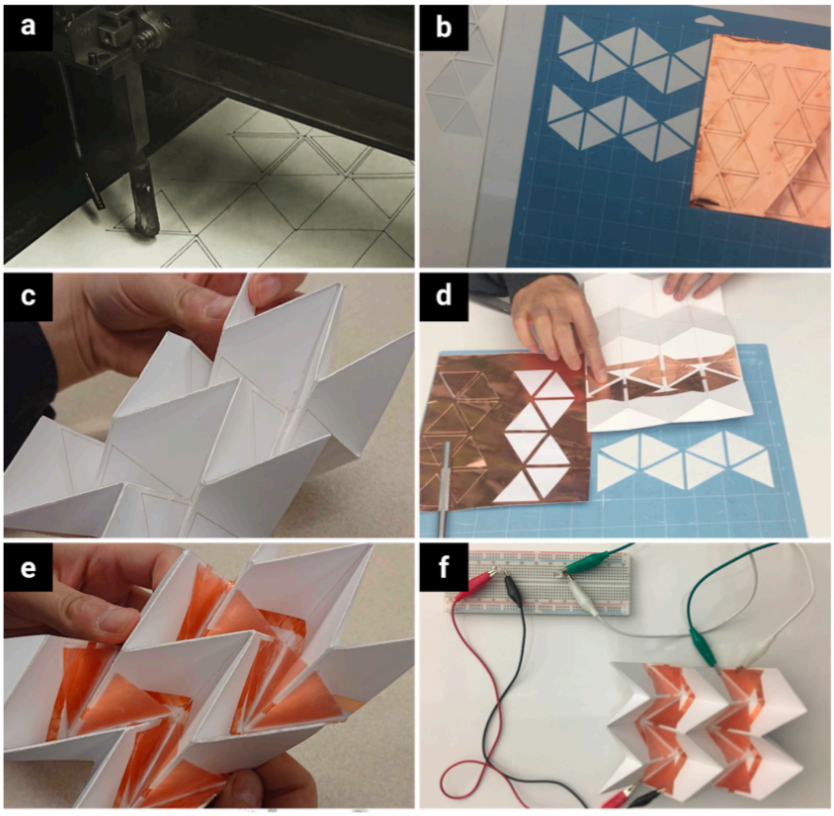

Figure 15. Fabrication Process of Origami Based TENG. a) Cutting and scoring paper by utilizing laser cutter. b) Cutting copper adhesive by utilizing vinyl cutter. c) Folding and creasing paper. d) Attaching copper adhesive onto origami structure e) Attaching PTFE adhesive onto the origami structure. f) Testing the origami-based nanogenerator's connections. [104]

Figure 15 shows the fabrication process that was done to create these origami-based triboelectric nanogenerator. The first step is to fold and crease paper, as shown in Figure 15c. Then, two copper adhesive layers were attached onto the rigid faces of the paper to make the electrodes of the origami-based triboelectric nanogenerator, as shown in Figure 15d. Next, PTFE layer were attached to one side of the copper electrode, as shown in Figure 15f. With this design, the triboelectric nanogenerator works as a contact-separation mode TENG. When a user press on the origami, the copper layer and PTFE layer would fully contact and separate producing electricity by the triboelectric effect.

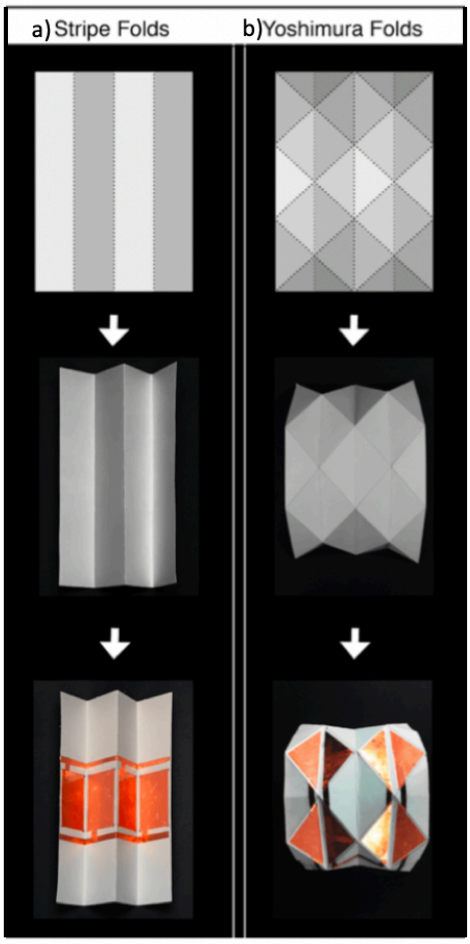

Figure 16. Different folds used for Origami Based TENG. a) Stripe fold. b)Yoshimura fold.
104

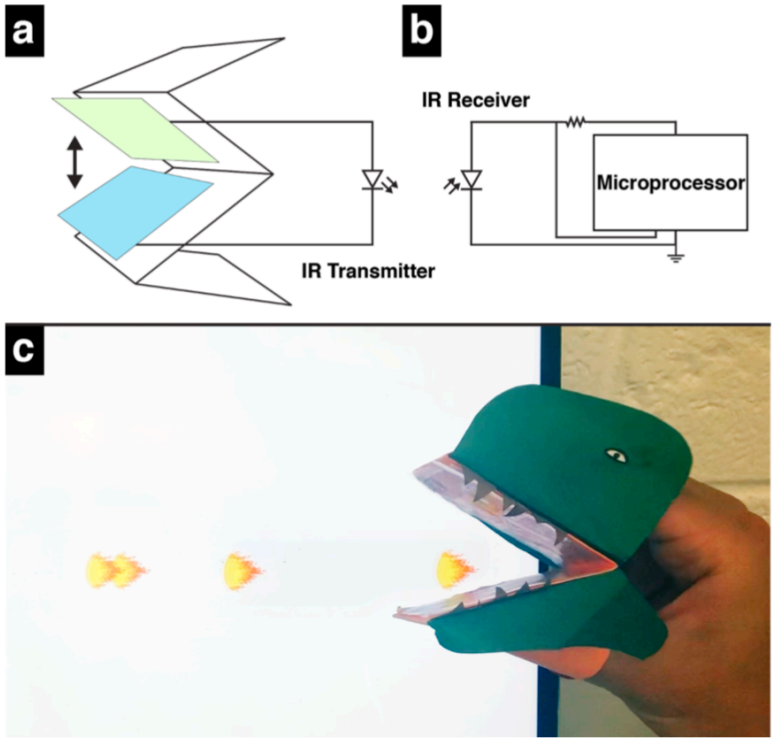

Figure 17. Origami Based TENG with Applications as a Finger Puppet. a) Schematic showing the connection of an origami-transmitter with a Stripe fold. b) Embedded schematic of the IR Receiver and Arduino Microprocessor. C) Application showing as a dinosaur puppet opens and closes its mouth, the laptop screen behind connected to the IR receiver generates shooting fire graphics.[104]

To demonstrate the broad possibility of the origami-based nanogenerator, two applications of the paper-based nanogenerator have been demonstrated for self-powered active sensing. The first application is it could be utilized as a finger puppet, and the second application is it could be utilized as a voting counter. For the finger puppet, it is created by utilizing a stripe-based fold, which is shown in Figure 16a, as the simplest origami pattern. The nanogenerator is then connected to an infrared (IR) light emitting diode (LED). In a previous work of the paper based nanogenerator, the IR transmitter was powered by the microcontroller, allowing the IR transmitter to produce different signal for different documents that were used.[105] For this application, the IR

transmitter could be powered direction by the nanogenerator; thus, it could show a broader application of self-powered optical communication. Also, Ding et al previously demonstrate the use of TENG with visible LEDs for an optical communication system.[106] However, the visible LED could be seen by human, which could limit some theatrical or security applications. This demonstrates an advantage of utilizing IR LEDs over using visible LEDs. Thus, in this case, visible LED was replaced with IR LED to demonstrate that IR LEDs could be powered by TENG and could be used as an optical communication system. When a user pinches the Stripe pattern, the copper and PTFE layers would contact, producing electricity to power an IR LED. The IR signal would be sensed by an Arduino Uno microprocessor, which is connected to a computer using Processing software. In response, there would be a fire shooting graphic that is displayed on the computer that is generated in response to the pinching motion, and IR light being sensed, as shown in Figure 17.

For the second application, a different fold of the origami is used. It is a yoshimiura fold, which is a fold that could make paper have a springy like texture. With the fold, the origami-based nanogenerator was used as a self-powered force and touch sensor, with the structure of the fold shown in Figure 16b. The applications adapt the spring-like property when it is folded into a playful pattern for a user to press and embraces it as a part of graphic design. In this application, the origami was made into a button like structure, as shown in Figure 18d. By tapping the button associated with the item, the user generates a voltage that can be sensed by a microprocessor; then, the microprocessor will detect the voltage and if the voltage exceed a threshold voltage set by the user, it will light another LED in the LED strip that is displayed back to the user on the item they tapped on, as shown in Figure 18. This shows that origami based TENG could be used as an effective power source for self-powered active sensing.

In this work, paper was transformed into a self-powered touch-based active sensors by using TENG technology and origami folds. The two different folds were made for the TENG to be used as a self-powered active sensor. These different folds allowed for different self-powered sensing applications, mainly for detecting if the paper-based nanogenerator is being pressed. It has been demonstrated that the paper-based nanogenerator could light up IR-LED, which expands a further application of optical communication technique. Also, it could be integrated with a microcontroller to further light LEDs, if the paper-based nanogenerator has been pressed, showing the application of a touch-based sensor. This concludes the section on transforming paper into self-powered sensors. In the next section, fluid based self-powered active sensors are discussed.

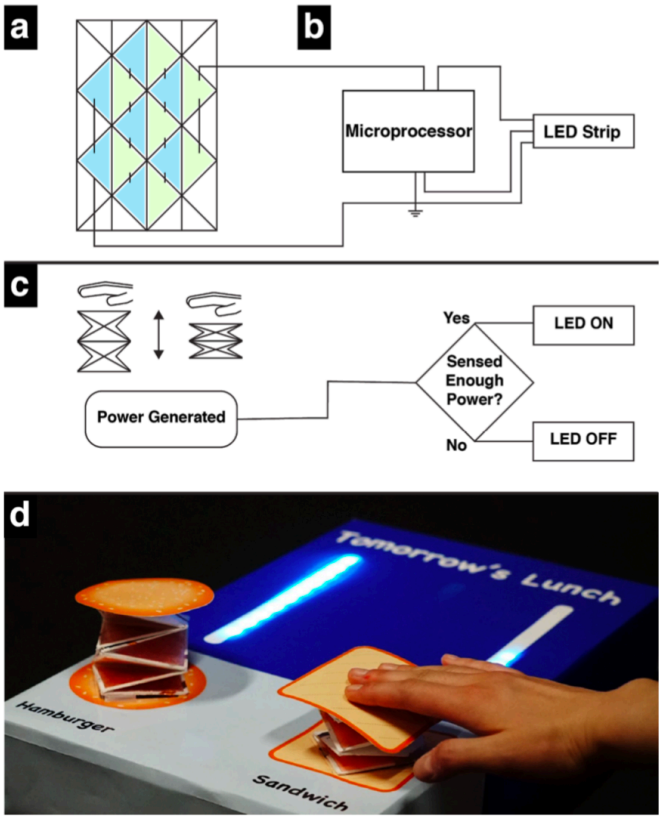

Figure 18. Origami Based TENG with Applications as a Voting Counter. a) applying the Yoshimura fold as a vote button. b) Embedded circuitry showing microprocessor connected with TENG and a LED strip. c) logic flowchart for sensing technology. d) Photograph showing as the buttons are pressed, the LED strips would light up on each side.[104]

2.4 Self-Powered Fluid Sensors

2.4.1 Aeroelastic Flutter Based Nanogenerator for Self-Powered Active Wind Speed Sensor

Recently, the interaction of a flag and a rigid plate as a powerful vibration source for TENG has attracted much attention for wind energy harvesting and self-powered active wind based sensors.[49, 107-112] Furthermore, in these previous works, they used output current peak to detect the wind speed, as in normal operating conditions, there is a linear relationship between output current peak and wind speed, as current is proportional to frequency and charge density. However, the electrical output of TENG, the charge density, is found to be influenced by high humidity, which would cause the current output to change.[49] Thus, new approaches are needed to improve the sensitivity and to lower the wind speed that the fluttering membrane starts to flutter.

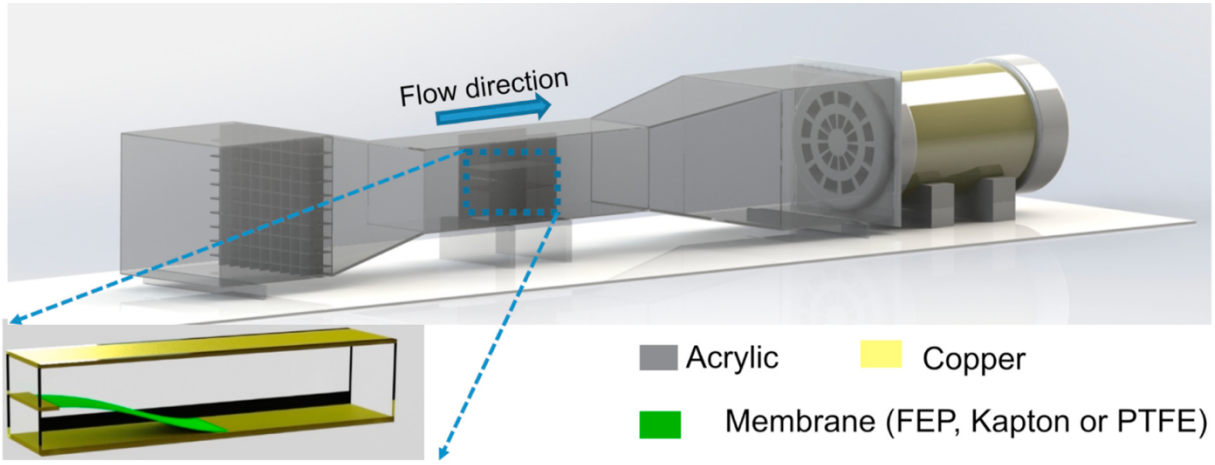

Figure 19. Experimental Setup of Aeroelastic Flutter TENG.[50]

In this work, a simple but practical design for an aeroelastic flutter based TENG, as shown in inset of Figure 19,[50] that could serve as a wind speed sensor by measuring the fluttering frequency instead of measuring the output voltage/current shown in previous reports.[49] The fabricated aeroelastic flutter based TENG consists of copper layer and a thin fluorinated ethylene

propylene (FEP) membrane (with thickness of 25.4 μm, length of 3 cm, and width of 1.8 cm) in a cuboid acrylic channel, as shown in Figure 19. When wind blows inside the tunnel, the thin FEP membrane would oscillate, and it would contact the copper electrode. Thus, it is capable in producing electricity by contact electrification and electrostatic induction, by repeated contact on the FEP electrode. It is necessary to note that FEP is one of the widely used electron withdrawing material for triboelectric nanogenerators, and it usually has a higher output performance compared to PTFE based films.[113]

The wind speed was set at 10.8 m/s from the blower in Figure 19 and the output performance was at different humidifies, which was changed by a commercial humidifier (TaoTronics Ultrasonic Humidifier) connected into the wind tunnel. The effect of relative humidity of AF-TENG performance was investigated by varying the relative humidity from 45% to 95%. Compared to that measured at humidity of 45%, the current and voltage output, which are measured by Kiethley 6514 electrometer, decreased by nearly 90% at humidity of 95%, due to the charge density on the membrane surface decreases dramatically at high humidity, as shown in Figure 20a and Figure 20b. However, humidity has no effect on fluttering motion of the membrane; thus, the corresponding fluttering frequency is independent to humidity, as shown in Figure 20c. Such finding proves that the fluttering frequency is a much more proper value to be used as the key parameter to detect the wind speed rather than average current output peaks used in previous study.[49] Thus, one could calculate the wind speed from frequency, as the frequency is directly related to the wind speed, as the higher wind speed, would cause faster vibrations, which would increase the frequency.

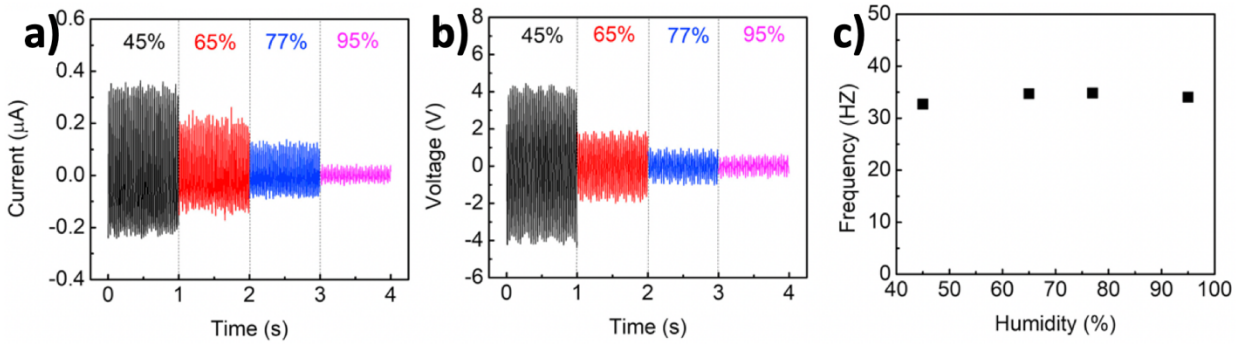

Figure 20. Effect of Humidity on Output Performance of Aeroelastic Flutter TENG. a) Output current with respect to relative humidity. b) Output voltage with respect to relative humidity. c) Measured frequency with respect to relative humidity.[50]

To test the performance of the aeroelastic flutter TENG as a wind speed sensor, the real-time speed of the aeroelastic flutter TENG TENG and a commercial hot-wire anemometer (Testo 405i) were compared, as shown in Figure 21a. The wind speed of the blower was manually changed, with an increase of 0.8 m/s every 20 s until the wind speed reached the maximum at 9.4 m/s. Then, the speed was decreased with a decrease of 0.8 m/s every 20 s until the wind speed reaches 2.2 m/s. The output voltage signal from the TENG was then measured and the real-time frequency f is obtained from the real-time voltage output of the aeroelastic flutter TENG with L=3cm using short-time Fast Fourier Transform (FFT), as shown in Figure 21b. Then, the wind speed U is obtained using the relationship between the frequency of the electrical signals e.g., voltage, and incoming wind speed, i.e., $U = 0.13f$. This equation was calibrated before by doing measurement of output signals of the aeroelastic flutter TENG. Thus, Figure 21c shows the relationship of the wind speed obtained by aeroelastic flutter TENG by utilizing this equation and output frequency of TENG, which is shown in Figure 21b. The wind speed obtained by both aeroelastic flutter TENG and the hot-wire anemometer agrees well, as shown in Figure 21c for both increasing wind velocity and decreasing velocity. This demonstrates that the aeroelastic flutter TENG, by utilizing frequency and not current, could be utilized effectively to sense wind speed.

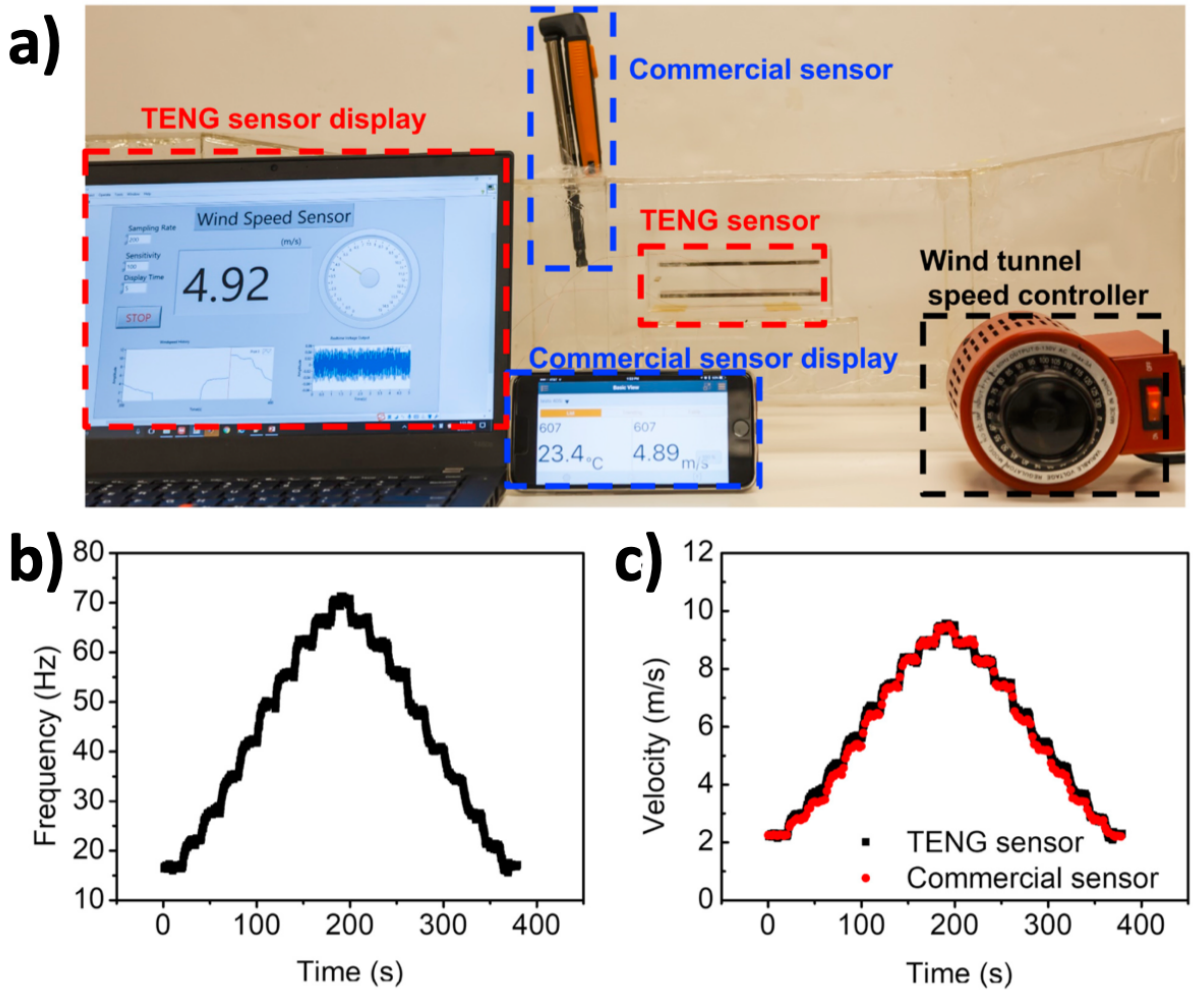

Figure 21. Application of Aeroelastic Flutter TENG as a Wind Velocity Sensor. a) Photos of the real time velocity measurement using aeroelastic flutter TENG sensor and a commercial sensor. b) Short time FFT frequency vs time with increasing speed from 0 to 200 s. and decreasing speed from 0 to 200 s. c) Comparison of aeroelastic flutter TENG wind speed sensor and commercial wind speed sensor with increasing speed from 0 to 200 s.[50]

In this work, a simple but practical design for an aeroelastic flutter TENG that could serve as an active wind speed sensor by measuring the fluttering frequency instead of utilizing the output current/voltage is performed. With this change, it could measure wind speed even at high humidity environments, where previous reports of wind sensors could not achieve, due to the previous reports use output current, which is dependent on the environment. Also, the real-time wind speed measured through analyzing frequency of the aeroelastic flutter TENG agrees well with a

commercial sensor with the speed sensitivity of about 0.13 m/s was utilized as the correlation between wind speed and frequency. The next section would discuss a self-powered fluid sensor that is able to sense the properties of water waves, such as the water wave height.

2.4.2 Liquid Solid Interfacing Triboelectric Nanogenerator for Wave Sensing

Wave monitoring is essential for marine engineering construction, development and utilization of ocean resources, maritime safety and early warning of marine disasters. Commercial wave monitoring techniques include water wave rider buoys, acoustic Doppler current profilers, and high frequency radar and remote sensing.[114] These commercial wave monitoring techniques are mainly applied for routine monitoring of waves and currents in offshore and nearshore regions.[115, 116] To enhance the environmental sensing ability of smart marine equipment, it is important to develop a highly sensitive and self-powered wave sensor to monitor the interaction between ocean wave and marine equipment, such as offshore platforms and ships. Thus, in this work, a novel wave sensor based of liquid-solid interfacing triboelectric nanogenerator is fabricated and investigated.

A schematic diagram of this wave sensor TENG for monitoring waves around marine equipment, such as a marine platform, is shown in Figure 22a. The long nanogenerator installed on the legs of the platform can precisely sense the instantaneous water height when ocean waves contact the nanogenerator's surface. The wave sensor TENG is comprised of a long rectangular copper electrode covered by a PTFE film, as shown in Figure 1b. When water height rises, as shown in 1b<i>, positive charges would be induced in the solution to neutralize the negative charges in the PTFE surface; furthermore, when water leaves the PTFE surface, as shown in 22b<iii>, positive charges would be transferred to a ground electrode in order to balance the electric field. Thus, the number of charges on the copper electrode would be inversely proportional

to the water height, allowing this device to be an instantaneous wave height sensor. Figure 1c shows data of when the wave sensor TENG is connected to a linear motor, and as the linear motor drives the substrate vertically up and down into water. The width of the electrode on the TENG is 10 mm. With the linear motor driving the wave sensor TENG up and down into the water, there would be an output open-circuit voltage signal that is measured by Keithley 6514 electrometer. In Figure 22c, it could be seen that as there is an linearly increase in height, there would be an linearly increase in the output voltage, showcasing this device as a wave height sensor. The sensitivity was then calculated by V_{OC}=kH, in which k represents the sensitivity of the sensor. The sensitivity comes out to be 23.5 mV/mm with this device with the electrode width of 10 mm. If the width is changed, the sensitivity of the device would be also changed, as the sensitivity is dependent on the contact area of the TENG and the water surface. If the contact area is increased by increasing the electrode width, the sensitivity factor would also increase.

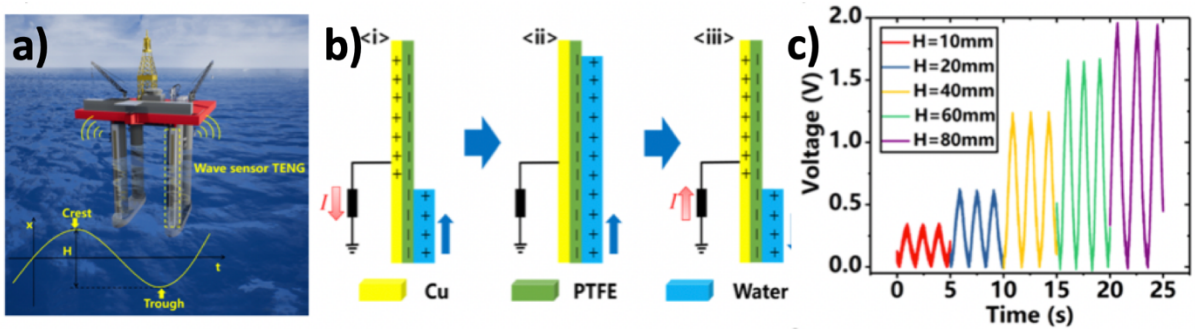

Figure 22. Structure, Mechanism, and Performance of Wave Sensor. a) Structure of wave sensor TENG on water platform. b) Mechanism of wave sensor TENG. c) Voltage vs time of wave sensor at different heights.[117]

Thus, in this a work, a novel wave sensor based on liquid-solid interfacing TENG is proposed.[117] The effect of wave height is found to be proportional to the output voltage peak; thus, allowing this liquid solid interfacing TENG to be a wave sensor. The measured sensitivity of this device is measured, and a high sensitivity of 23.5 mV/mm is observed. In the next chapter, I would

also discuss about fluids, especially water's effect on TENG, but I would mainly focus on it for energy harvesting purposes instead of self-powered active sensing.

CHAPTER 3. TENG AS ENERGY HARVESTER

One major application for triboelectric nanogenerator is for it to be used as an energy harvester that is able to scavenge energy from ambient environment and use the harvested electrical energy to drive electronic devices. Based on recent studies, the main advantage of TENG over previous energy harvesters, in particular, electromagnetic generators (EMG) is its effectiveness in harvesting low-frequency (<5 Hz) vibration energy.[51, 118] Recently, Wang proposed the concept of using TENG networks for harvesting kinetic energy of water waves towards the dream of large-scale blue energy.[43] In this section, I would introduce couple works of utilizing TENG for harvest energy from ocean waves, and demonstrate a new method to improve the TENG's efficiency in harvesting from ocean waves, that involves mitigating an electrostatic screening effect. Furthermore, for TENG to harvest energy effectively and deliver maximum power to a load, the load impedance of the energy harvester needs to decrease, as it is currently too high for powering most electronic circuitry. Thus, another work is demonstrated to lower the impedance of the TENG when harvesting ocean waves by constructing multi-level based triboelectric nanogenerators. Furthermore, I would further investigate the electrostatic effect on different substrate material in freestanding mode TENG, and it is found that the substrate material that had the smallest dielectric constant had the highest performance. Another research field is for a TENG to be used as a wearable energy harvester, so that it could harvest energy from body motions and use the harvested energy to power wearable sensors. Also, in this section, I would introduce a novel work to effectively harvest energy from body motion by utilizing a hybrid EMG-TENG device and demonstrate its applications in powering wearable electronic devices.

3.1 TENG for Harvesting Ocean Waves

The energy harvested from the ocean is regarded as an important renewable and clean energy source, which has been estimated to be over 75 Terawatt totally around the world.[1, 119, 120] Ocean energy is typically regarded as having five specific forms, i.e., tidal energy, water wave energy, ocean current energy, temperature gradient energy, and salinity gradient energy, among which ocean wave energy referring to the kinetic and potential energy from ocean surface waves. The global power of waves breaking around the coastlines worldwide have been estimated to be around 2-3 TW.[120] Thus, wave energy has become one of the key directions of ocean energy development. However, it has rarely been exploited due to the lack of economical energy scavenging techniques.[121]

Currently, harvesting energy from the ocean wave starts with extraction of wave energy, and the wave motion is first translated into linear or rotational mechanical motion, and then relies on EMG to generate electricity from the produced mechanical motion.[122, 123] Major drawbacks of utilizing EMG includes that it requires a permanent magnet, which makes the device heavy, bulky, and costly. Also, the heaviness of the structure would increase the structure's damping factor, as it would require a larger wave to move the structure, causing most of the energy to be not effectively harvested. Furthermore, the coils and magnets easily suffer saltwater corrosion and turbines have low efficiency in harvesting low-frequency energy, such as ocean waves, which are typically less than 1 Hz. Also, EMG generates a relatively low amount of voltage, which would require the electric signal to pass through a transformer to mitigate power losses from low voltage transmission. Due to these drawbacks, current ocean wave energy utilizing electromagnetic generators exhibit unsatisfactory energy harvesting efficiency and high cost.

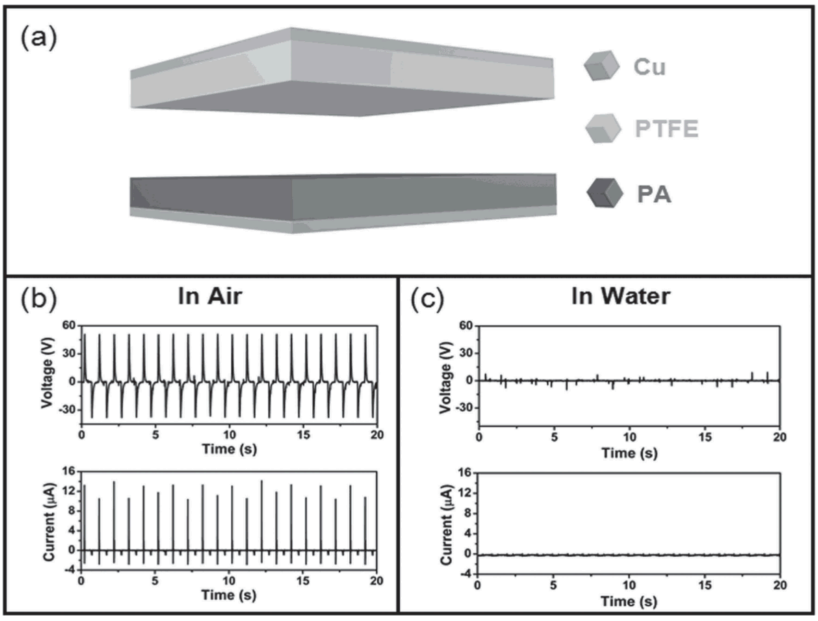

Figure 23. Performance of Nanogenerator in Presence of Air and in Water. a) Schematic diagram of the fabricated conventional TENG without packaging using two insulator materials. b) Measured output voltage and current of TENG in air. c) Measured output voltage and current of TENG in water.[124]

Thus, the TENG could provide a new strategy for wave energy conversion and have huge potential toward large-scale blue energy harvesting from the ocean. Also, previously TENG has been showed to have the lowest levelized cost of electricity (LCOE) compared to all energy harvester.[125] Thus, if one could use TENG to harvest ocean wave energy has direct commercial value due to its low cost in producing electricity. However, the main challenges for TENG for wave-energy harvesting is the effectively packaging of the structure, and also eliminating a water electrostatic shielding effect, which I have discovered in one of the works, which I would explain below. For effectively packaging a structure to harvest energy from harsh environment, Yang et al first fabricated a conventional TENG, which consists a Cu film as a top electrode, a PTFE film, a PA film and a Cu film as the bottom electrode, as shown in Figure 23, and showed that in air, the voltage (V_{oc}) and short-circuit current were about 50 V and 14 μA, respectively.[124] However, once

the same TENG was placed in water, there was no observed output voltage or current signal as if water have infiltrated the TENG. This work then further showed that the device needs to be fully packaged, for it to work in harsh environments, such as for harvesting energy from water waves. The authors have further stated that the humidity from water have a direct effect on TENG's performance, as water molecules is able to take away triboelectric charges. Investigating the effect of causing low output voltage signal would be the priority of the next section, in which I would discuss about a rationally designed sea snake TENG for effectively harvesting ocean wave energy and harvesting the ocean wave energy with a minimized water screening effect.[126]

3.1.1 Rationally Designed Sea Snake TENG For Effectively Harvesting Ocean Wave Energy with Minimized Water Screening Effect

3.1.1.1 Harvesting Ocean Wave Energy with Miniaturized Electrostatic Screening Effect

Even though humidity has a direct negative effect on the TENG, it was not the only effect that have a negative effect on the TENG's performance. Another effect that I've explored was the electrostatic shielding of TENG, which could drastically reduce the output voltage of the TENG when harvesting in ocean environment. In this work, a sliding-mode freestanding TENG in a fully packaged structure was designed to explore the effect of electrostatic shielding in a TENG device in a simulated ocean environment.[126] To explain the electrostatic shielding effect of the TENG, one has to look into the theory of the triboelectric nanogenerator. By looking into the theory of TENG proposed by Niu et al,[9] the TENG acts as a capacitive device explained by Equation 5 below,

$$V_{OC} = \frac{Q_{tribo}}{C_0} \tag{5}$$

in which V_{OC} is the output open-circuit voltage of the TENG, Q_{tribo} is the charge on the dielectric layer, and C_0 is the capacitance between the two electrodes, which is assumed constant for sliding-mode freestanding TENG with a dielectric as a mover. The capacitance between the two electrodes is dependent and proportional on the dielectric constant of surrounding medium. Since water has a much higher dielectric constant (~70) compared to air (~1), when a sliding mode freestanding TENG device is placed and tested in water environment, C_0 would greatly increase, and since Q_{tribo} is the same, the open-circuit voltage would greatly decrease, leading to a much less energy harvested, and a lower efficiency.[126] To first verify the effect, COMSOL Simulation were done at two conditions, one with the TENG device have an airgap and another with the TENG device having no airgap, and the only separation between the TENG device and water is acrylic. The COMSOL Simulation, shown in Figure 24, showed that with an airgap, the voltage remained high, at 300 V peak to peak, whereas without an airgap, the voltage was low, at 60 V peak to peak, verifying the effect of electrostatic shielding of TENG from the water. Furthermore, by utilizing COMSOL simulation, the effect of air gap in three different structures with different length of electrode L and gap between the electrode d placed in a water environment was investigated, and it is found that increasing the length of electrode exhibits a larger reduction in output voltage, and also increasing the gap between electrode also exhibits a larger reduction in output voltage, as shown in Figure 25.

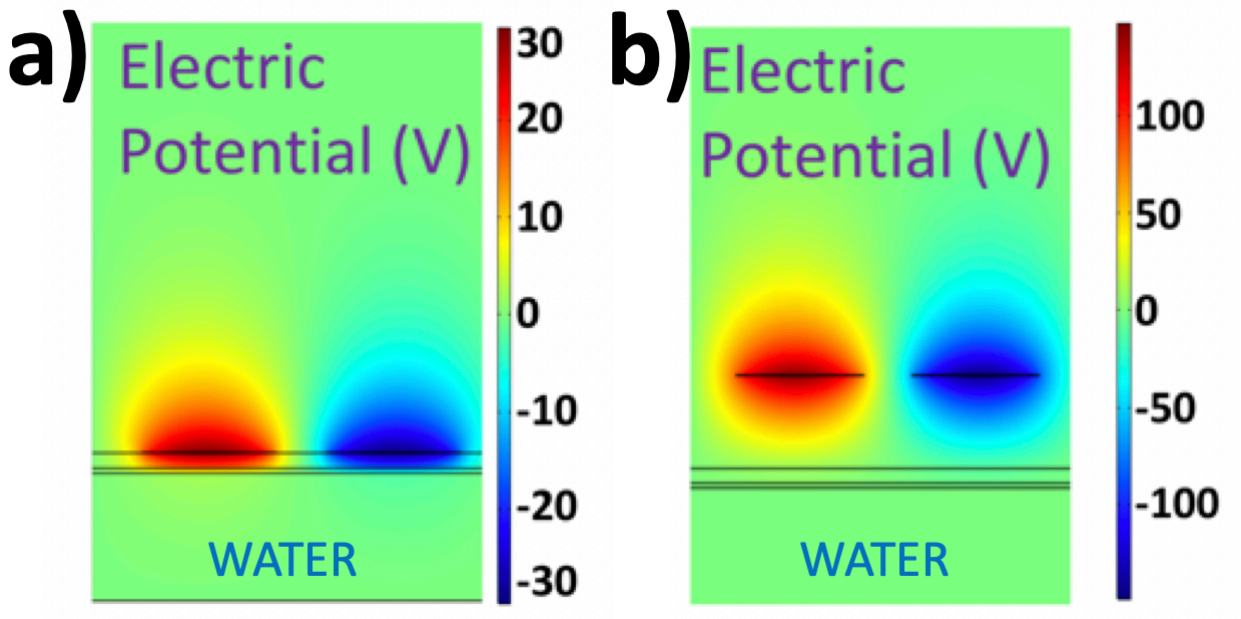

Figure 24. Finite Element Simulation showing the Effect of Air Gap on the Device's Output Voltage. a) Finite element simulation with electrodes having no air gap above water. b) Finite element simulation with electrodes having 2.0 cm. air gap above water.[126]

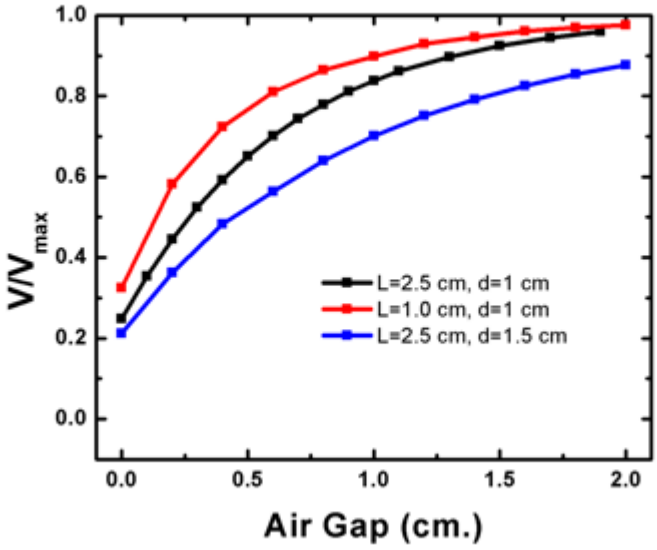

Figure 25. Finite Element Simulation showing the Effect of Length of Electrode L and Gap between Electrode d on the Device's Output Voltage.[126]

Not only simulation was performed, experiments were performed to further verify this effect. For the setup of the experiment, a freestanding mode TENG shown in Figure 26 is tested. This TENG has an air gap distance h from the bottom acrylic to the acrylic holding the TENG

structure. The structure is fully packaged, so no water could enter the interior acrylic structure, where the PTFE Balls and copper electrode are located. The mechanism showing how this TENG work is shown in Figure 27, and it is based on a freestanding mode TENG. Under an external triggering, such as a water wave move across the acrylic structure, the acrylic box would bend due to the curvature of the incoming water wave. In turn, the inner acrylic box consisting the TENG would be inclined, causing the balls to roll down the nylon film. After the first contact between the PTFE balls and the film, the PTFE balls would become negatively charged due to contact electrification with the thin film. While the balls are sliding down, they would induce positive charges on the bottom left electrode, shown in Figure 27d, which would produce a current to flow onto the upper electrode. Furthermore, after the water wave move past the acrylic structure, the structure would be inclined in the other direction. This would allow the PTFE balls to roll down in the other direction, which would produce electricity in the bottom right electrode, producing a net current in the opposite direction. Overall, this design is a freestanding rolling mode triboelectric nanogenerator, as the balls act as a dielectric layer above the electrodes, and due to the movement of the balls, there exist a charge transfer between the electrode.

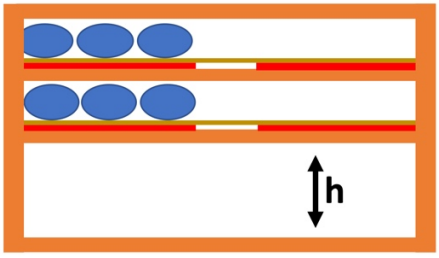

Figure 26. Structure of Freestanding Mode TENG with Air Gap[126]

The device shown in Figure 26 was placed in a plastic container that is filled with 2 cm tall of tap water. The container was then placed on a rotational shaker with operational frequency of 0.5 Hz , allowing it and the device to rotate back and forth, being inclined at different angles. The

rotational shaker was placed at the maximum amplitude setting. A systematic study was done with the air gap height of the structure changed from 0 cm. to 1.5 cm. by adding spacers in between the bottom acrylic and the acrylic holding the freestanding mode TENG, and the output open-circuit voltage and transferred charge are measured. Figure 28a shows that when the device is operating in water, the output voltage decreases to only 20 V if no air gap is present, as shown on bottom inset of Figure 28a. With an increasing air gap, the output voltage increases as well. Once an air gap is added onto the structure with a height of 1.5 cm, the voltage of the air gap structure remains the same as the device when operating in ambient air conditions, which has the peak to peak value of 250 V, as shown in top inset of Figure 28a. Also, it is important to note that in Figure 28b, the short-circuit output charge is the same and independent with regards to the air gap. The results matched identically with the simulated results.

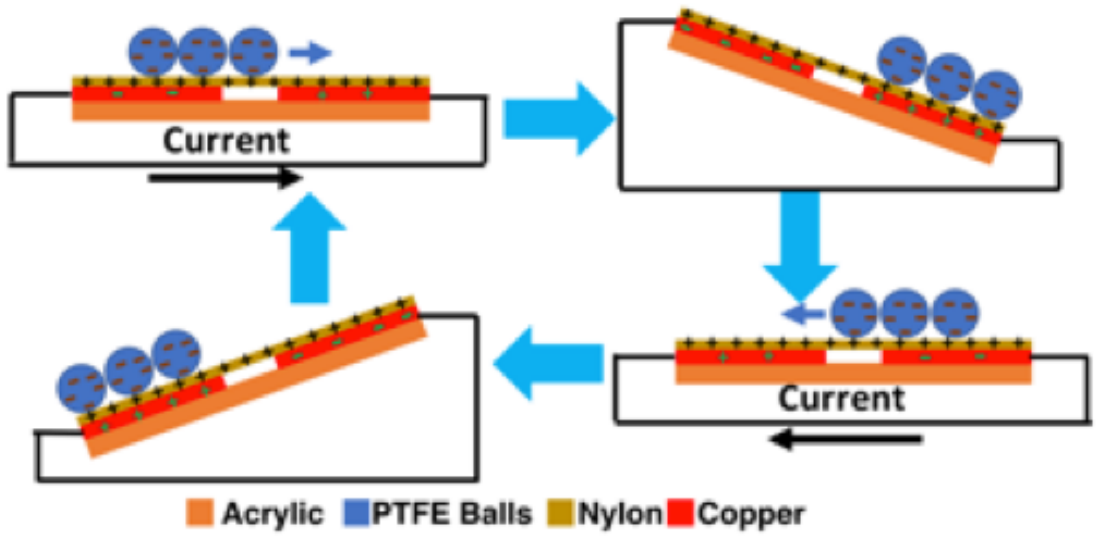

Figure 27. Working Mechanism of Freestanding Mode TENG[126]

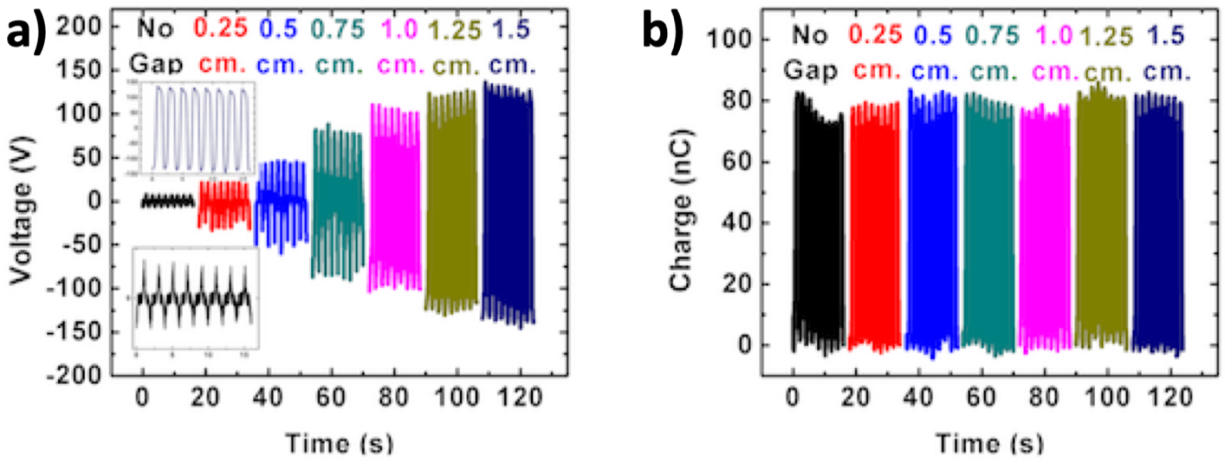

Figure 28. Effect of Air Gap on Open-Circuit Voltage and Transferred Charge. a) Effect of Air Gap on Open-Circuit Voltage. b) Effect of Air Gap on Transferred Charge.[126]

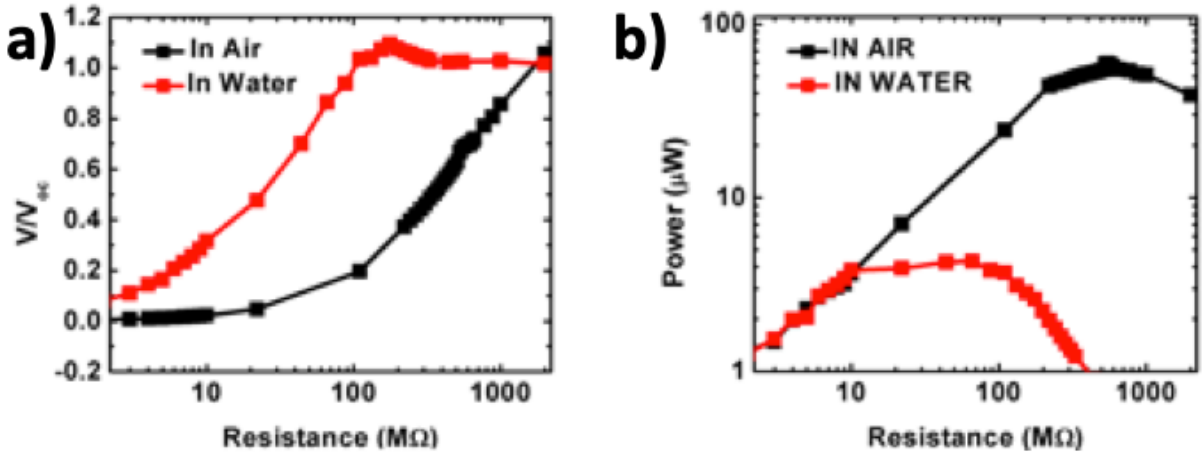

Figure 29. Comparison of Resistance Curves in Water and in Air. a) Comparison of actual voltage/Voc with different resistance with TENG with no air gap in air and in water. b) Comparison of output power with different resistance with TENG with no air gap in air and in water.[126]

To also demonstrate the effect, since the internal capacitance increase due to the presence of water without an air gap, there would be a large decrease in the impedance of the nanogenerator. This is because of Equation 6 below, as the impedance of the nanogenerator, Z, is inversely proportional to the internal capacitance of the TENG when operating at the same frequency.

$$Z = \frac{1}{2\pi f C_0} \tag{6}$$

To evaluate the impedance of the nanogenerator, the voltage across the resistor was measured. The voltage across very small resistance would be low, and it would increase once the resistance is high, as shown in Figure 29a. The relative voltage is displayed here, as the calculated voltage divided by open-circuit voltage, due to the large difference in output potential when the device is placed in water. Furthermore, the power is measured by Equation 7 below, and the power would increase at low resistance due to the increase of the voltage across the resistor, and at higher resistance, the power would decrease with respect to resistance, due to the voltage would be constant.

$$P_L = \frac{{V_L}^2}{R} \tag{7}$$

According to the maximum power transfer theorem,[127] the impedance of the nanogenerator could be evaluated at the resistance when the power is the maximum, as the maximum power is transferred when the load resistance matches the generator impedance. Thus, from Figure 29b, with an air gap, the impedance of nanogenerator is calculated to be 660 MOhms, whereas without an air gap, the impedance of the nanogenerator is only 60 MOhms. This proves the fact that without an air gap structure, there would be a low voltage due to the increase of capacitance from the water screening effect, as seen in Equation 6, as the internal resistance had decreased by 11 times, showing that the capacitance would have increase by 11 times. This demonstrates the order of increase in the triboelectric nanogenerator's capacitance due to the dielectric shielding effect from the water. Also, there is a significantly lower output power when the device is in water if no air gap present, as the power decreased from 90 μW to 6μW.

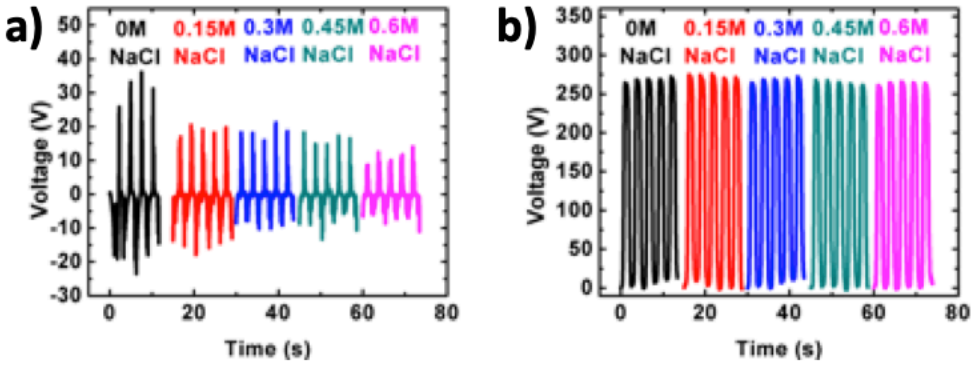

Figure 30. Comparison on Effect of Salinity on Structure Without and With an Air Gap. a) Effect of Salinity with an Air Gap. b) Effect of Salinity without an Air Gap.[126]

Also, since the device needs to be operated in ocean environment, the effect of salinity, concentration of salt in water, on the electrical output is also observed with a device that has an air gap of 1.5 cm. and a device without an airgap. The electrical performance of the device with an air gap showed the same output voltage (260 V) when the device is placed in saltwater at different concentration from 0 M to 0.6 M, as shown in Figure 30b. The latter concentration is used, because it is the concentration of salt in the ocean. However, with the air gap, the device degraded when adding more salt in the water, as the output in only water is around 40 V, and at 0.6 M, the device output voltage decreased to only 15 V, as shown in Figure 30a, showing the device with an air gap is useful in scavenging energy from the ocean wave, while the device without an air gap's performance would decrease with increasing salt concentrations, due to the increase of dielectric constant in salt water compared to deionized water.

Thus, in summary of this work, the electrostatic screening effect was explored in detail in both simulation and experimentally, and it is considered a negative effect for harvesting ocean energy. It occurs when a freestanding mode TENG lies too close to water, and since water has a high dielectric constant, the output voltage of the freestanding mode TENG would be considered low. Thus, too address this issue, air gap of 1.5 cm was added, and the output voltage is high, as if

it is operating in ambient air conditions. The capacitive model by looking at impedance was also explored, and it further verifies this effect of electrostatic screening.

3.1.1.2 Increasing Output Power of Air Gap Structure with Springs and Application of Sea Snake TENG

Even though this work first demonstrates the effect of electrostatic screening when harvesting from ocean waves, it is considered a negative effect, as with an air gap structure, a larger volume is needed, which would decrease the volumetric power density harvested of the device. Thus, it is necessary to use the space of the air gap to increase the performance of the device. The platform placed on ocean will incline at an angle θ due to the curvature of the wave. For the TENG box directly placed on the platform, the inclination angle of the TENG element is φ. For the TENG box being fixed on the platform with the spring, the inclination angle of the TENG box as φ resulted from the ocean wave was denoted. An evaluation of the inclination angle of the platform θ is compared to the inclination angle of the TENG element φ is shown in Figure 31a. Also, a stainless-steel mass weighing 0.4 kg. was further added on top of the acrylic box structure. containing the PTFE balls and electrode to increase the rotational angle of the device, as well as lowering the resonant frequency. For the TENG box connected with the spring, its inclination angle can be evaluated with the spring-mass system, as shown in Figure 31a**.** Under the harmonic excitation of the ocean wave with $\theta=\theta_0 \sin \omega t$, the inclination angle of the TENG of the box can be written as $\varphi=\varphi_0 \sin \omega t$. The θ_0 and φ_0 are the maximum amplitude of the inclination angle. With the energy conservation equation, the equation of motion of TENG could be easily derived, as shown in Equation 8

$$ml^2\ddot{\varphi} - mglsin\,\varphi + k(\varphi - \theta)\left(1 - \frac{\dot{\theta}}{\dot{\varphi}}\right) = 0 \quad (8)$$

where g is the gravitational acceleration, and the over dot denotes the time differentiation. According to the real experiment, the inclination angle φ is not too large. Thus, by simplifying the Equation 8, the following nonlinear relationship below, as shown in Equation 9, is obtained,

$$\frac{\varphi_0}{\theta_0} = \frac{1}{1-\frac{\omega}{\omega_n} l\sqrt{(1+\frac{g}{l})}} \tag{9}$$

where $\omega_n = k/m$ is the natural frequency of the spring-mass system. It can be seen that the amplitude of the inclination angle mainly depends on the TENG's mass, the spring's stiffness and length. Thus, by using Equation 9, Figure 31b was derived using m=1.8 kg., l=1.25 cm, and k=0.8 N/m at different oscillating frequencies, and it shows that the φ_0 is greater than θ_0 , showing the increase in inclination angle with the addition of the added tampered spring.

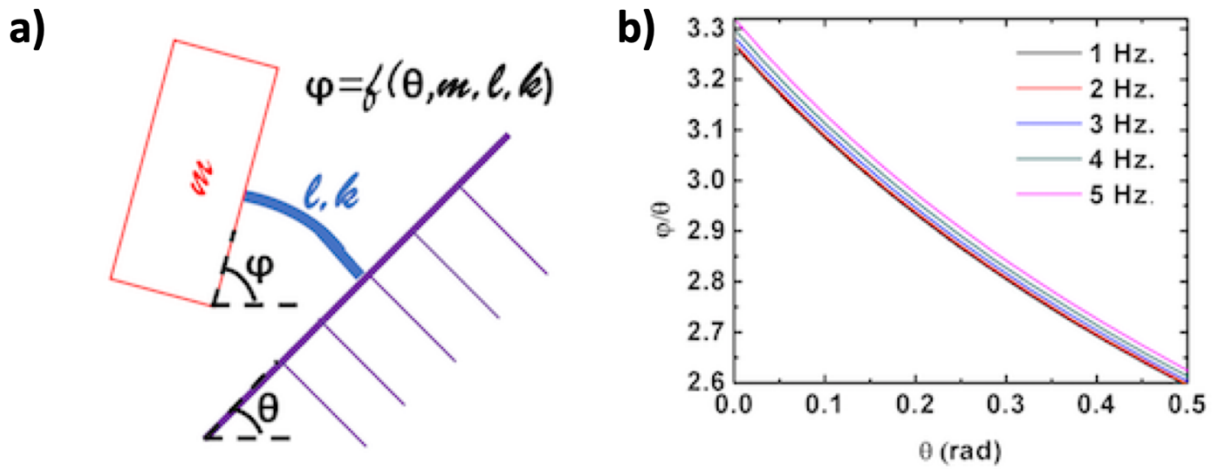

Figure 31. Physical model of TENG with Attached Spring and ANSYS Simulation. a) Physical model of TENG with spring and ANSYS simulation showing ϕ dependence on θ. b) The simulated result of rotational angle of device with spring to original rotational angle.[126]

Figure 32a shows the experimental data of the performance of the TENG with and without a tampered spring under the actuation of the rotational shaker. With the tampered spring, the performance was enhanced by 350% at a rotation angle of 2 degrees This is due to, without the tampered spring, the balls could not slide down the slope all the way, at a low inclination angle of the TENG element, and with the tampered spring, the entire structure is able to be inclined at a

high inclination angle and the balls are able to easily roll down and is able to have a higher maximum velocity. Also, it is important to know that without the spring, the device's output voltage would always be increasing as the inclination angle of the entire device increases from 2 degrees to 45 degrees by increasing the maximum rotational angle of the shaker. This is because the balls are able to slide down easily at higher inclination angle. For the device with the spring, the device's output voltage is nearly constant for inclination angle of the entire device above an inclination angle of 20 degrees, whereas for the device output without the tampered spring, the performance decreases always with decreasing rotational angle, as shown in Figure 38c. This means that below 20 degrees, the inclination angle of the TENG element is still increasing due to the restoring force on the tampered spring, and above 20 degrees, the inclination angle of the balls stops increasing, and the balls reached its maximum terminal velocity. Overall, this shows that the use of the tampered spring exhibit much better performance than without a spring, especially at lower inclination angle.

Figure 32b shows the output charge on the device when the ball is moving at the maximum inclination angle of the segment at 45^0. The output voltage increased by nearly 150%, from 75 V to 112 V. Figure 32c shows the output power of the device with the spring and comparing the output power of the device without the spring at the maximum inclination angle of 45^0, and the output power is able to increase from 100 μW to 600 μW. This is because both charge and voltage increased with the addition of the tampered spring, which contributing to a higher power. Also, the power with the spring is at a lower resistance, thus increasing the power, as $P=V^2/R$. Also, the maximum power occurs at a lower resistance; this means that the instantaneous frequency of the balls moving down would increase, which is expected, as the balls were able to move down at a higher speed due to the larger inclination angle ϕ with the tampered spring. Also, the effect of

charging a 100 μF capacitor was studied, and with the spring, the capacitor was able to charge to a maximum of 3.5 V in 5 minutes, while without the spring, it can charge up to only 2.5 V in 5 minutes as shown in Figure 32d.

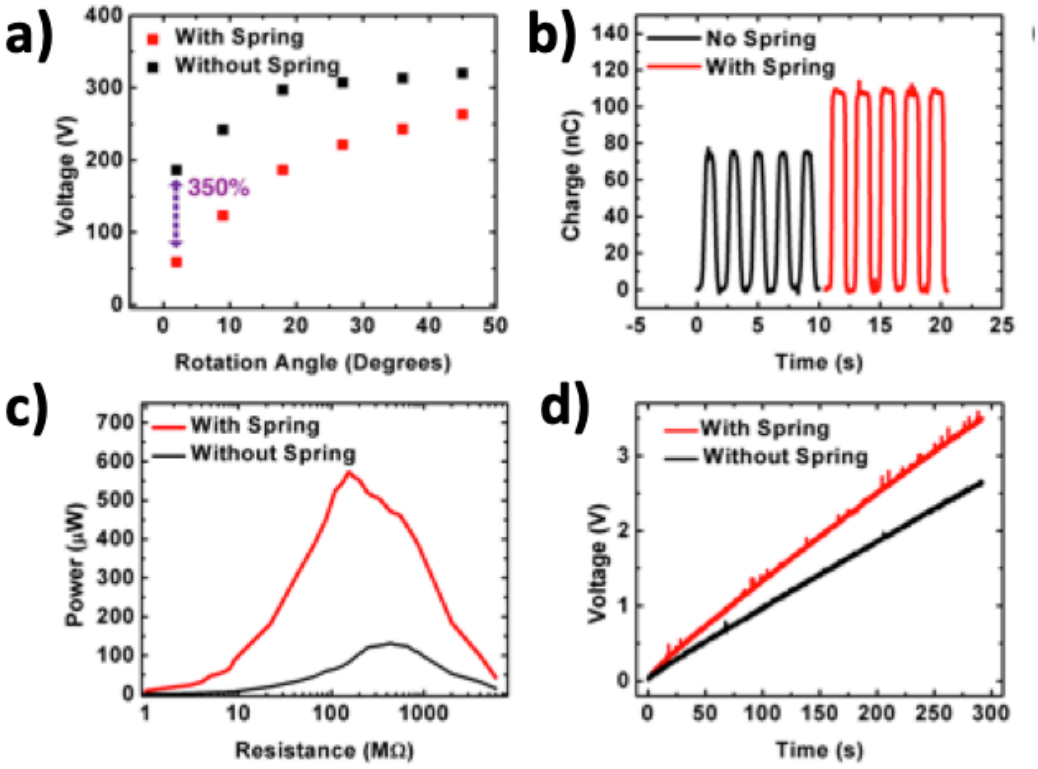

Figure 32. Comparison of TENG With and Without Spring. a) Comparison of TENG with spring and TENG without spring on voltage vs rotational angle. b) Charge vs time of TENG with spring and without spring at rotational speed of 30 rpm. c) Comparison of output power with different resistance with TENG with TENG with Spring and without spring. d) Charging a 100 μF with TENG with spring and without spring on shaker with rotational speed of 30 rpm.[126]

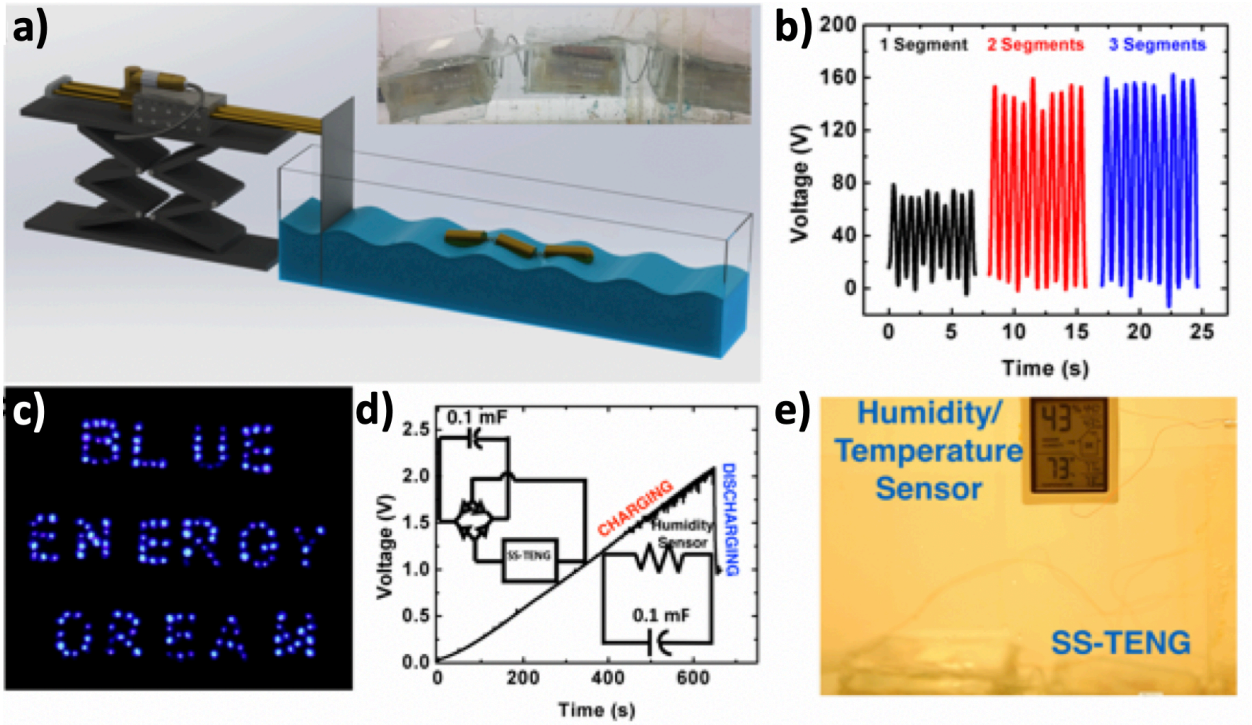

Figure 33. Applications of the SS-TENG. a) The placement of the SS-TENG in the water environment with a linear motor actuating the water waves. b) The Voltage vs time of one segment with respect to different number of segments of the SS-TENG with attached tampered spring. c) Lighting up 152 LEDs in the words "**Blue Energy Dream**" with SS-TENG with attached tampered spring. d) The charging profile of a 100 μF capacitor by the SS-TENG in water. e) The application of driving and powering the humidity sensor with SS-TENG with attached tampered spring.[126]

To show some practical use of the nanogenerator, three segments of sea snake TENG with the attached tampered spring was then placed in a homemade water tank made with acrylic glass. The Sea Snake TENG (SS-TENG) with the attached tampered spring was used due to its superior performance. The tank was filled with three segments in of tap water. On one end of the tank is an acrylic plate, shown in Figure 33a, that is attached to a linear motor. The linear motor is able to be moved in a periodic motion with displacement of 8cm and acceleration of 2 m/s^2 to produce periodic water waves. The Sea Snake TENG device, which is show in the inset of Figure 33a, in response to the periodic water waves would move up and down. It is important to study the effect of number of segments on the output voltage of the device, because the added springs are able to add a balance force, which greatly increase the inclination angle of the segment and the horizontal

motion of the device, creating a coupled structure. This is shown in Figure 33b, as with taken from the output of one segment of the TENG, the output voltage is only 55 V, whereas with 2 and 3 segments connected, the output voltage is greatly enhanced to 160 V, and this is due to the spring force by adding the springs. The maximum angle of the large box under the horizontal motion of water waves is around 10 degrees, and the output voltage could be expected to be lower under shaker actuation, in which the applied angle is 45 degrees. Also, due to the periodic motion, the balls would be able to slide back and forth, producing a high voltage. The voltage was able to light 152 LED lights connected in series, which showed the phrase “Blue Energy Dream” as shown in Figure 33c, and this was done without the use of a capacitor to help with the energy accumulation.

Also, the effect of charging the capacitor is explored, and one device is able to charge a 100 μF capacitor in to 2 V in 10 minutes, which took longer time than in Figure 32d, due to the decrease in the inclination angle, as the box is only able to incline by 10 degrees and the less impact of the wave on the device. The diagram for the circuit to charge the capacitor is show on the top left of Figure 33d, in which there was a rectifier to only allow current to flow in one direction connected to the SS-TENG, and then it was connected to the capacitor. Then, to power the humidity sensor, 2 V was required, and the capacitor was able to successfully power the temperature and humidity sensor, which is shown in Figure 33e.

In summary of this work, a nanogenerator based of Pelamis wave energy converter was designed, using balls that are able to move with the structure of the sea snake. The device was utilized to verify the electrostatic shielding of TENG in water, in which when a triboelectric nanogenerator is placed next to water, there would be a large decrease in the electric potential of the device. Thus, to address the problem, the device needs to have an air gap, and with the air gap, the nanogenerator was able to operate in high salinity environment, such as simulated ocean

conditions. This work further demonstrates how one to design freestanding mode triboelectric nanogenerators for harvesting ocean waves. Due to the air gap have a negative effect on the output power density, tampered springs have been added to fill the air gap to increase the operating angle of the device, and the device could rotate under low actuation angles, up to 2 degrees. The nanogenerator was then placed in water, and it was able to light up 152 LED lights in water, with the air gap structure, allowing the high output voltage in simulated ocean conditions. The next section would explain how I could further enhance the output performance of the sea snake triboelectric nanogenerator by utilizing multiple layers.

3.1.2 High-Power Tower-Based Nanogenerator with Low Intrinsic Impedance for Harvesting Arbitrary Direction Water Wave Energy

One important aspect of energy harvesting is how could one improve the power density that is harvested from the device. For TENG, one necessary goal is to lower the output impedance of the nanogenerator, as most current electronic device's impedance is low, and the nanogenerator's impedance must match the electronic device's impedance for maximum power transfer, based on the Maximum Power Transfer Theorem.[127] In this work, a tower-like triboelectric nanogenerator (T-TENG) is designed and systematically investigated, and it is an extension to the previous sea snake nanogenerator work, in which I wanted to show that with more layers, there would be a lower impedance and a higher output power.[128]

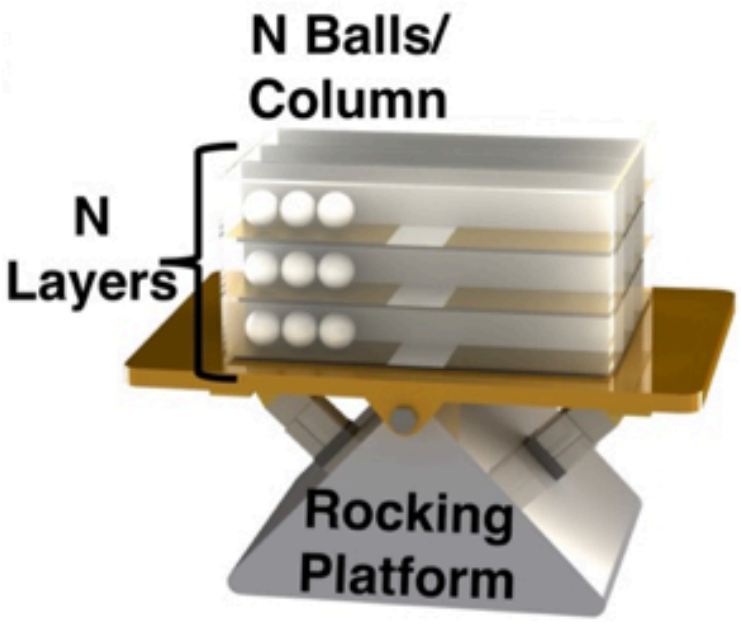

Figure 34. Schematic of Single Section of SS-TENG on Rocking Platform.[126]

First, before looking into the structure of this T-TENG, I wanted to provide some more background of this project, and this work is based on a data from previous work that is surprising.[126] The freestanding mode triboelectric nanogenerator (single section of SS-TENG) from the previous section in was tested in ambient conditions with a rocking platform, as shown in Figure 34, moving the SS-TENG at a frequency of 0.5 Hz for a simulation of open wave movement condition. This single section of SS-TENG currently has N number of layers, and the number of layers effect on the TENG was measured. Each layer refers to the effect of the previous layers included, as they are measured in parallel. The open circuit voltage, short-circuit current, and short-circuit charge were measured with different layers connected in parallel. All three signals increased with increasing the number of layers, shown in Figure 35.

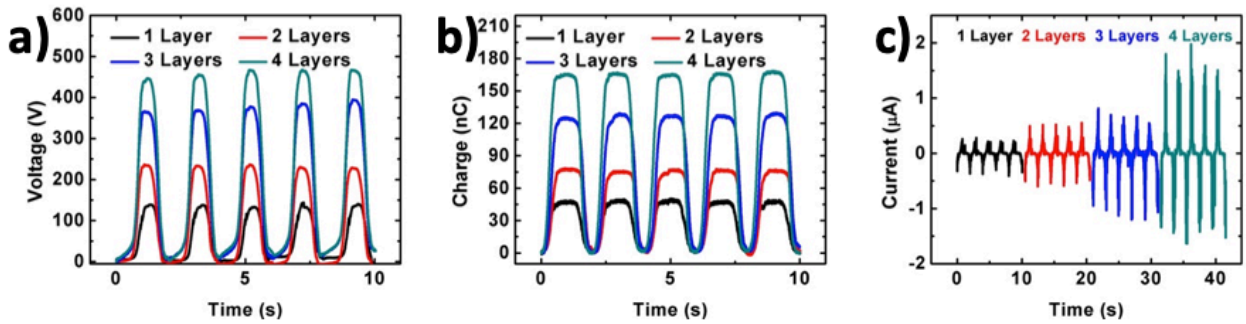

Figure 35. Effect of Layers on Sea Snake Nanogenerator Output Performance a) Open-circuit voltage vs time with dependence on different layers connected in parallel. b) Transferred charge vs time with dependence on different layers connected in parallel. c) short-circuit current vs time with dependence on different layers connected in parallel.[126]

For voltage to increase with number of layers connected in parallel is contradictory, as one is usually taught that if you have components in parallel, the voltage should actually decrease with more components or roughly the same in parallel, as connecting comments in parallel would not cause an increase in voltage. Thus, by looking into the previous circuit model of TENG, as shown in Figure 1c of Section 1.3, a new circuit model to fit the design of two TENGs connected in parallel in an attempt to explain this finding was established. The elements of the multimeter, which has a capacitor that could be assumed with capacitance of 0.3 nC., was included. This was based on a previous work, which showed when measuring the open-circuit voltage, the capacitance of the meter is 0.3 nC.[57] This circuit model is shown below in Figure 36. It is important to note that C_1 and C_2 are not position variant capacitances, because in a freestanding mode case, with the mover as a dielectric, it is assumed that capacitance are independent of mover's position.[9] Thus, from this circuit model, the open-circuit voltage of just 1 layer could be calculated by Equation 8. Furthermore, with the open circuit voltage of two layers could be found by Equation 9, based on the assumption that C_1 and C_2 are the same and $Qsc,_1$ and $Qsc,_2$ are the same, due to the two layers are similarly constructed.

$$V_{1-layer,OC} = \frac{Q_{sc,1}}{C_1+C_v} \tag{8}$$

$$V_{1+2,OC} = \frac{Q_{sc,,1}+Q_{sc,,2}}{C_1+C_{2+}C_v} = \frac{2Q_{sc,1}}{2C_1+C_v} \quad (9)$$

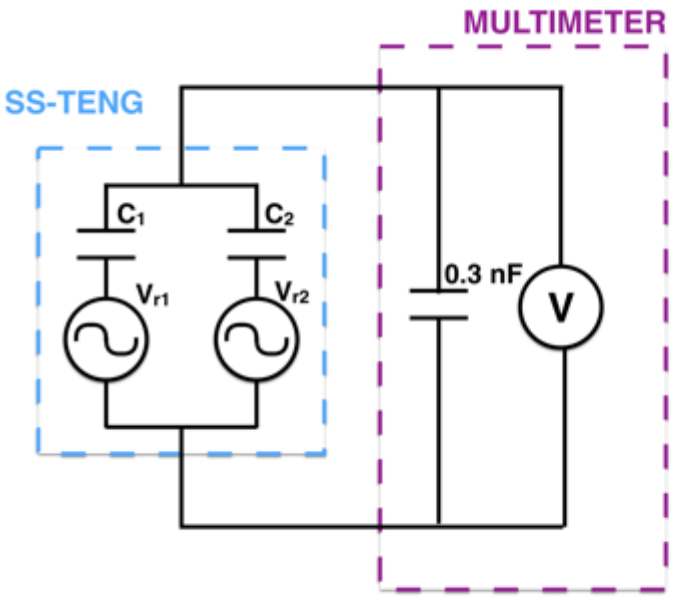

Figure 36. Circuit Diagram of SS-TENG with Two Layers Connected in Parallel.[126]

The case that voltage of two layers would hold always greater than the voltage of 1 layer would hold true for any values of $Q_{sc,1}$ and C_1, proving the fact that the measured open-circuit voltage would increase with multiple layers in parallel. With this, questions were asked of whether the current could also increase with the number of layers, and if the current increase, then we could show there would be an increase in the power density, which would be the aim of this new work.

Thus, a T-TENG consists of multiple units in one block, and each unit is made of polytetrafluoroethylene (PTFE) balls and a three-dimensional (3D) printed arc surface coated with melt adhesive reticulation nylon film, as shown in Figure 37a and Figure 37b.[128] The power generation model coupled with the kinetic model for the T-TENG is proposed. The T-TENG can

be fully packed in one block to harvest arbitrary directional wave energy and solve the effect of humidity and dielectric screening at the same time.

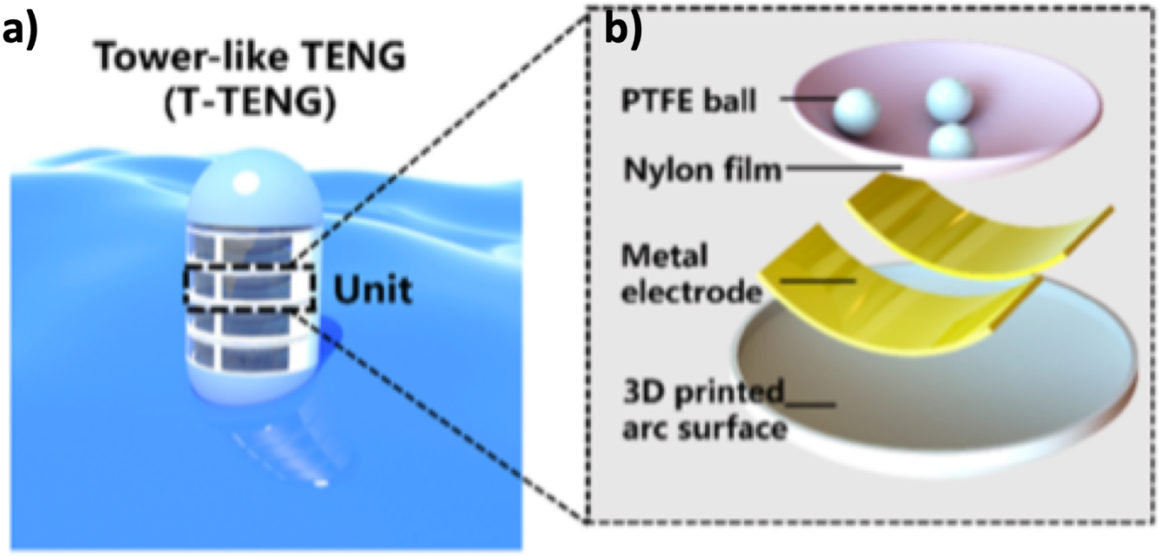

Figure 37. Structural Design of the T-TENG. a) Schematic diagram of the designed T-TENG consisting of multiple units. b) The internal structure of one unit and the nylon film coated on the 3D printed arc surface.[128]

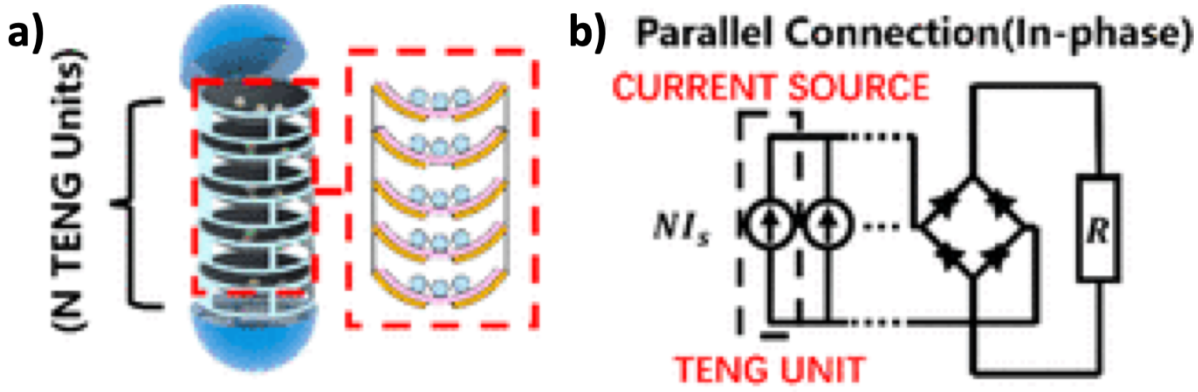

Figure 38. Diagram and Corresponding Equivalent Circuit Diagram of T-TENG.[128]

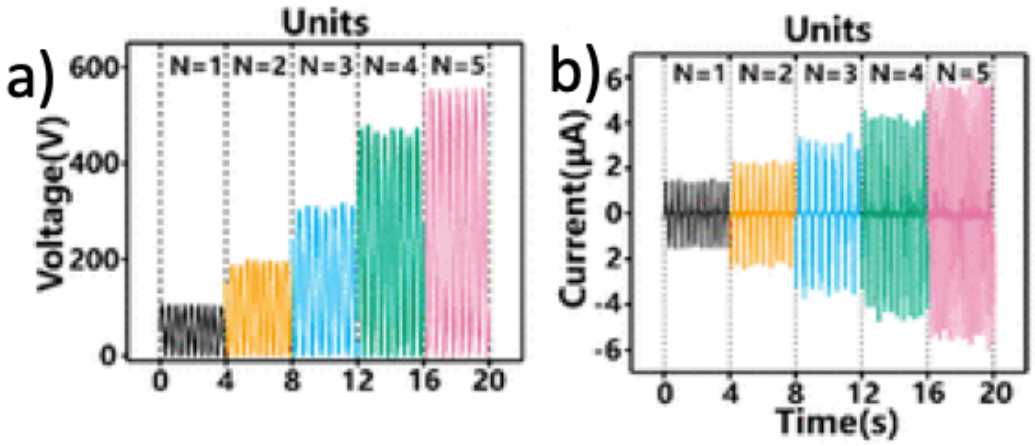

Figure 39. Electrical Performance of T-TENG with Number of Layers in Parallel[128]

To harvest wave energy more effectively, a T-TENG consisting of multiple units connecting in parallel in one tubular block is designed, as shown in one tubular block is designed, as shown in Figure 38a. Due to all PTFE balls moving in the same phase, it is unnecessary to utilize rectifiers for connecting units. The T-TENG could be treated as a current source with a TENG's capacitance in parallel and power marine sensors with just one rectifier. This is based on applying Norton's theorem on the circuit shown in Figure 1d. The equivalent simplified circuit of the T-TENG without taking regard to the TENG's capacitance is shown in Figure 38b. Also, the circuit with taking regard to the TENG's capacitance is shown in Figure 40a From the equivalent circuit, the current ($I_{T\text{-}TENG}$) of T-TENG with N multiple units in parallel can be regarded as N times relative to the current of one unit (I_1), which is shown in Equation 10 below.

$$I_{T-TENG} = \sum_{i=1}^{N} I_i = NI_1 \tag{10}$$

Thus, the voltage ($V_{T\text{-}TENG}$) across the resistance (R) of the T- TENG is also found to be N times relative to the voltage (V_1) of one unit, as shown in Equation 11 below

$$V_{T-TENG} = I_{T-TENG}R = NI_1R \tag{11}$$

To verify this, experiments were performed. To simulate ocean like conditions, the T-TENG was placed on the linear motor with a swaying motion of a frequency of 2 Hz. The voltage across the resistance, short-circuit current were measured with different number of units connected in parallel. Both increased with increasing the number of units, as shown in Figure 39a and Figure 39b. It is worthwhile to note from the result shown in Figure 35a from sea snake based nanogenerator, only Voc previously increased with the numbers of layers; now, it is clear that also voltage across a resistor and short-circuit current also increased with the number of layers. Furthermore, the power density could be obtained by Equation 12 below,

$$P_{T-TENG} = \frac{I_{T-TENG}V_{T-TENG}}{NA_1} = \frac{N^2{I_1}^2R}{NA_1} = NP_1 \quad (12)$$

where A_1 is the area of the device, and P_1 is the power density of one TENG unit. From Equation 12, it demonstrates that the power density is proportional to the number of units in parallel. Thus, if there are more units in parallel, the larger power density could be harvested, which shows it could be a more effective energy harvester.

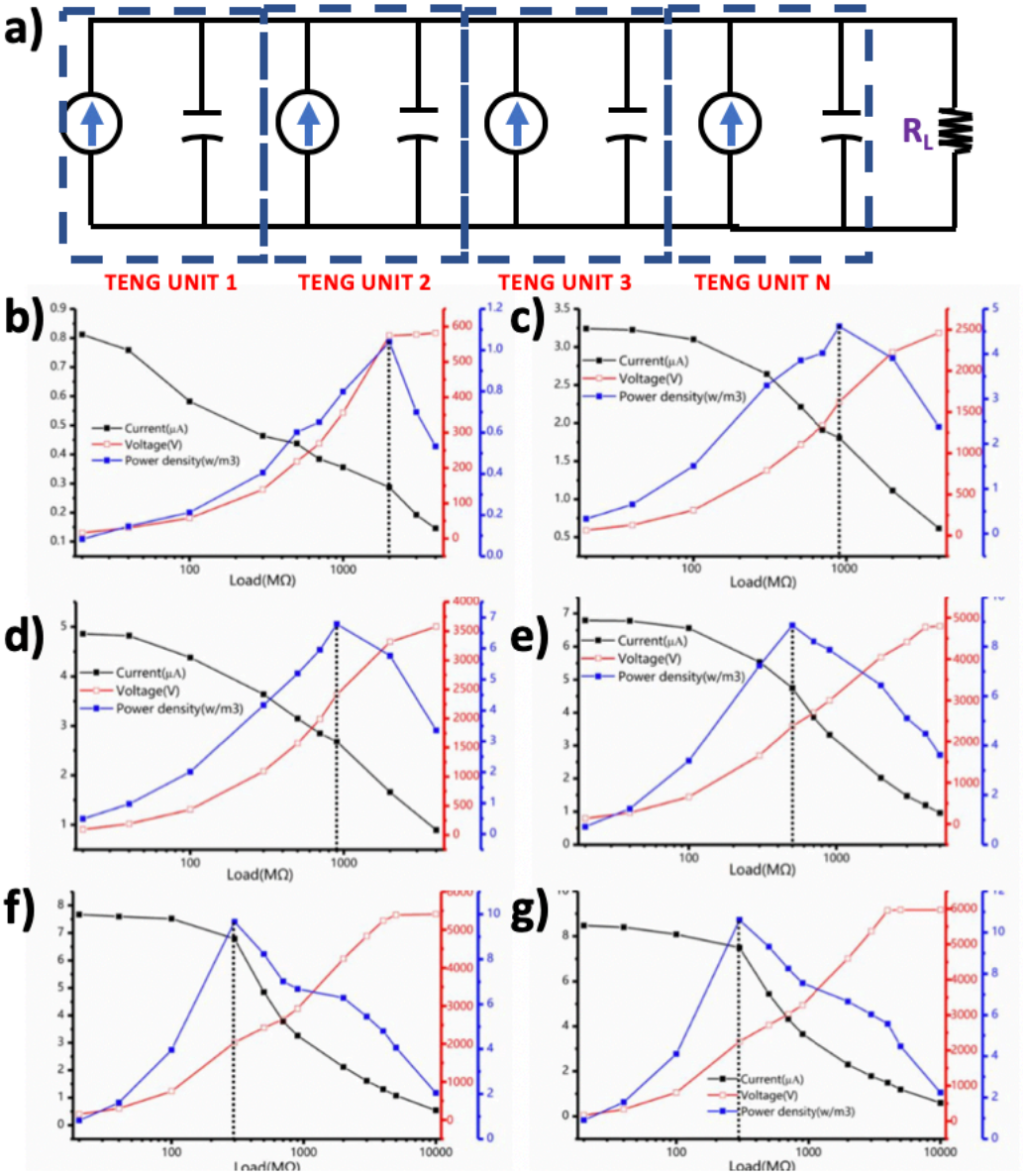

Figure 40. Circuit Model to Evaluate N TENGs in Parallel, and Schematics Showing N TENGs in Parallel Decrease Load Impedance. a) Circuit Model with N TENGs in parallel. Dependence of the output voltage and current, and power density for T- TENG with (b) 1 units, (c) 4 units, (d) 6 units, (e) 8 units, (f) 9 units, and (g) 10 units on the resistance of the load.[128]

Also, with more triboelectric nanogenerator in parallel, the internal impedance of the nanogenerator would decrease, which is beneficial for the nanogenerator to power low impedance electronic device. This is due to each nanogenerator is a capacitive device, in which the TENG is modeled as a current source with capacitor in parallel, as seen in Figure 7a. From the equivalent

circuit, the capacitance ($C_{T\text{-}TENG}$) of T-TENG with N multiple units in parallel can be regarded as a single capacitor with N times relative to the capacitance of one unit (C_1), which is shown in Equation 13 below.

$$C_{T-TENG} = \sum_{i=1}^{N} C_i = NC_1 \tag{13}$$

Since the impedance of the nanogenerator ($Z_{T\text{-}TENG}$) is inversely proportional to the capacitance, the impedance would decrease with more layers connected in parallel, as shown in Equation 14, where f is the operational frequency of the device.

$$|Z_{T-TENG}| = \frac{1}{2\pi f C_{T-TENG}} = \frac{1}{2\pi f N C_1} \tag{14}$$

The power density reaches maximum value when the external resistance equals the internal impedance. From Fig 40b-g, the internal impedance of the TENG initially with 1 unit is shown to be at 200 MOhms, whereas for 10 units in parallel is shown to be 30 MOhms, representing a large decrease in impedance, verifying Equation 14. As well from Figure 40b-40g, it was found that the power density of the T-TENG also increases with the number of layers, in which at 1 layer the power density is at 1.1 W/m^3, whereas at 10 layers, the power density is at 11 W/m^3. This is consistent with the prediction of Equation 12, which shows the power density is proportional to the number of layers.

In this present work, a design of triboelectric nanogenerator based on a tower structure is proposed and investigated. The T-TENG can effectively convert arbitrary directional and low-frequency wave energy into electrical energy by utilizing charged PTFE balls rolling on an arc surface. As all PTFE balls in one block move in the same phase and the TENG unit is treated as current source, the power density of the T-TENG is proportional with the number of units (N)

connected in parallel. This shows that adding more layers significantly increase the power density of the nanogenerator device. Furthermore, by adding more layers, a decrease in the impedance of the energy harvester was observed, which is important for it to transfer power into commercial electronics, as most electronic devices have a low impedance. Therefore, this design of T-TENG provides an innovative and effective approach toward large-scale blue energy harvesting just by connecting more blocks to form T-TENG networks. In the next section, I would go back in discussing the electrostatic screening effect and relate it to how it affects solid materials instead of liquid.

3.2 Effect of Different Substrate Material on TENG's performance

Based on the conclusions drawn from Section 3.1.1.1 that the freestanding TENG's output decreased by electrostatic shielding effect from water, the electrostatic shielding effect from various materials are studied in detail. In this work, a simple design of freestanding mode TENG, which is shown in Figure 41a, was fabricated with PTFE and nylon as triboelectric layers. The substrate layer was then changed between a silica aerogel ($\varepsilon_r = 1.1$), acrylic ($\varepsilon_r = 3.4$), and alumina ($\varepsilon_r = 9.1$). All three of the material were purchased from McMaster-Carr and are cut into 2.5-inch (63.5 mm.) width x 1-inch (25.4 mm.) length. The materials all had the same height of 1/8 inch (3.175 mm.). The aerogel was cut by utilizing scissors; the acrylic was cut by utilizing a laser cutter; the alumina was cut by utilizing a waterjet. The mover was constructed with an acrylic with a width of 1.25-inch (31.75 mm) x 1-inch (25.44 mm.) length, and a foam layer and copper tape were taped onto the acrylic structure.

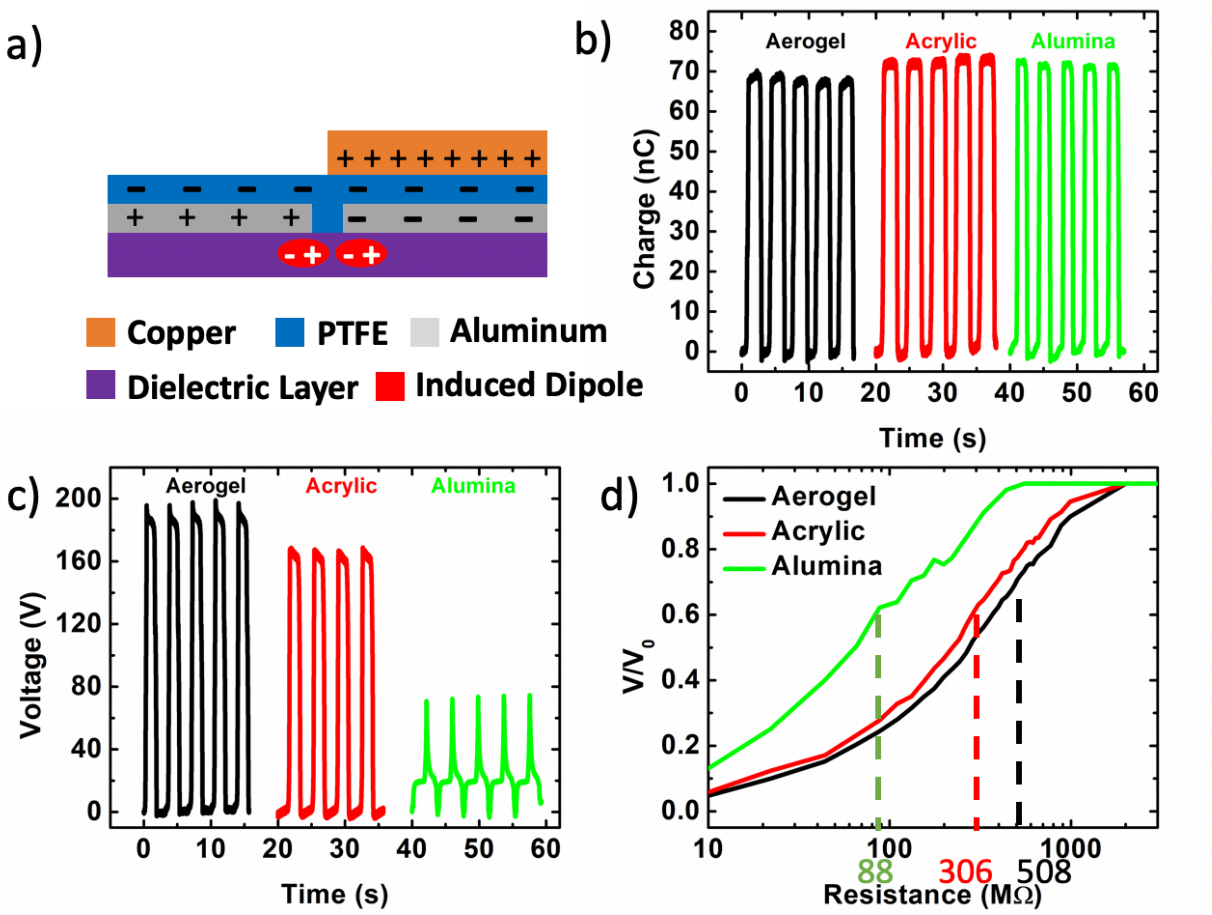

Figure 41. Different Substrate Material on TENG's Output Performance. a) Schematic showing the freestanding-mode TENG. b) Charge vs time comparison of the freestanding mode TENG with different materials. c) Voltage vs time comparison of the freestanding mode TENG with different materials. d) Comparison of actual voltage/V_{OC} with different resistance with different materials.

The mover was attached onto a linear motor with actuation of 30 mm at a frequency of 0.33 Hz. The electrical performance was then measured, and all three different substrates had a similar transferred charge output, which is around 72 nC, as shown in Figure 41b. This is similar to Figure 30a, when the gap distance between the bottom of the TENG and the water had been changed. It is important to note that the aerogel had a smaller charge, at around 68 nC, due to the aerogel is porous, making it difficult to have full contact, causing a smaller charge output. However, the small discrepancy in the charge does not change too much in the analysis. For the

output open circuit voltage, it is important to note that aerogel had the highest voltage at 191 V, the acrylic had a moderate output voltage at 167 V, and the alumina substrate had the lowest voltage at 71V, as shown in Figure 41c. This is further tabulated in Table 3. Furthermore, if the capacitance of the TENG is assumed constant with the position of the mover, as it is with most freestanding mode TENG with a small dielectric constant on the mover, the capacitance of the TENG could be approximated by Equation 15 below,

$$C_{TENG} = \frac{Q_{tr,p-p}}{V_{oc,p-p}} - 0.31\ nC \tag{15}$$

Where $Q_{tr,p-p}$ is the peak to peak transferred charge, and $V_{oc,p-p}$ is the peak to peak open-circuit voltage, and 0.31 nC is known to be the capacitance that the meter (Kiethley 6514) when measuring open-circuit voltage. It could be evaluated that the capacitance of the TENG, C_{TENG} for alumina substrate is 0.7 nF, for acrylic substrate is 0.121 nF, and for aerogel is 0.046 nF. This is further tabulated in Table 3. Also, similarly to Figure 45d, to evaluate the impedance of the nanogenerator, the voltage across a resistance was measured. The relative voltage is displayed here in Figure 41d, as the calculated voltage divided by open-circuit voltage, due to the large difference in output potential when the device is placed in water. The impedance of the nanogenerator was then obtained, with the impedance of alumina substrate being 88 Ω, acrylic substrate being 306 Ω, and aerogel being 508 Ω. This is also tabulated in Table 3. Furthermore, by using the actual voltages, the power was then calculated and tabulated in Table 3. It could be clearly seen from Table 3 that aerogel had the highest output power, whereas alumina had the lowest power, and this is due to a greater electrostatic screening effect for substrates with higher dielectric constant.

Table 2. Effect of Different Substrate Material on Output Characteristics of TENG

Substrate Material	Dielectric Constant, ε_r	Transferred Charge (nC)	Open-Circuit Voltage (V)	Capacitance (nF)	Impedance of Nanogenerator (Ω)	Maximum Output Power (μW)
Aerogel	1.1	68	191	0.046	508	180
Acrylic	3.4	72	167	0.121	306	143
Alumina	9.1	72	71	0.7	88	20

In summary of this work, the electrostatic screening effect was evaluated by changing substrates of the triboelectric nanogenerator. The three substrates tested are aerogel, acrylic, and alumina. It was found that aerogel had the least electrostatic screening effect, and the highest output power, whereas alumina had the most electrostatic screening effect, which its performance had the lowest output power. This was due to the electrostatic screening effect is dependent and proportional to the substrate's dielectric constant. This work details the first experiments done on the effect of substrate material on TENG's output performance. The next section is about a hybrid energy harvester that is able to harvest and store energy.

3.4 Hybrid TENG and EMG for Harvesting and Store Energy

With an increasing development of wearable electronics and wearable IoT sensor networks, extensive research has been focused on how one could provide power to these sensors. One way involves utilizing a wearable solar cell, but then the device would only operate in presence of light and could not operate during night or during cloudy weather. Another solution is to utilize batteries; however, batteries would constantly need to be replaced or recharged. Thus, my group believes the best way is to scavenge wasted biomechanical energy from human locomotion. Triboelectric nanogenerators have been shown to effectively convert mechanical energies from the environment into electrical energy. However, most generators that harvest waste biomechanical energy generates a pulsed AC signal, which makes them unsuitable for driving electronic devices directly. An energy storage device instead needs to be first used to store the

energy generated by the energy harvesters, and then deliver direct current to power the electronic device. One good type of energy storage device is Li-ion battery; however, batteries have a limited cycle lifetime, and have known safety concerns due to toxic electrolyte and reactive Li metal. Meanwhile, another type of energy storage device, electrochemical microsupercapacitors, can offer high power and longer cycle life, making them a safe and excellent candidate to be integrated with energy harvesters to create a self-charging power unit to power microelectronics.

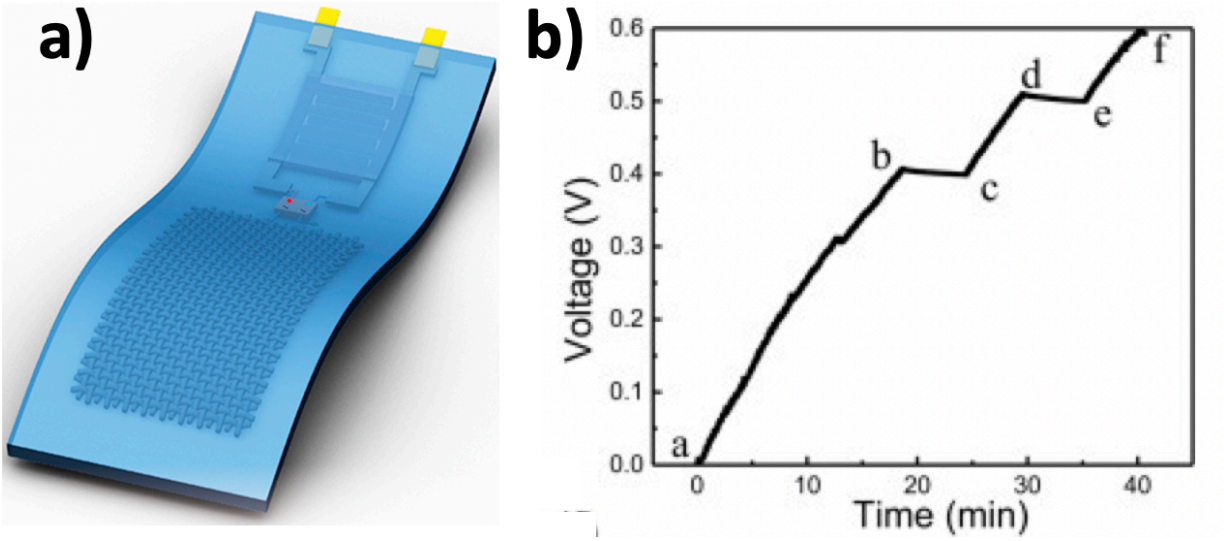

Figure 42.Wearable Self-Charging Power Unit. A) Schematic diagram of the wearable self-charging power unit. b) Charging curve showing the voltage increase of the single microsupercapacitor (Capacitance: 4 mF) powered by TENG.[129]

Qiu et al previously reported a single self-charging power unit, which integrates TENG device with solid-state microsupercapacitor, as shown in Figure 42a,in order to simultaneously and effectively convert and store mechanical energy of human biomechanical motions into electro-chemical energy.[129] However, just utilizing a TENG, the power output is low and it took roughly 40 minutes of continuous clapping to charge a microsupercapacitor with capacitance of 4 mF to 0.6 V, as shown in Figure 42b. Thus, it is necessary to hybridize multiple generators together to provide higher voltage or current than individual generators.[51, 118, 130, 131] In this work, an energy

harvesting bracelet is designed utilizing the cooperative operation of both EMG and TENG to deliver a high output performance, as shown in Figure 43.[132] The harvested energy is then stored into an integrated electrochemical microsupercapacitor that is attached onto the bracelet to power electronic devices and sensors, the charging of the electrochemical microsupercapacitor could easily be charged to high voltages quickly with the user by engaging in daily activities, such as walking and running.

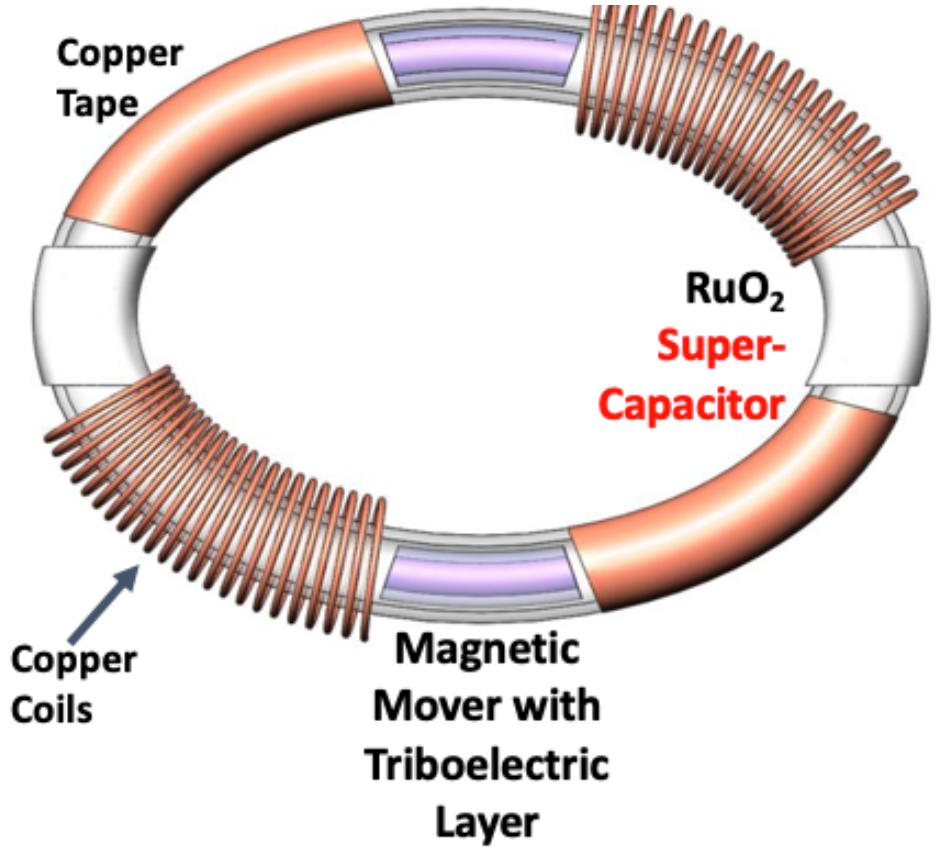

Figure 43. Schematic of Energy Harvesting Bracelet[132]

The energy harvesting bracelet consists of two magnetic coils for EMG, two copper tapes attached on a shell structure for a TENG component, a magnetic mover with an electret

polytetrafluorethylene (PTFE) material acting as a triboelectrification layer inside the shell, and a power management circuit containing an RuO_2 supercapacitor in the connector region. The fabrication process to make the bracelet is shown in Figure 44. Polyethylene Terephthalate Glycol (PETG) Tube (0.375 in. ID, 0.5 in. OD., McMaster Inc.) was first cut by a coping saw to have the length of 4.5 inches. Then, the PETG was heated by a heat gun, and placed in an ovular shaped mold. The resulting structure would be the PETG shape would have the similar structure as the ovular mold. Then, copper coils were wrapped around the side of the PETG tube with the number of turns equal to 1000 to fabricate the EMG element. The copper tape is then wrapped outside of the PETG tube to create the electrode for the TENG.

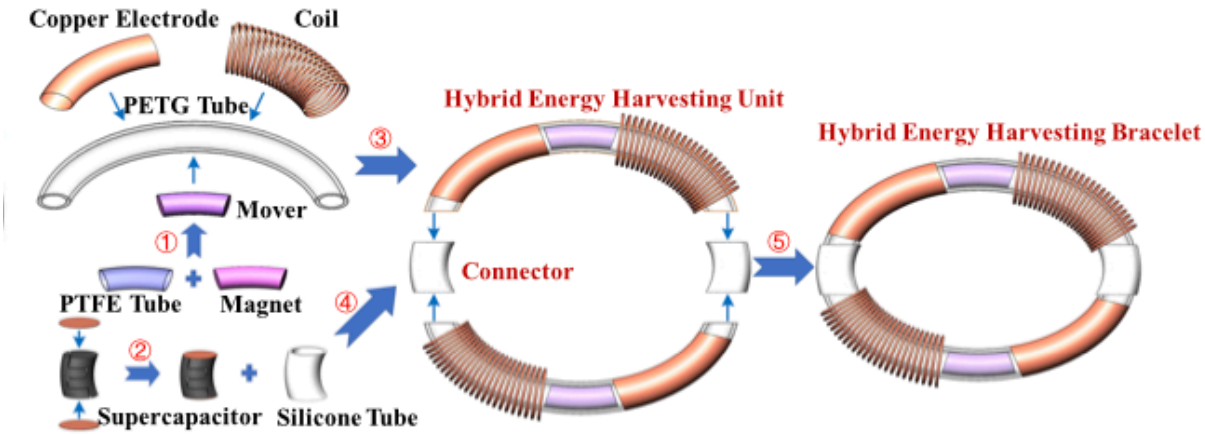

Figure 44. Fabrication Process of Energy Harvesting Bracelet.[132]

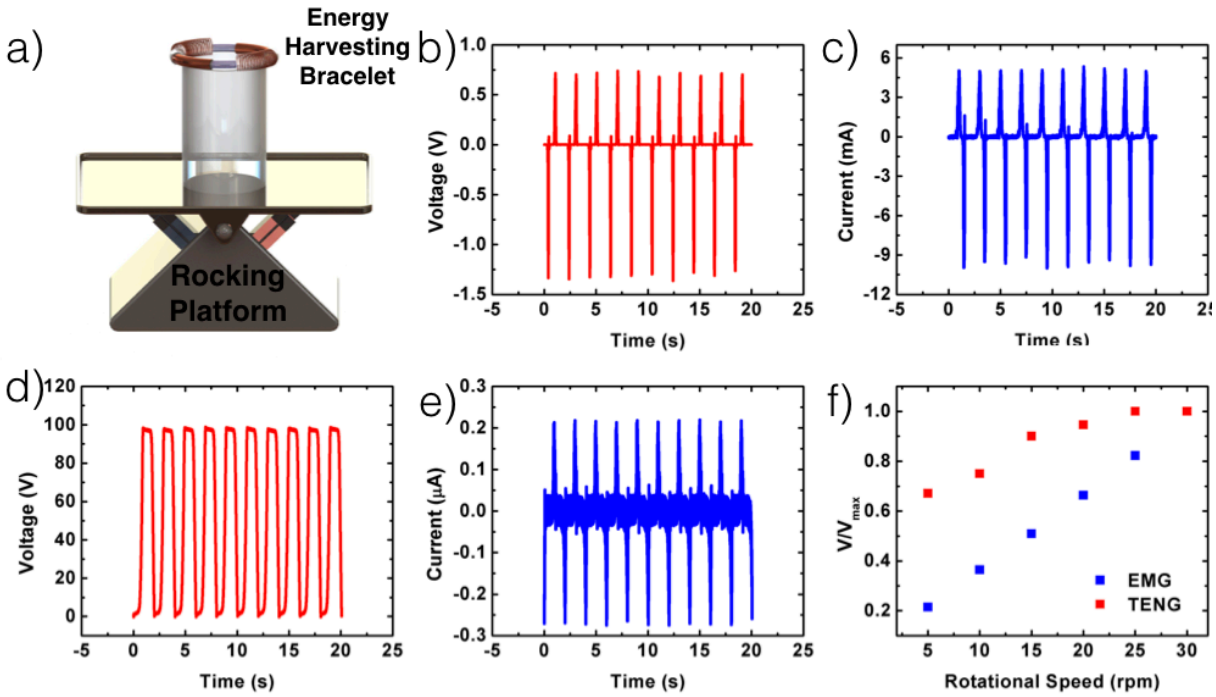

Figure 45. Electrical Performance of the Hybrid Energy Harvesting Bracelet: a) The 3D schematic of the energy harvesting bracelet on top of the rocking platform, b) The output open circuit voltage of the EMG. c) the output short circuit current of the EMG, d) The output open circuit voltage of the TENG, and e) the output short circuit current of the TENG. f) The normalized open circuit voltage dependence on the rotational speed of the rocking platform for both the TENG and the EMG.[132]

The energy harvesting bracelet operates by shaking motion while engaging in physical activities, such as walking, running, etc. As the bracelet is shaken by wrist motion, the magnetic mover would move from one end to the other, which could produce electricity by both the electromagnetic and the triboelectric effects.

To test the performance of the energy harvester, the energy harvesting bracelet was placed on top of a rocking platform, as shown in Figure 45a. The rocking platform is used to simulate the wrist shaking motion at low frequencies, such as when the user is walking. Due to the magnetic material present inside the rocking platform, a separator is needed to separate the rocking platform and the energy harvesting bracelet, and to allow the mover element to move freely. The rocking platform is inclined back and forth at a low frequency (frequency of < 0.5 Hz). As a result, the

magnetic mover element in the tube oscillates back and forth, moving from one end of the tube to the other due to gravitational force. The output performance for a single EMG is shown in Figure 45b and Figure 45c, in which the peak-to-peak open circuit potential difference could reach 1.9 V, and the short circuit peak-to-peak current reaches 15 mA. The output performance for a single TENG is also measured and is shown in Figure 45d and Figure 45e. The maximum open circuit voltage of the TENG is measured to be 100 V, with the maximum short circuit current measured as 0.5 μA. It could be seen that the effect of both the EMG and the TENG are complimentary, as the EMG has a high output current, but a low voltage, while the TENG has a high output voltage, but a low current. In addition, Figure 45f shows the effect of the rotational speed on both the EMG and on the TENG's performance. The EMG's open circuit voltage decreases linearly with rotational speed and is related linearly to the frequency of actuation of the device. For the TENG, the open circuit voltage remains constant at high rotational speed, but then starts to decrease afterwards. In principle, the TENG's output voltage should be constant with frequency, but the decrease of TENG output voltage at low frequency is due to the lack of sufficient kinetic energy to overcome the frictional force to slide fully down the tube. This shows that a lower open circuit voltage is obtained at low rotational frequency.

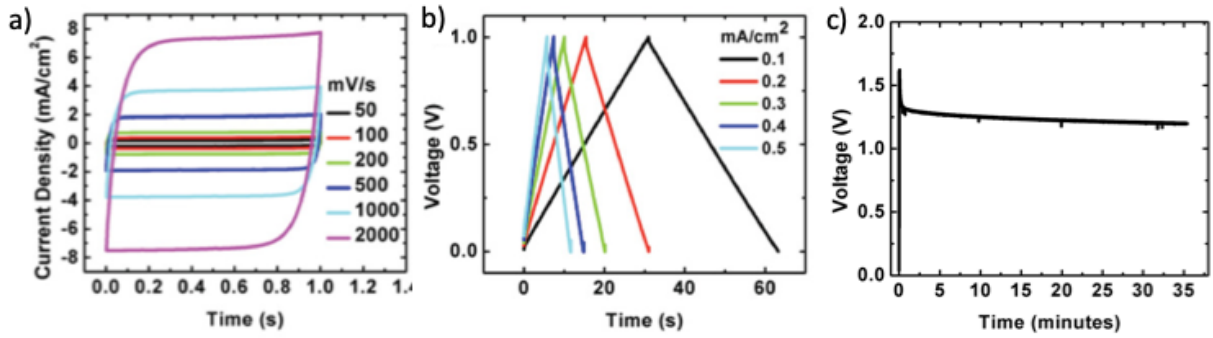

Figure 46. Characteristics of RuO_2 Microsupercapacitor.[132]

A ruthenium dioxide (RuO_2) supercapacitor was then fabricated and attached onto the bracelet. The electrochemical performance of the RuO_2 microsupercapacitor was evaluated by cyclic voltammetry (CV) at different scan rates. As shown in Figure 46a, CV curves shows symmetric and rectangular curves in the 0.8 V window, indicating excellent rate performance. Figure 46b shows the charge-discharge curve of the supercapacitor. The curves are quite linear with no voltage drop in the window of 0-0.8 V, indicating good conductivity and coulombic efficiency of the supercapacitor. Furthermore, the areal capacitance was calculated from the charge-discharge curve, in which the areal capacitance is 3 mF/cm^2. Due to the anhydrous and compact nature of the sputtered RuO_2, the areal capacitance is low compared with state-of-art microsupercapacitors.[133-136] However, the critical parameter of microsupercapacitor for real integration is the self-discharge rate, RuO_2 was chosen in this study mainly because of its slow self-discharge rate, which is extremely beneficial for energy harvesting applications, as the charges that is harvested would not be quickly lost, due to a quick self-discharging rate in other microsupercapacitors.[137] With the use of the RuO_2 electrochemical mirosupercapacitor, a low discharge rate is observed, as after 35 minutes, the voltage only dropped to 1.2 V, and remains constant afterward, as shown in Figure 46cillustrating the good performance and low leakage current of the RuO_2 microsupercapacitor. Figure 47a shows two EMGs connected in series, to obtain a higher output voltage, and two TENG connected in parallel to obtain a higher output current. Two RuO_2 were connected in series, because the working voltage of each of the capacitors can only go up to 1 V, and 1 V is not enough voltage to power most electronics. Thus, connecting two in series could get the working voltage to 2 V, which is enough voltage to power most devices. The charging curve of two RuO_2 microsupercapacitors connected in series is shown in Figure 47b under an actuation frequency of 0.5 Hz. on the rotational stage. The microsupercapacitors could

be charged to 1.5 V by single actuation and remains constant at this voltage with continuous actuation.

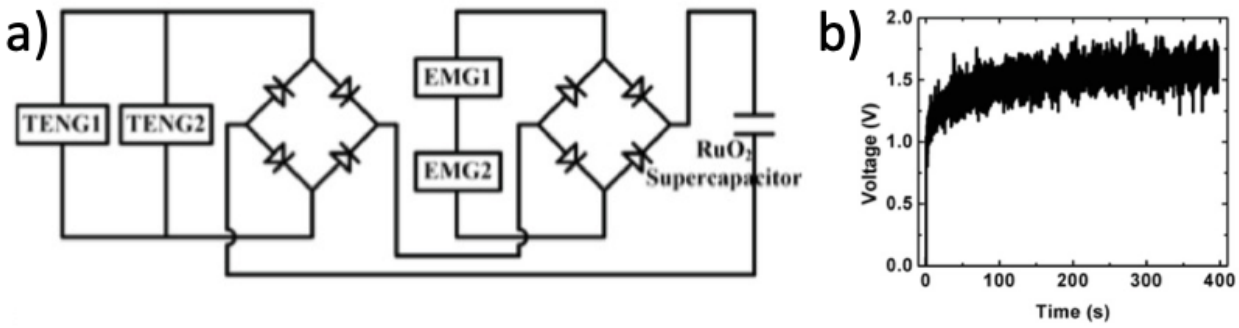

Figure 47. Circuit Model and Performance of Charging RuO_2 Microsupercapacitor[132]

Figure 48 shows the hybrid energy harvester's performance under different daily activities. The activities that were tested include slow walking, fast walking, and running. During these motions, the wrist motion allows the magnetic rod to move back and forth inside the PETG tube. The reported measurements were done with 25 seconds of actuation followed by 10 seconds of rest. As shown in Figure 48a, during slow walking, the excitation frequency is low, and the supercapacitor could only be charged to 0.5 V in 2.5 seconds. Furthermore, in Figure 48b, during faster walking speed, the excitation frequency is higher, allowing the supercapacitor to be charged to 1 V in 5 seconds. Also, in Figure 48c, while running, the supercapacitor could be charged to 2.5 V in 5 seconds. For the running case, the voltage starts to decrease after 25 seconds, due to the lack of actuation. With these simple daily activities, the supercapacitor could easily be charged to high voltages, which are sufficient to power most electronic devices.

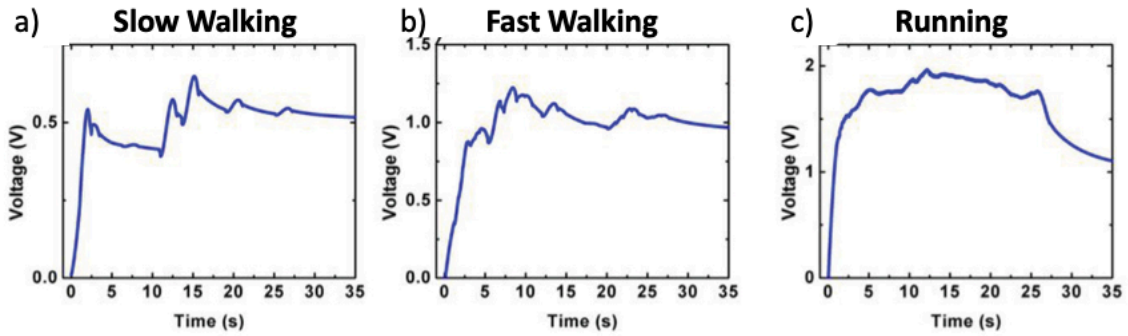

Figure 48. Energy Harvesting/Storage Performance of the Hybrid Energy Bracelet and RuO_2 Microsupercapacitors Under Human Locomotion Voltage of supercapacitors measured under a) slow walking, b)fast walking c) running[132]

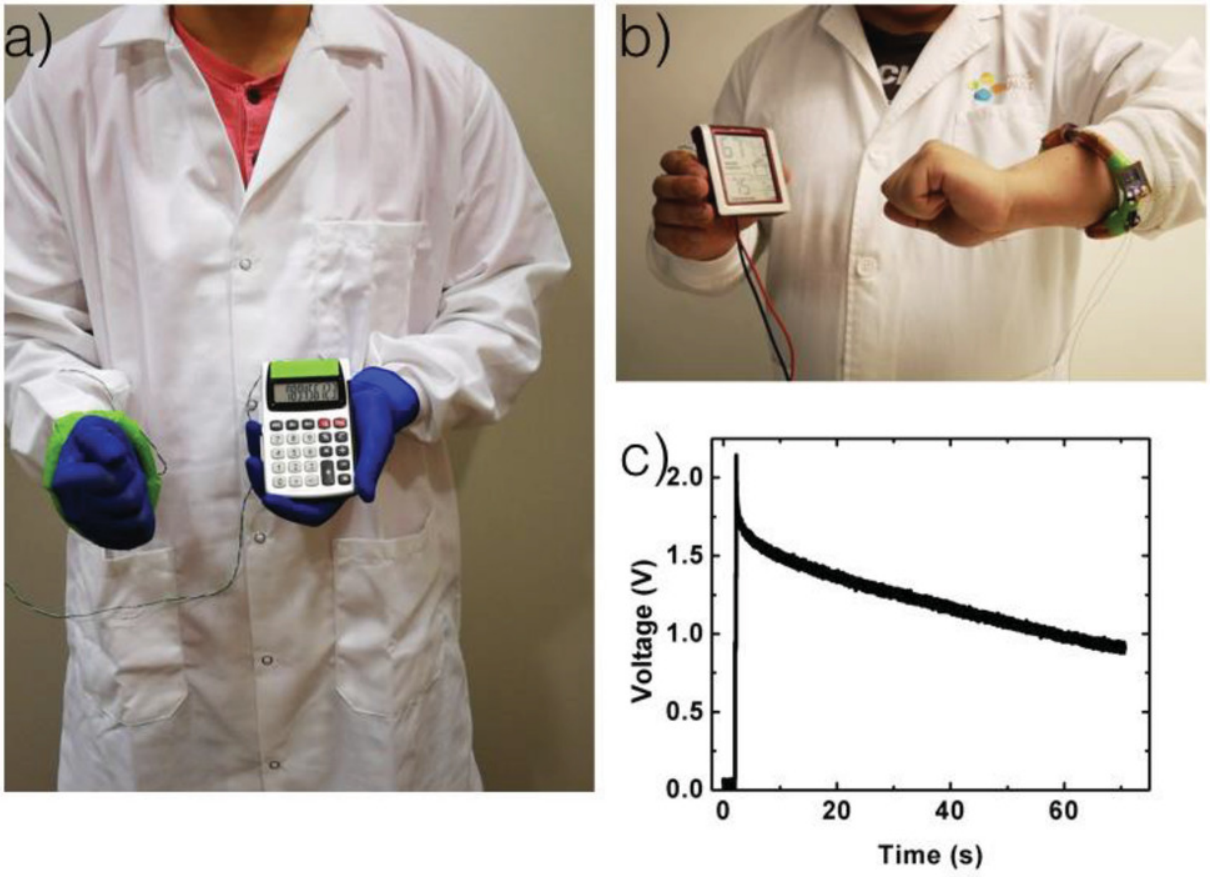

Figure 49. Applications of the Hybrid Energy Harvesting Bracelet a) Photograph of the hybrid energy harvesting bracelet powering a calculator. b) Photograph of the hybrid energy harvesting bracelet powering a relative humidity and temperature sensor. c) Voltage of the two RuO_2 microsupercapacitors connected in series when connected with a relative humidity and temperature sensor.[132]

There are many applications that can benefit from the hybrid energy harvesting bracelet, mainly it could act as energy harvester to power commercial electronic device. Figure 49a,b shows that the hybrid energy harvesting bracelet can power electronic devices, such as a calculator and a relative humidity temperature sensor by a single gesture. This is important, as previously with just the triboelectric nanogenerator device, it took 30 minutes to charge a microsupercapacitor to 0.6 V. Figure 49c shows the charging profile of the micro-supercapacitor powered by single shake of the energy harvesting bracelet and the discharge of the micro-supercapacitor powering the calculator. The single shake of the energy harvesting bracelet could charge the supercapacitor to 2V, and the calculator could be operational for 60 seconds, until the voltage across the calculator reaches 1 V.

In this work, a wearable hybrid energy harvester integrated with a supercapacitor is fabricator. Both the electromagnetic generator and triboelectric nanogenerator have been systematically studied and optimized. The hybrid energy harvester can charge efficiently a RuO_2 electrochemical microsupercapacitor, which showed exceptionally low leakage current, and excellent capacitive performance. With this integration, a self-powered humidity sensor or a calculator could be powered by a single shaking motion, whereas with previous devices, it could take a long time of continuous tapping to charge a supercapacitor.[129] In the next chapter, the high voltage application of TENG is discussed.

CHAPTER 4. TENG FOR HIGH VOLTAGE APPLICATION

TENG has emerged as a novel alternative of conventional high voltage (HV) applications in recent years. [56, 58, 138-142] The first use of TENG as a high voltage source is as a self-powered air cleaning system, in which the TENG could electrostatic precipitate flying dust particles and oxidizing SO_2 given its high voltage nature.[58, 143] Its intrinsic characteristic of HV eliminates the need of sophisticated power converters, and thus greatly reduces the system complexity and cost. Furthermore, the limited charge transfer per operation cycle of TENG offers an unprecedented way of accurately controlling HV-driven processes and provides extra safety to personnel and instruments in the meantime, as TENG has a high impedance, and thus a low current is also delivered through the high voltage process.

One representative work for high voltage application is the use of TENG to generate a nanoelectron spray for highly sensitive nano-coulomb molecular mass spectrometry, which not only utilizes the HV output of TENG, but due to the high impedance of the nanogenerator, also transforms the limitation of charge transfer and current into an advantage of unprecedented control over ion generation.[57] As shown in Figure 50a, a discrete amount of pulsed charges from the a high performance TENG were supplied to a nano electrospray ionization emitter and triggered highly repeatable ionization pulses with minimum sample consumption. The duration, frequency and ion polarity were all tunable via TENG actuation on-demand, and the HV (5-9 kV) of the TENG provided nanoESI with enhanced sensitivity at low concentrations, as demonstrated by the signature fragment ion (m/z 182.118) only observable in the TENG-driven nanoESI mass spectroscopy when analyzing a cocaine solution (10 pg./ml). This was due to with less current that is supplied, there would be less electrical noise in the mass spectroscopy analysis.

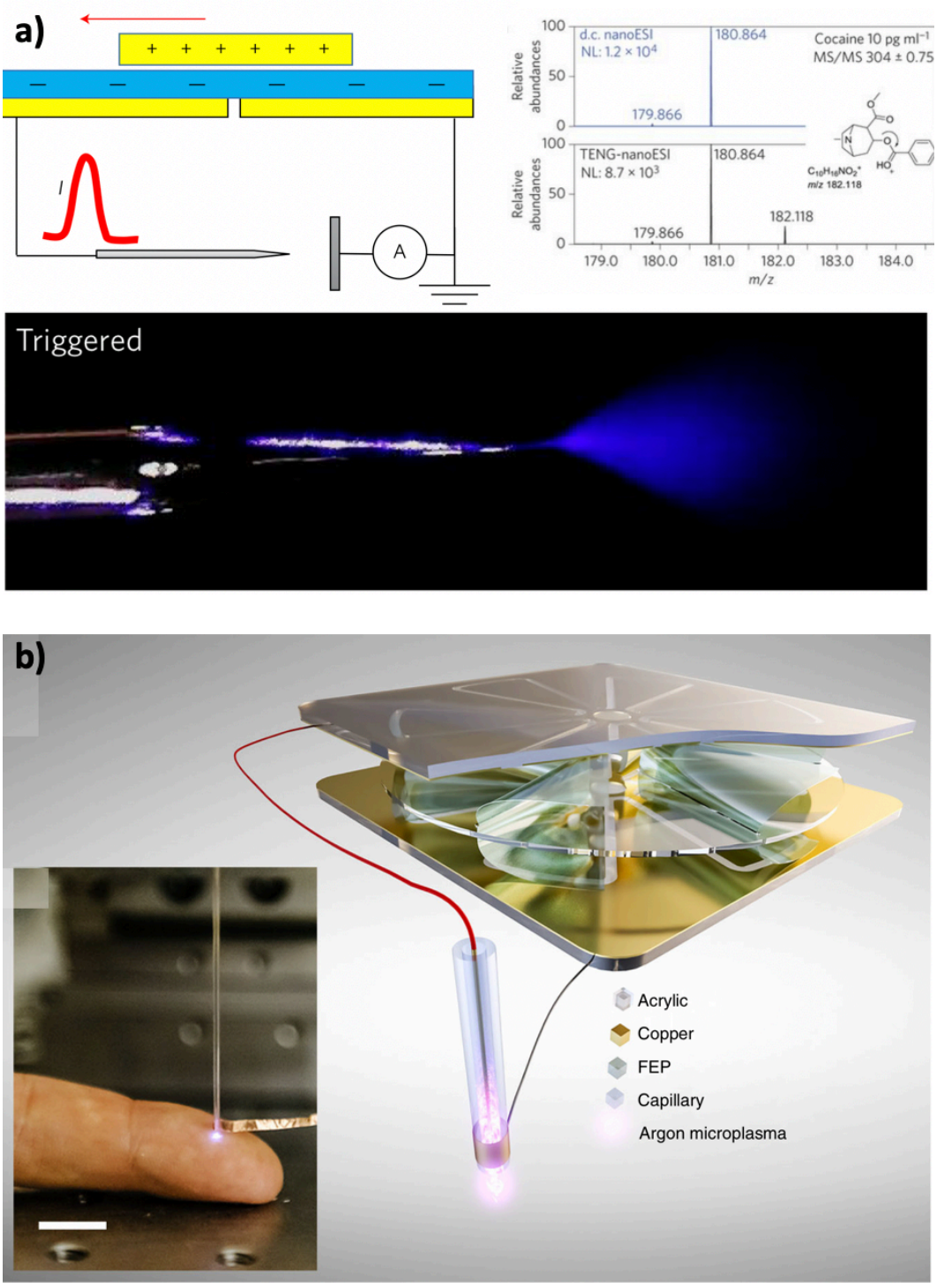

Figure 50. Applications of TENG for High Voltage Power Source. a) Sensitive nanocoulomb mass spectroscopy with freestanding mode TENG.[57] b) Generation of microplasma with rotational-based TENG.[56]

Another example is use of triboelectric nanogenerator to generate microplasma, which was realized by Cheng et al.[56] By the integration of TENG with a plasma source, and atmospheric-pressure plasma powered only by mechanical stimuli was achieved, as shown in Figure 50b. This shows that the high voltage of the triboelectric nanogenerators, over 10 kV, has the ability to break down gas. They also show there are several different types of microplasma, and discharge driven by TENG were achieved successfully, which opens up possibilities for using TENG to generate diverse microplasma. Taking natural advantage of TENG, high voltage, low current and charge, the triboelectric microplasma might has enormous potential value in applications of individual cell culture, treatment and apoptosis, species detection, elemental analysis, and ultraviolet excimer etc.

Recently, the high voltage produced from TENG has been used for a new mode of TENG called direct current-TENG (DC-TENG).[144] The working mechanism and the structure of this energy harvester is shown in Figure 51, and it has numerous advantages over conventional modes shown in Section 1.4, due to it does not need a rectification system to store the generated charges and its performance is not limited by air breakdown; thus, it allows it to have a larger charge density. In the initial state, as shown in Figure 51i, the frictional electrode is in left alignment with PTFE film and is in contact with PTFE, and there are positive charges on the frictional electrode and negative charges on PTFE caused by the triboelectrification effect. When the top mover moves forward, as shown in Figure 51ii, a very high electrostatic field is built between the top copper and the negatively charged PTFE film. As long as it exceeds the dielectric strength of air, it causes the nearby air to partially ionize and begin conducting. This will result in electrons flowing from the PTFE to the copper electrode, thus reducing the potential difference. Thus, since the copper is connected to an outside load, it would collect the charge. Because the inner flow direction of electrons is fixed from the frictional electrode to the PTFE film to the top copper electrode, the

output current would be in a single direction, making it direct current. When the slider moves backward to the initial state, no current flows in the external circuit, because there is not enough potential difference across the top electrode and PTFE film for dielectric breakdown to occur. The physics model of this DC-TENG is made up of electric charge source and a capacitor.[144]

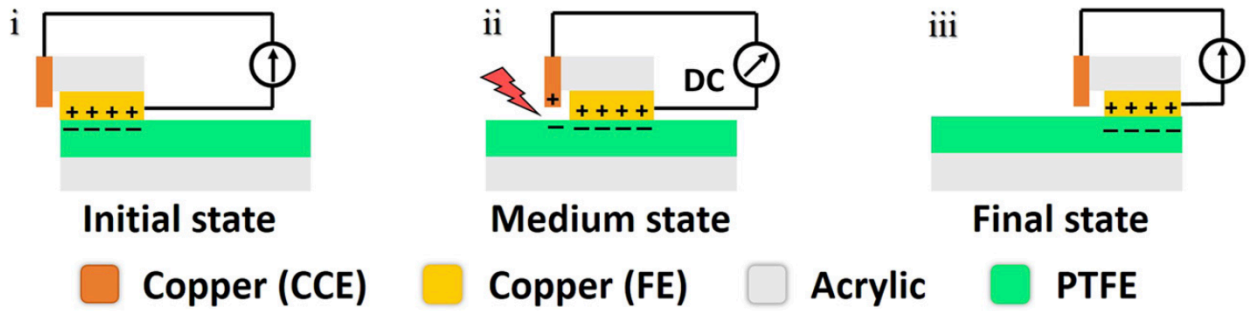

Figure 51. Working Mechanism and Structure of DC Mode TENG[144]

In this section, since TENG use of high voltage is a relatively new field, the effect of high voltage on different electronic components, such as resistors and capacitors is restored. First, I would look into applying a high voltage on a resistive system, which would cause the fuse to break, which could have important applications in personal security and a fully self-powered active sensor. Next, similarly for the DC-TENG work, there was an integration of TENG and a capacitor. I would then evaluate the type of electrostatic discharge in capacitive system and show a potential application in creating a high instantaneous current and power density TENG.

4.1 EMP Triboelectric Nanogenerator with Application in Sensing and Security

The motivation of this work are firstly, even though there are many TENG-based self-powered sensors being reported, as seen in Chapter 2, only the sensor element is self-powered in the designs.[145] This means that most other components of a sensing systems, such as the signal processing, analysis tool, and data transmission, are powered by an external power source. In this

work, a fully self-powered sensing system, without the use of external power supply is created.[146] This is done by utilizing TENGs high voltage as a trigger to break a fuse. Secondly, as more sensors are being developed, it is necessary to consider protecting privacy and to enable users to quickly change sensitive information if it is at risk of exposure. Thus, to address these issues, other researchers have turned to electrical fuses or antifuses powered by Joule heating or nano-electromechanical switches.[147-149] Using an electrical fuse, an instant transition between the 0 and 1 binary states can be achieved. When current passes through the electrical fuse, it can instantly turn from a short circuit (binary state 0) to an open circuit (binary state 1). Therefore, electrical fuses have been shown as effective embedded security elements that can be rapidly utilized to change sensitive information.

In this work, an electromagnetic pulse-based TENG (EMP-TENG) that could be utilized both as a self-powered sensing system, as well as a self-powered personal security device, was created.[146] The EMP-TENG system consists of two main elements: a high-powered sliding freestanding mode TENG device and a Direct Ink Write (DIW) 3D-printed electrical fuse element, as shown in Figure 52. DIW 3D printing provides a powerful manufacturing tool that could create geometrically complex shapes that can be mass customized, because design concepts are translated into products through direct digital manufacturing.[150].

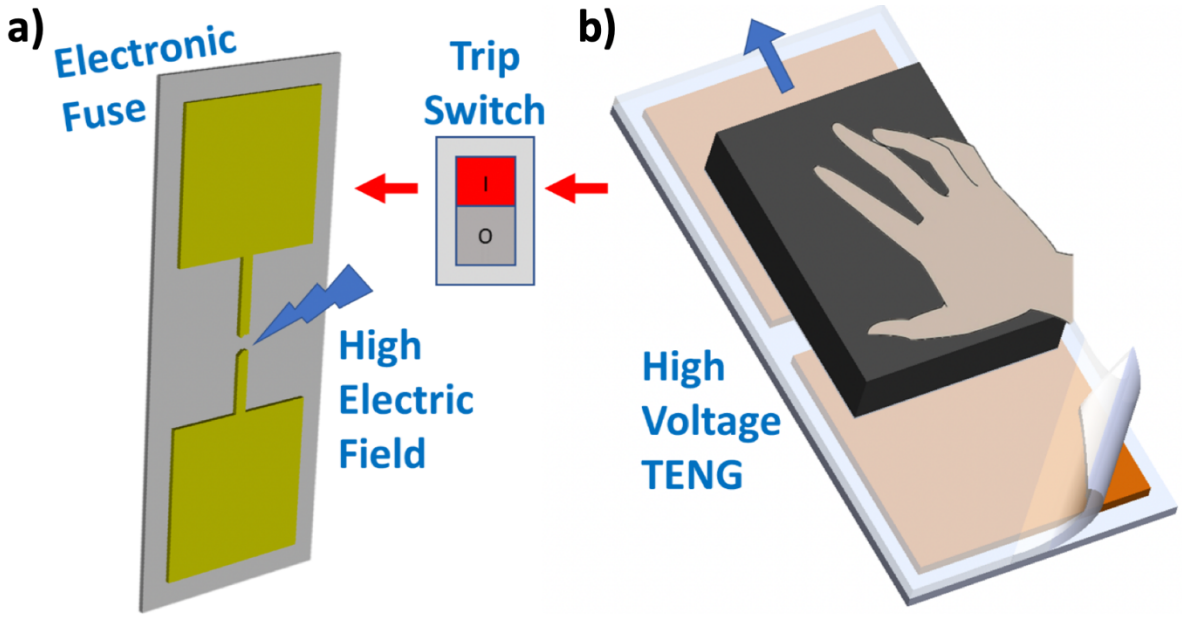

Figure 52: Concept of Triboelectric Electromagnetic Pulse System. A) Schematic of the Direct Ink Write (DIW) 3D-printed electronic fuse. Sliding the TENG triggers the trip switch to produce a high electric field across the fuse causing it to break. B) Schematic of the TENG used to trigger the trip switch of the fuse. Combining these two devices creates EMP-TENG system.[146]

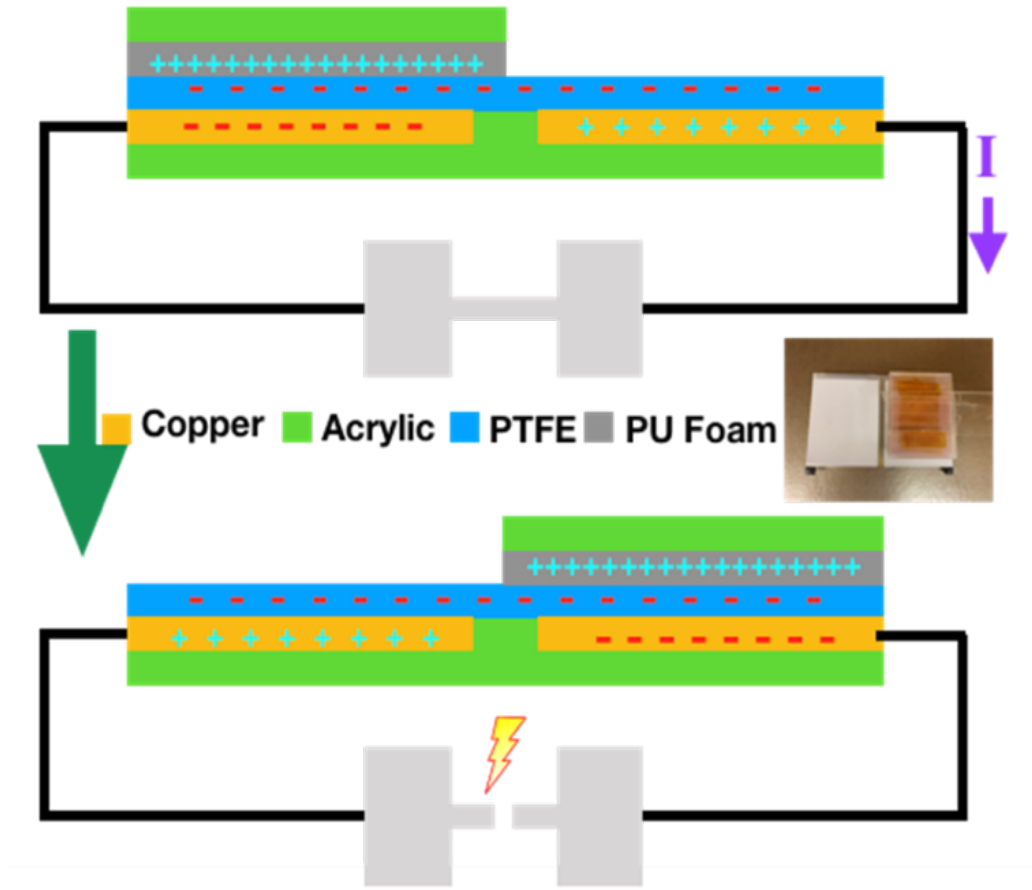

Figure 53: Mechanism of EMP-TENG in Breaking the 3D-printed Electronic Fuse.[146]

In this work, an electromagnetic pulse-based TENG (EMP-TENG) that could be utilized both as a self-powered sensing system, as well as a self-powered personal security device, was created. The EMP-TENG system has two main elements: and a Direct Ink Write (DIW) 3D-printed electrical fuse element, as shown in Figure 52a and a high-powered large scale sliding freestanding mode TENG device, as shown in Figure 52b. The freestanding mode TENG has a size of 175 mm x 100 mm. x 80 mm. These two components constitute destructible electronics by which a user could break the thin line of the fuse, causing a large change in the resistance of the fuse by an external mechanical motion. The mechanism of this process is shown in Figure 53, in which as the top triboelectric friction layer, consisting of a polyurethane (PU) foam, slides over the

polytetrafluoroethylene (PTFE) film, there would be a current pass through the fuse. If the produced AC current is high enough, the silver fuse will break, triggering a large change in resistance. Furthermore, by detecting the change in resistance, it could be utilized in security and sensing applications. Given that external mechanical motion generates enough energy to trigger the fuse, no external bias is required for activating the fuse, symbolizing this system is entirely self-powered, whereas in previous nanogenerator devices, only the sensor units are considered self-powered.

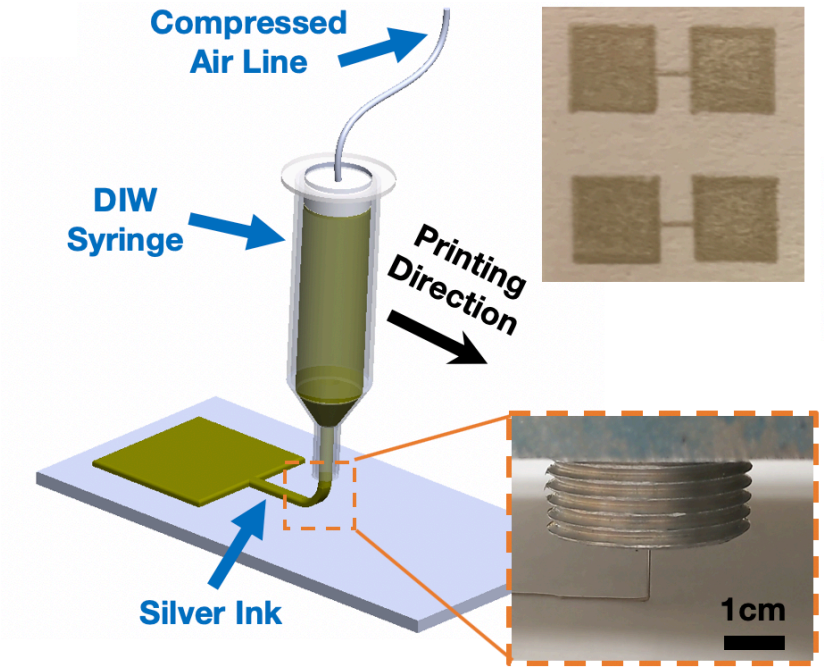

Figure 54: Direct Ink Write of Fuse on Paper Substrate. Left: Schematic showing the direct ink write 3D printing process. Inset (top): produced fuse on paper substrate. Inset, bottom: photograph illustrating the printing process.[146]

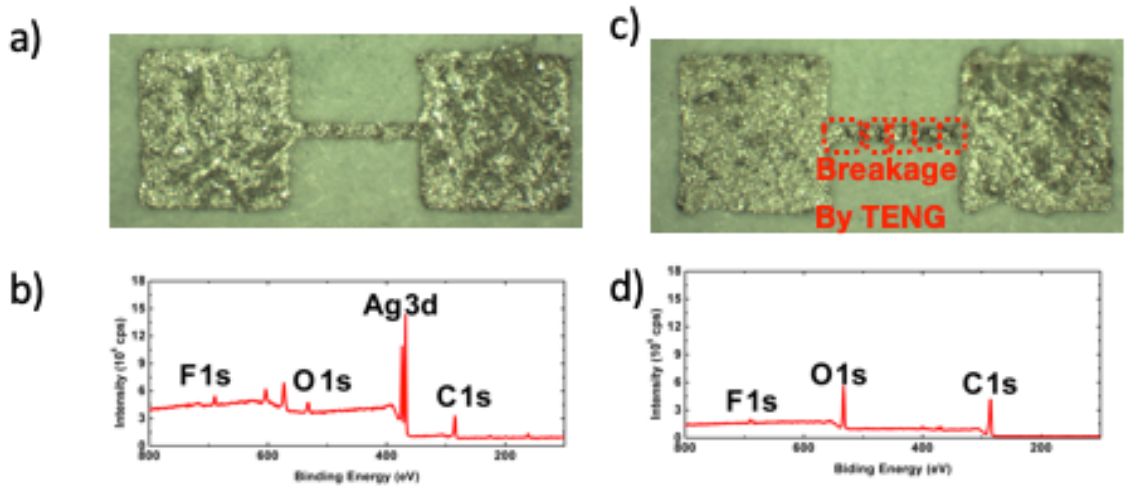

Figure 55: Optical Micrograph and XPS of Printed Fuse. a) Optical Micrograph of the fuse before being triggered by the TENG. b) XPS of the fuse before being triggered by the TENG. c) Optical Micrograph of the fuse after being triggered by the TENG. d) XPS of the fuse before being triggered by the TENG.[146]

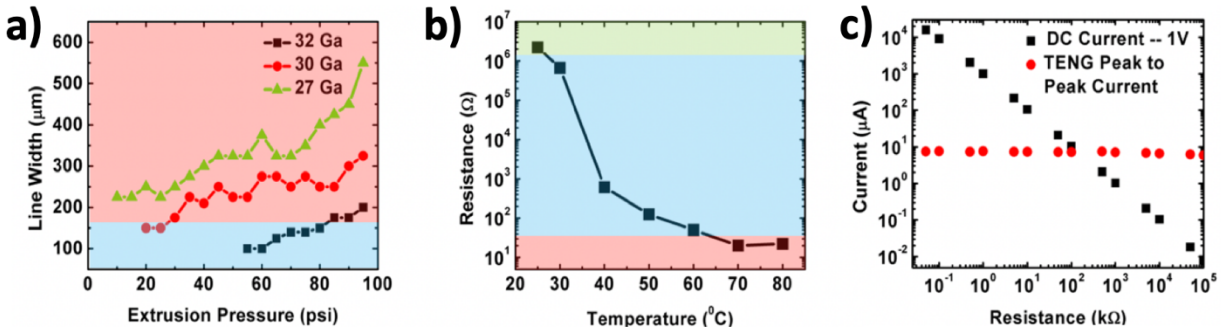

Figure 56: 3D Printing and Curing Parameters and its Effect on Fuse Performance A) Demonstration of printed electronic fuse line width as a function of extrusion pressure and nozzle diameter (red region: shows it could not be broken easily by EMP-TENG, blue: shows it could be broken easily by TENG). B) Demonstration of fuse resistance as a function of curing temperature (red region: shows it could not be broken easily by EMP-TENG, but could be broken by DC of 1 V, blue: shows it could be broken easily by TENG and by DC current, green: shows it could be broken by only EMP-TENG. C) The produced current of both the EMP-TENG and 1 V DC through different resistance.[146]

With this device structure in mind, it is first necessary to understand how the electronic fuse is fabricated. Figure 54 shows the fabrication process of the 3D-printed fuse, which is done by DIW 3D printing. In this process, pressure is applied to the syringe to extrude the viscous silver nanoparticle conductive ink (DuPont 603, Wilmington, DE, USA) onto the paper substrate. The

internal pressure within the syringe is controlled using a pressure regulator (Ultimunus V, Nordson EFE, East Providence, RI, USA). Thus, one could tune the extrusion pressure of the system. A computer-controlled motion stage then moves along the x and y-directions in a prescribed pattern that is controlled by an open source software Repetier (Hot-World GmbH. & Co. KG, Willich, Gernany) to form the electronic fuse. The optimal 3D printing and subsequent curing parameters were extensively studied by Mu, et. al.[151] In this work, since the fuse need to break, more research on the optimal 3D printing needed to be studied in this research to create a 3D-printed fuse element able to be triggered by the EMP-TENG.

Figure 55 shows the microstructure of the DIW 3D printed fuse prior to being triggered by the EMP-TENG. As seen by the data from X-Ray Photoelectron Spectroscopy (XPS) performed on the thin line of the fuse shown on Figure 55b**,** the Ag 3d duplex peak can be seen, which illustrates the large presence of silver in the device. Furthermore, the F 1s, O 1s and C 1s peaks can be seen due to the signal from the fluorinated paper below the 3D-printed fuse. However, after breakage by the triboelectric nanogenerator, the microstructure changed to that shown in Figure 55c**,** which shows dark spots that are caused by the breakage of the EMP-TENG. As shown in Figure 55d, performing XPS on the dark spots did now show the Ag 3d peak and only showed the F 1s, O 1s, and C 1s peak. Since there is no Ag 3d peak, this demonstrated that the silver is not oxidized, as silver would have remained on the sample, but instead the main cause for breakage is due to Joule heating. As the current passes through the fuse, a large amount of heat is generated causing the paper substrate to combust and thus removing the conductive silver.

Since Joule heating is the main principle, it is important to understand the various factors that affect Joule heating. The most important parameter for Joule heating is the resistance of the fuse. If a constant current is delivered, the resistance is directly proportional to the power produced.

For the silver 3D printed fuse, the resistance of the fuse must be above 30 Ω to be triggered by this EMP-TENG. When the resistance of the fuse is less than 30 Ω, the fuse will be difficult to break and require multiple cycles before it triggers as there is not enough power from the EMP-TENG to cause the paper substrate to combust. The silver trace line width is another key parameter for Joule heating as it has a direct effect on the resistance of the fuse. If the line is thicker, the resistance of the fuse will decrease, and the emissivity of the fuse will change. Thus, to ensure the silver-based fuse can be easily broken by the EMP-TENG, it is necessary to print the silver trace as thin as possible by precisely controlling the 3D printing parameters. To determine the 3D printing parameters needed to create an optimal silver-based fuse, a parametric study was performed where the two primary parameters, extrusion pressure and nozzle diameter, were adjusted. For this study, nozzles of three different diameters were used (27 Gauge (360 μm.), 30 Gauge (250 μm.), 32 Gauge (200 μm.)), while the extrusion pressure was adjusted from 10 to 95 psi for the 27 Gauge nozzle, 20 to 95 psi for the 30 Gauge nozzle, and 55 to 95 psi for the 32 Gauge nozzle; each was done with an increment of 5 psi. The reason for the increase of minimum pressure for smaller diameter nozzles was that at too low of pressures, the silver ink would not extrude through the nozzle. The resulting fuse width as a function of nozzle diameter and extrusion pressure can be seen in Figure 56a. Furthermore, an evaluation of the fuse's ability to be tripped by the EMP-TENG causing breakage was performed. It was concluded that neither line printed using the 27 Gauge nozzle could be broken with a single slide of the EMP-TENG. Also, fuses printed using the 30 Gauge nozzle, only the low extrusion pressure (below 30 psi) were able to be broken by the EMP-TENG, and for the 32 gauge, only fuses printed using pressures below 80 psi were able to be broken with the EMP-TENG. Thus, in Figure 56a, different regions were drawn with a cutoff at line diameter of 160 micrometers. The teal region (below 160 microns) represents the fuse could

be broken by EMP-TENG with a single slide, whereas the red region (above 160 microns) represents the fuse prove difficult to be broken using the EMP-TENG.

Furthermore, since the resistance must be 30 Ω and greater to be tripped by the EMP-TENG causing breakage, control over the resistance of the fuse is necessary. Here, standardized tests were performed on the fuse to ensure the fuse has a resistance above 30 Ω. This was done by printing fuses using a 32 Gauge nozzle at 60psi and placing them in the furnace at different temperatures for 10 minutes. As shown in Figure 56b, the resistance decreased with higher curing temperatures, and thus, if the fuse is over-cured, it could not be triggered by the EMP-TENG device, due to the low resistance demonstrated by the fuse, and thus, not enough power would be supplied from the EMP-TENG to burn the paper substrate. Therefore, in Figure 56b, three different regions are defined. First, the red region represents printed silver traces with resistance below 30 Ω, and in this region, the fuse could not be broken by the EMP-TENG but could be broken by DC power supply of 1V. Second, the teal region represents printed silver traces with resistance greater than 30 Ω and below 1.2 MΩ and is defined by the fuse could be broken by both the EMP-TENG and a DC power supply voltage of 1 V. Third, the light green region represents a resistance greater than 1.2 MΩ. In this region, the DC-power supply of 1 V was not able to break the fuse, whereas the EMP-TENG could easily break the fuse. This demonstrates the unique advantage of EMP-TENG over DC power supply, as it is able to break fuses with high resistances, such as in uncured silver ink, due to a higher peak current generated by the EMP-TENG than DC power supply at high resistance, as seen in Figure 56c. The peak current of a freestanding mode TENG would remain constant, until GΩs of resistance is achieved, and then the peak current would decrease with increasing resistance.

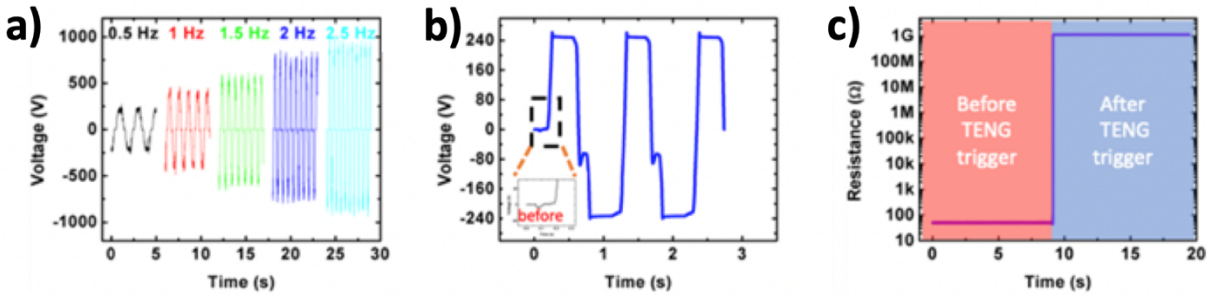

Figure 57. Electric Characteristics of TENG and EMP-TENG System. A) Open-circuit voltage of TENG. B) Open-circuit voltage of TENG when connected to fuse. C) Measured Resistance of Fuse.[146]

The electronic characteristics of the EMP-TENG is shown in Figure 57. This was tested by moving the top mover of TENG with a linear motor. In this figure the voltage was measured by a high voltage probe with a resistance set to 100 MΩ, and it could be shown to reach over 1000 V, demonstrating the high performance and the voltage produced of the device, as seen in Figure 57a. Further experiments were than performed when the EMP-TENG is connected to the fuse. Figure 57c shows the measurement of the fuse resistance, in which at the initial state, the resistance is measured to be 90 Ohm and after the fuse is triggered by the TENG, the resistance instantly increases to 1.5 GΩ. Furthermore, voltage was measured across the fuse, as shown in Figure 57b. At the initial state, the output voltage is low, as shown in the inset of Figure 57b, since it operates in a short circuit condition. After the fuse trigger, the output voltage reaches the maximum value of the meter (-250 V to 250 V).

After showing that the fuse could change its resistance by multiple orders of magnitude by simply sliding the EMP-TENG, different applications of the EMP-TENG triggering fuse were demonstrated. The first application is a fully self-powered package drop detection sensor, as shown in Figure 58a. The device operates as after the package slides down the EMP-TENG, the fuse

would be opened, causing a large change in resistance. Previously, for TENG devices, only the sensor part is self-powered, as the system still requires energy for analysis of the detected signal. Here, the EMP-TENG triggering the fuse is entirely a self-powered system and does not need additional energy for the sensed signal analysis. At the initial state, the package is placed on top of the top electrode, and it is held in place by electrostatic force, as shown in Figure 58b. As shown in Figure 58c, as the package falls, the resistance instantly changed from 46.8Ω to 0 L, where 0 L means the resistance is too high to be measured by the multimeter. This is due to the current passing through the fuse is high enough to break the fuse, causing the large change in resistance. Furthermore, for full realization of the self-powered system, the fuse could be placed under the microscope to see the change in the microstructure, as depicted in Figure 55a and 55c. With this, the first self-powered system based on EMP-TENG is developed, showing its potential in package drop detection sensor, and this area of utilizing the fuse could be extended into other self-powered sensing systems.

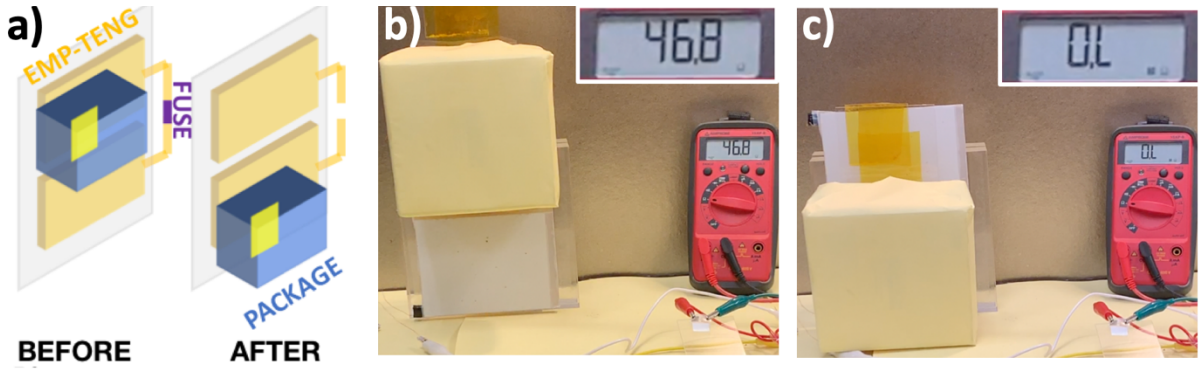

Figure 58: Applications of EMP-TENG for Self-Powered Package Detection A) Schematic showing application of EMP-TENG as a self-powered package detection system. B) Images showing the package and multimeter measuring resistance before it is dropped. Top inset: Zoomed in image showing the resistance value from multimeter C) Optical images showing the package and multimeter measuring resistance after it is dropped.[146]

The second application for EMP-TENG triggered fuse shows its potential usage for security purpose. Figure 60a shows the circuit diagram of the half adder circuit with the EMP-TENG and the fuse placed in parallel to the inverter. At the initial state, the circuit operates as a half adder circuit, with the information of input and output shown in Figure 59a-b, since the inverter would be shorted. When sliding the EMP-TENG intentionally, the fuse can be broken, even when actuated with a low frequency slide, and the inverter would be no longer shorted. This would cause the half adder circuit to be changed to a half subtractor circuit, which would have different output. The information of the input and output of the half subtractor circuit is shown in Figure 59c-d. With the input of A 1 and B 1, the initial output from the half adder circuit would be G 0 and R 1, which is shown by the green LED light off and red LED light on, as shown in Figure 9e. Also, from Figure 60b, on the DC power source, it displays a positive flow of current, which is required to light up the red light. As the top frictional layer of the TENG slides from left to right, the fuse is no longer shorting the inverter, and the circuit change from the half-adder to a half subtractor circuit. The output were then G 0 and R 0, which is symbolized by the green LED light off and red LED light off, as shown in Figure 60c. Half-adder and Half-subtractor logic circuits are the most basic system in computing, and a simple slide of the TENG can cause a transition between the two. If a TENG can easily change these two elements, it could be further implemented to change logic circuit elements in a more complex system, like data stored in a computer. This demonstrates a potential application in security, as a simple switch could change the states of logic circuit elements, which could be used as a quick way to change sensitive data stored on computer.

In summary of this work, a Direct Ink Write 3D-printed silver fuse was integrated with TENG technology to create a self-powered security device and fully self-powered sensor. The parameters of the 3D-printed fuse were first examined and optimized so that a thinner fuse with a

higher resistance could be broken, or triggered, by the EMP-TENG and by DC current. Utilizing the high voltage during operation of the freestanding mode TENG, a low frequency mechanical motion can instantly and quickly break the 3D-printed fuse. The fuse's resistance was able to change quickly from 50 Ω to 1 GΩ just by a simple sliding motion on the TENG. Different applications were then demonstrated, and the integration between the TENG technology and the fuse could be utilized for a fully self-powered drop detection system, which could operate without external power. The physical change in the fuse could be viewed visually after being triggered, as the microstructure of the fuse would be changed. Lastly, the integration of the fuse and TENG was utilized to create a logic circuit element for a self-powered security application. After a single sliding motion using the TENG, a half adder circuit was able to change to a half subtractor circuit instantly, providing a basis for irreversibly changing sensitive data.

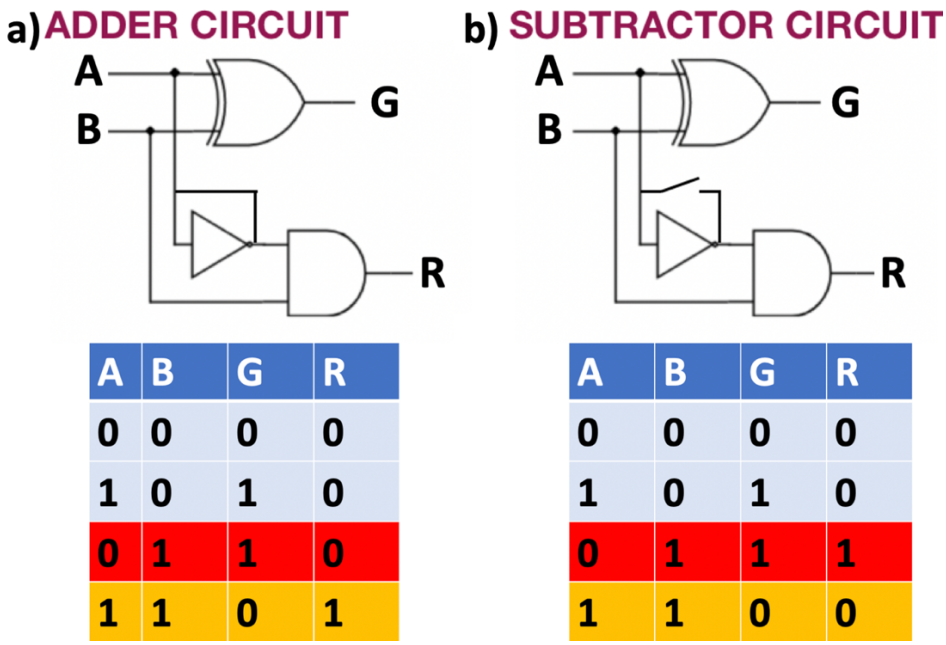

A	B	G	R
0	0	0	0
1	0	1	0
0	1	1	0
1	1	0	1

A	B	G	R
0	0	0	0
1	0	1	0
0	1	1	1
1	1	0	0

Figure 59: Schematic Showing the Half-Adder and Half-Subtractor Circuit: A) Circuit Diagram of a Half-Adder Circuit. B) Truth table of Half-Adder Circuit with Input A,B and output G,R. C) Circuit Diagram of a Half-Subtractor Circuit. B) Truth table of Half-Subtractor Circuit with Input A,B and output G,R.[146]

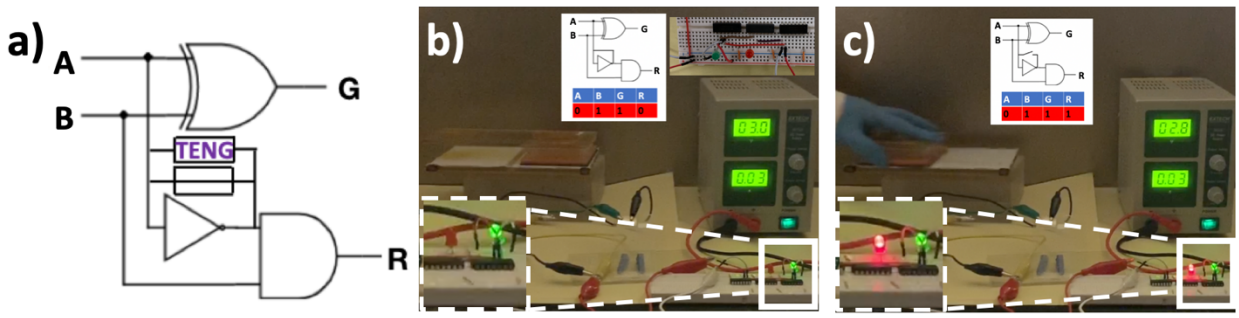

Figure 60: Applications of EMP-TENG for Personal Security. A) Circuit model for EMP-TENG coupled with logic circuitry to be used as security element. Top inset: Zoomed in image showing the resistance value from multimeter. B) Optical images showing the red light on and green light off before sliding of TENG. Top left inset: zoomed in image of the logic circuit element. Top middle: Output of half-adder circuit with input A 1 and B 1, Bottom right: zoomed in schematic of LED lights C) Optical images showing red light off and green light on after sliding of TENG demonstrating the EMP-TENG as a logic security element. Top middle: Output of half-subtractor circuit with input A 1 and B 1. Bottom right: zoomed in schematic of LED lights.[146]

4.2 TENG induced Breakdown in Capacitors for High Instantaneous Current and Power Density

Research have been focused on increasing the instantaneous power output of the TENG, as it was thought that the higher the instantaneous power output of the nanogenerator, the better the performance of the nanogenerator. For a TENG, the output voltage is high, but the output current is low; thus, it is easier to increase the current of the TENG. Since a nanogenerator is assumed to deliver a constant charge per cycle, an approach to increase the short circuit current density is to decrease a period per cycle, T, or increase the frequency of operation, *f*. This is because TENG's short circuit current I_{sc}^{TENG} is equivalent to the variation rate of short-circuit charge, Q_{sc}, of nanogenerator with respect of time, as shown in Equation 16.

$$I_{sc}^{TENG} = \frac{dQ_{sc}}{dt} \tag{16}$$

Thus, the average short-circuit current could be derived as

$$|I_{SC}^{TENG}|_{avg} = \frac{\int_0^T |I_{sc}|dt}{T} = \frac{2Q_{sc,max}}{T} = 2Q_{sc,max}f \quad (17)$$

From Equation 17, the average short-circuit current is proportional to the frequency of operation. Thus, much research has been focused on utilizing rotational device to obtain a higher frequency of output; thus, a higher short-circuit current.[152-156]

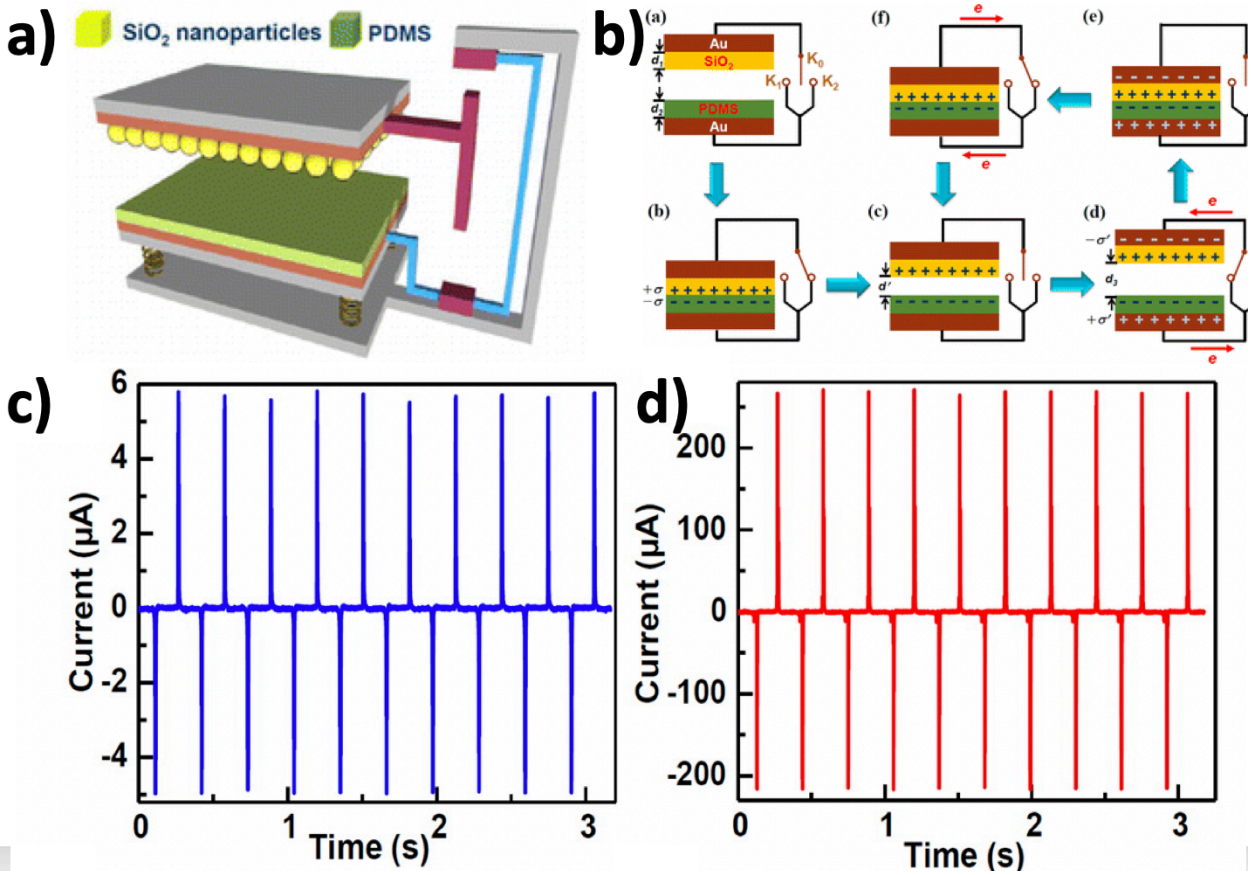

Figure 61. Schematic, Working Mechanism, and Performance of ID-TENG. a) Schematic of ID-TENG. b) Working Mechanism of ID-TENG. c) Output short circuit current characteristics of CD-TENG. d) Output current characteristics of ID-TENG with a load of 1 MOhms.[157]

However, this is not the only method for largely increasing the output current. Cheng et al proposed a design,[157] as shown in Figure 61a, based on an off-on-off contact based switching during mechanical triggering that largely reduces the duration of the charging/discharge process, with the working mechanism explained in Figure 61b. They called their design instantaneous

discharging TENG, as the charges are discharged instantaneously when the switch is closed. Through Equation 17, due to the large decrease in the period, the duration of charge/discharge process, the instantaneous output current pulse is hugely improved without sacrificing output voltage. Thus, they had claimed their instantaneous discharging TENG (ID-TENG) could gigantically enhance the instantaneous output power compared to continuous discharging TENG (CD-TENG). Furthermore, utilizing this approach, various papers have been constructed with different modes of nanogenerator, but still utilize the contact-based switching during mechanical triggering.[157-164] Also, the theoretical calculations show that utilizing the switch is the key to solving TENG's impedance matching problem and achieving the maximum output energy from the TENG.[162]

Even though this design did hugely improve the current density, as the current density of the ID-TENG could reach 480 μA peak to peak compared to 11 μA peak to peak in the CD-TENG as shown in Figure 61c and Figure 61d. The design has some drawbacks, such as the current device have a complex structure, which makes it impractical to use, and also, the added switch significantly increases the area of the device, which would decrease the output instantaneous power density. These devices are not durable, as the mechanical contact between metallic contacts could easily cause breakage in the device, which would limit its operation in long term usage. To address this issue, I wanted to utilize the high voltage of the TENG to create an electrical switch that would limit the duration of the charge/discharge process, which in turn, would cause a higher output instantaneous current density. Previous work of utilizing TENG as a switch, called tribotronics, with a name based on conjunction with a transistor and TENG, had utilized electrostatic potential created by triboelectrification as a 'gate' voltage to tune/control energy transport in semiconductor for human-machine interaction.[165-169] However, for tribotronic devices,

there needs to be a conversion of the random and irregular pulse output voltage in hundreds of kilovolts into steady and continuous DC voltage of 2-5 V to power the gate of the semiconductor to act as an electrical switch. In this work, I wanted to demonstrate the pulse output voltage of nanogenerator could create a novel design of an electrical switch, without the use of conversion circuits, which would draw outside electrical power to convert the random and irregular pulse output voltage to steady and continuous DC Voltage to power gate of semiconductors.

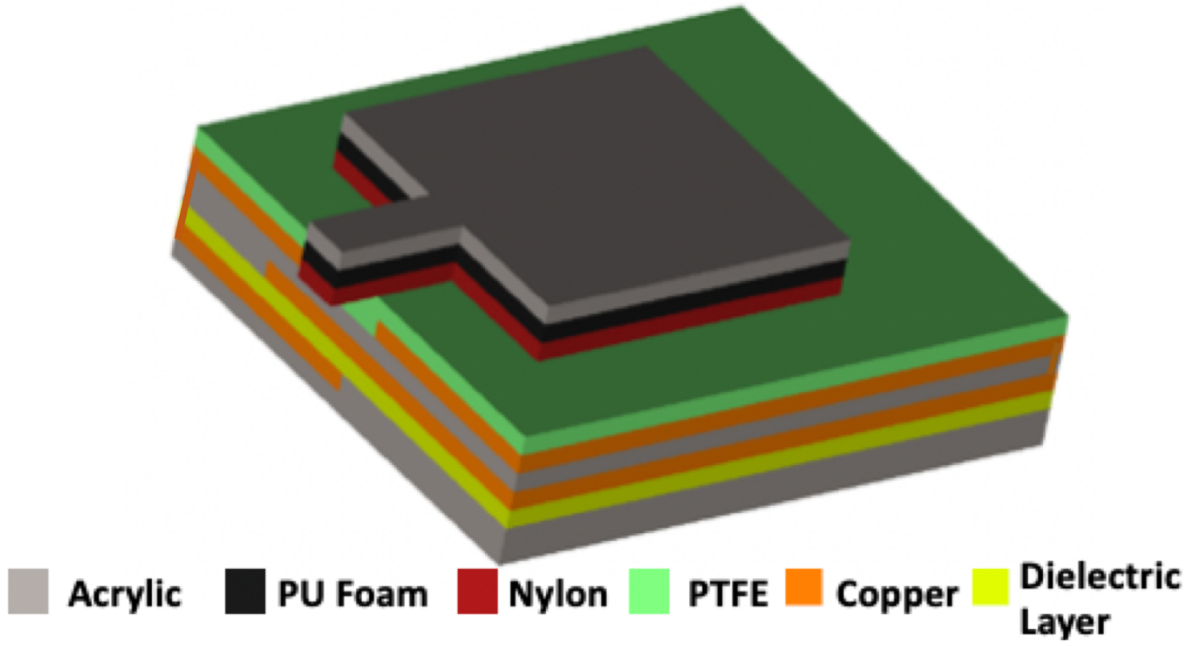

Figure 62. Schematic and Mechanism of Dielectric Layer Triboelectric Nanogenerator

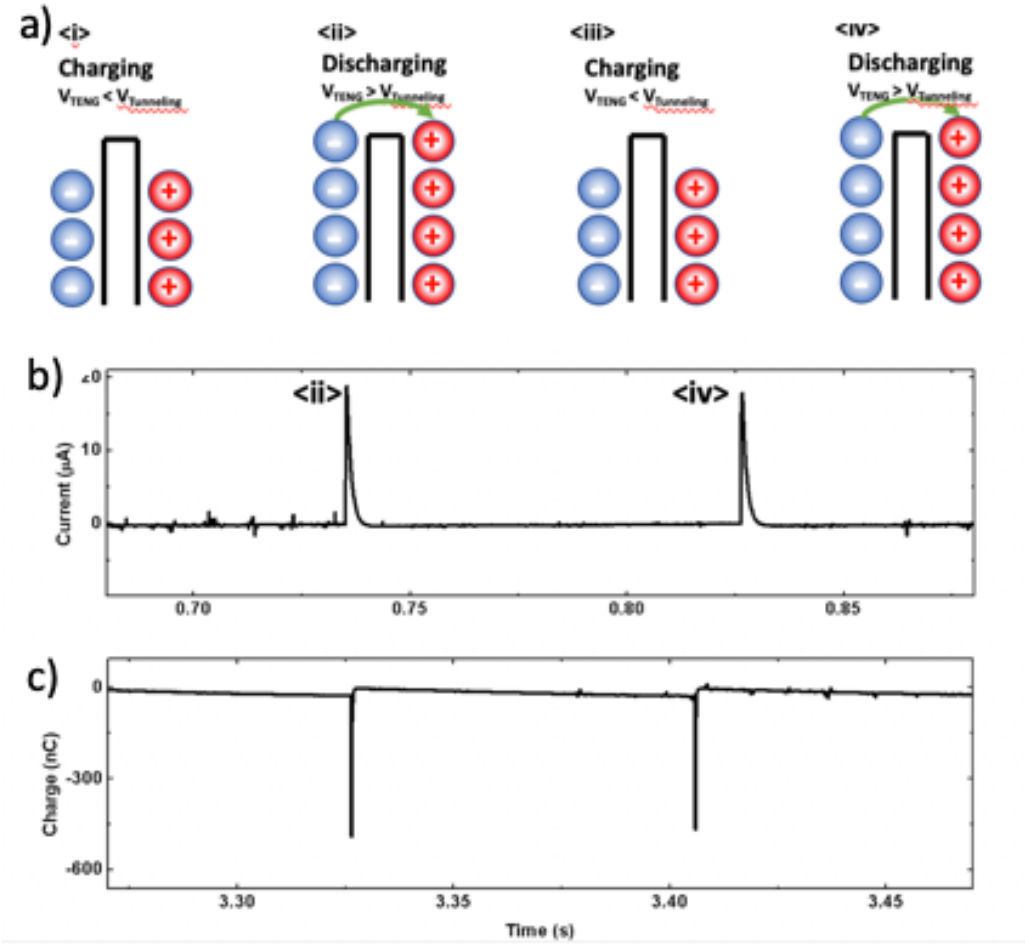

Figure 63. Schematic of Tunneling Effect and Output Performance of Current and Charge. a)Schematic demonstrating the tunneling effect of the Dielectric Layer-TENG, which include charging and discharging through tunneling layer. b) Current vs time of the effect of dielectric layer, illustrating the charging and discharging effect. c) Charge vs time of the dielectric layer, illustrating the charging and discharging effect.

After much thought, I concluded that a it is possible to create a switch by utilizing a high voltage discharge that is generated by the TENG. The idea is that by having a freestanding mode TENG with the electrodes of the nanogenerator shown in Figure 62a connected to a copper-dielectric layer-copper layer beneath the nanogenerator that is separated by an acrylic sheet. Thus, with this device, by sliding the top foam layer with nylon across the PTFE layer, a potential

difference is produced on the nanogenerator and directed to the Cu-dielectric layer-Cu load, as positive charges would be stored on one side of the copper layer and negative charges would be stored on the other copper layer, as shown in Figure 63a<i>. The potential difference on the Cu-dielectric layer-Cu would increase, as more opposite charges get stored on the copper layer. As more charges gets stored on the copper surface, the potential difference would eventually be greater than the threshold potential difference for discharge to occur, as shown in 63a <i> and charges are able to transfer from one electrode to another producing a current, as shown in Figure 63b. Recently, it was found that this discharge in air is found to be caused by partial discharge, or corona discharge with no dielectric. Thus, in this case, the main mechanism could be assumed to be dielectric barrier discharge, which is also partial discharge with a dielectric. The discharge lifetime is really short; thus, a high current is produced. After the discharge occurs, the potential difference would be less than the threshold potential for discharge to occur, and since the nylon mover is still moving across the electrode, more charges are being stored, and once the potential difference would be greater than the threshold potential, breakdown would occur, and the process is repeated. Figure 63b and Figure 63c verifies the effect, as it displays the output short-circuit current and charge when utilizing a freestanding mode TENG with a Cu-Polyethylene Terephthalate (PET) (0.002-inch thickness)-Cu layer, and one could see the time of charge transfer is only 0.1 millisecond.

To explain the role of the dielectric layer, a circuit model is constructed for the dielectric layer in Figure 64. The dielectric layer is modeled as a switch and a capacitor, and the TENG is modeled as a sinusoidal charge source with a capacitor in parallel. The reason that a sinusoidal charge source is used is due to the mechanical motion induced by the linear motor is programmed to be sinusoidal. This technique is usually used when investigating theoretical models of TENG. When the TENG is charging, the capacitor modeled for the dielectric layer is connected to the TENG, meaning that switch is closed at A. Thus, the voltage across the capacitor could be calculated by Equation 18 below.

$$V_{cap} = \frac{Q_0 \sin(\omega_0 t)}{C_{TENG} + C_{d,layer}} \tag{18}$$

Thus, the calculated charge on the dielectric layer of the capacitor is shown in Equation 19

$$Q_{cap} = \frac{Q_0 \sin(\omega_0 t) C_{d,layer}}{C_{TENG} + C_{d,layer}} \tag{19}$$

Once the voltage across the dielectric layer is greater than the threshold voltage for breakdown, switch would move from A to B, and the circuit is identical to a RC circuit, consisting of R_d, discharge resistance, and C_d, dielectric capacitance. It is important to note for that without any partial discharge, R_d would be very large, approaches infinity ; however, when there's partial discharge, R_d decreased and approaches 0.[170, 171] Thus, the discharge current as a function of time would be shown in Equation 20. Since R_d approaches 0 during discharge, discharge current would be high.

$$i_{discharge}(t) = \frac{V_{cap}}{R_d} e^{-\frac{t}{R_d C_{d,layer}}}. \tag{20}$$

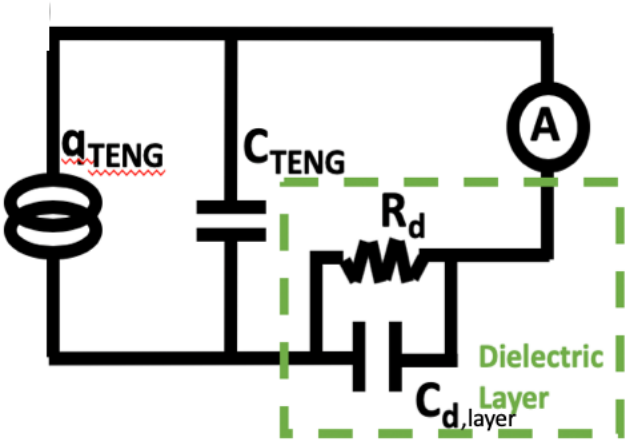

Figure 64. Equivalent Circuit Model of Dielectric Layer TENG

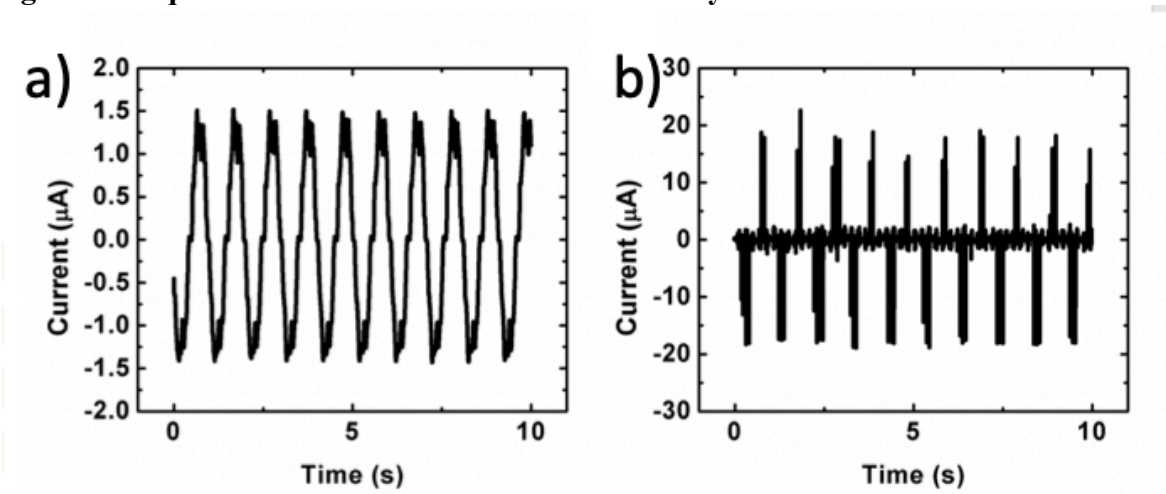

Figure 65: Output Current Without and With Dielectric Layer. a) output current without dielectric. b) output current with dielectric.

With these equations in mind, the current of the TENG when connected to a dielectric layer of PET (0.002 in (0.0508) mm., 4x4 cm^2 (1600 mm^2) (area)), k (dielectric constant=3.0)calc, as seen in Figure 65b, was compared to the current of the TENG without connect to a dielectric layer, which is shown in Figure 65a. With the dielectric layer, the current has increased from 3 μA peak to peak to 40 μA peak to peak, showing a 1333% increase in the instantaneous current. This shows that without dielectric layer, the instantaneous current could be greatly improved. Due to the great

improvement in instantaneous current, instantaneous power could also be improved as well. However, a goal for this research is to see if the instantaneous current could be increased to an even higher value. One way to increase the current is to increase the charge on the capacitor, as current is the derivative of charge, and the time for discharge would not change; thus, by increasing charge, a higher output current could be achieved. From Equation 19, as capacitance increase, the charge on the capacitor would also increase; thus, by increasing capacitance, the charge could be increased; thus, increasing the current. However, if the capacitance is increased too high, V_{cap} would decrease, which there would not be discharge. Thus, experiments were performed, in which by varying the capacitance and measuring the current, and at low capacitance, 40 pF, the output peak to peak current is 40 μA, as seen in Figure 66b. Furthermore, with 160 pF, the output peak to peak current is 120 μA, which correspond to a 4000% increase in instantaneous current. However, at above 200 pF, there is no discharge, and the current observed is low. Furthermore, from Figure 66a, the charge transferred did increase with increase of capacitance, which further verifies this effect. Furthermore, the capacitance of the PET layer comes out to around 80 pF, by using parallel plate capacitor equation, shown in Equation 21, which from Figure 66b, should produce an output of 40 μA peak to peak, which is exactly verified with Figure 65b.

$$C = \frac{\varepsilon_0 \varepsilon_r A}{z} \tag{21}$$

in which A is the area of the dielectric layer, and z represents the thickness of the dielectric layer.

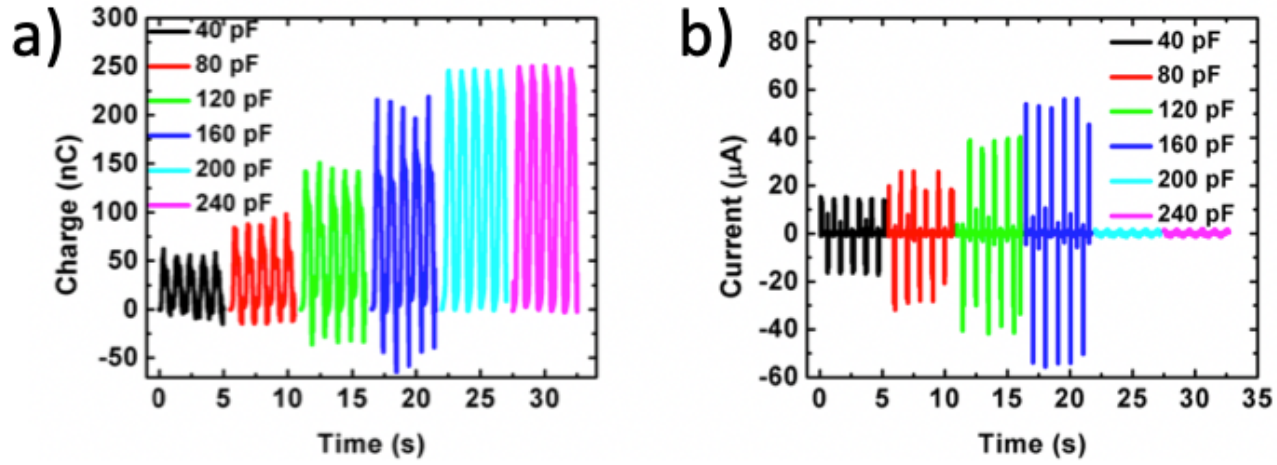

Figure 66: Effect of Capacitance of Dielectric Layer on Output Performance. a) Effect of capacitance on charge transferred. b) Effect of capacitance on short-circuit current.

In this work, I have demonstrated a simple process to achieve a high current by lowering the discharge time of the nanogenerator. Unlike previous work, which utilizes the mechanical motion as a mechanical switch to reduce the lifetime, this work incorporates a new switching methods and investigates the use of high voltage through a dielectric layer as a simple electrical switch.[157] The advantages of the new design are less area added to the device, which would cause an increase in the overall instantaneous power density, and higher durability due to lack of metal-metal contacts in the electrical switch. If there is sufficient high voltage across the dielectric layer, there would be partial dielectric breakdown of the dielectric layer, which would allow high current to pass through in short period of time. Furthermore, the dielectric layer was modeled as a capacitor, and different capacitance were tested, and it was found that the discharge could only occur at low capacitance, where voltage across the capacitor would be higher. Also, there is an optimum capacitance that could be used to achieve a very high instantaneous current, and with further increase of capacitance, no electrostatic discharge was seen. With the very high instantaneous current, a high-power density could also be achieved. This work had further led to

theoretical analysis of DC-TENG, which had the similar model of electric charge source and capacitor.[172]

CHAPTER 5. CONCLUSION

This dissertation documents my major research achievements in the field of triboelectric nanogerator as a Ph.D. student at Georgia Institute of Technology for the past five years. Triboelectric nanogenerator is a promising technology that has potential in vast applications ranging from energy harvesting, high-voltage power sources to active sensing. In this chapter, I would briefly summarize my research achievements and technological innovations. Furthermore, some proposed future works in advancing triboelectric nanogenerators are also posed.

5.1 TENG as Self-powered Active Sensor

As a sustainable power source, TENG can convert mechanical input into an electrical output. The electric output signals generated could then be used to tell information of a typical mechanical motion, making the TENG a self-powered active sensor. Part of my dissertation research involve on developing TENG into self-powered active strain sensors with higher sensitivity and selectivity, transforming commonplace materials, such as paper, into a self-powered sensing platform, and fabricating new self-powered fluid sensors to detect wind speed and water wave height.

5.2 TENG as Energy Harvester

Applications of TENG for energy harvesting have been explored. First, to obtain a higher output power, a new theory on electrostatic screening effect was performed, and this is the first work that showed the TENG's performance is dependent on the substrate material and objects around the TENG. This is particularly useful for harvesting ocean wave energy, as the dielectric constant of nearby water to the TENG device could cause the TENG's performance to be very low. Thus, an air gap to separate water to a distance of at least 1 cm. was needed to harvest ocean

wave energy efficiently. Furthermore, another key aspect to a low performance of TENG is that it could only deliver maximum power at very high impedance. Thus, a multi-layer TENG was developed, and it is able to effectively reduce the impedance of the triboelectric nanogenerator, and also producing a much higher power density. Also, from investigating the effect of substrate material on performance of TENG, it was found that aerogel had the highest performance due to its low dielectric constant. Finally, a key issue for TENG is a lack of energy storage element. Thus, my co-workers and I address this issue by integrating a wearable TENG/EMG system with a microsupercapacitor.

5.3 TENG as High Voltage Power Source

Research in TENG as a high voltage power source have been increasing lately, but it is still a relatively new field and the in-depth mechanism of high voltage power source still needs to be examined. Thus, in my work, the effect of high voltage on different electronic components, such as resistors and capacitors, are examined. For investigation of high voltage source on resistive systems, a TENG was able to short a fuse, causing an electromagnetic pulse. With this device, application in fully self-powered system and personal security was performed. For high voltage on capacitive system, I explored the characteristic of electrical discharge across the capacitor, and this could be utilized in creating a very high instantaneous current and power output. This work has also led to the theoretical analysis of DC-TENG, which is a new mode of TENG that it does not require a rectification system to store the harvested power.

5.4 Future Directions for Research

The discovery of triboelectric nanogenerator has helped created various fields, such as self-powered active sensors, energy harvesting, and high voltage applications. TENGs have experienced a very rapid development both in fundamental understanding and technological improvements. In order to move towards commercialization of TENG, future works still need to be done in making this technology applicable as commercial products. In this section, I would first focus on future works that could be done on TENG in general.

Firstly, one major issue of TENG is its device durability. A requirement of high surface friction between two contact materials is needed for a decent output from TENG. Thus, there remains a challenge that material abrasion and constantly generated heat will make the device nondurable under continuous operation or even in cases when the mover moves very quickly. It has been observed that the polymers used currently in TENG could eventually lose its rigidity after continuous working. Thus, more durable materials, self-healing materials, or different structural design are necessary for achieving a high output performance without compromising device robustness.

Secondly, the fundamental physics of triboelectrification still remains unclear, and there needs to be more investigation to its underlying physics. Furthermore, since it is just found that solid-solid contact electrification is due to electron transfer. A question that still remains to be answered is that ‘How could we maximize the amount of surface charges transferred between surfaces?’ To address this question, a new material or surface treatment techniques to increase the triboelectric charge density transferred needs to be considered.

Especially for self-powered sensing case, the output performance is highly subjected to environmental factors, such as humidity and temperature. Thus, packaging is highly desirable for TENG for applications in self-powered active sensor.

For ocean wave harvesting, currently these TENG that is created are currently very small compared to the vast area of the ocean. Thus, there needs to be methods to mass produce large area TENG so that it could harvest large areas in the ocean.

Lastly but not least, for high voltage on different components. In this thesis, currently only capacitors and resistive based structures are studied. Further work involves studying the effect of high voltage on inductive based components for creating a magnetic field, also on memristor based devices, for creating a TENG activated switch.

REFERENCES

[1] Wang, Z. L.; Jiang, T.; Xu, L., Toward the blue energy dream by triboelectric nanogenerator networks. *Nano Energy* **2017,** *39*, 9-23.

[2] Xu, C.; Zi, Y.; Wang, A. C.; Zou, H.; Dai, Y.; He, X.; Wang, P.; Wang, Y. C.; Feng, P.; Li, D., On the electron-transfer mechanism in the contact-electrification effect. *Advanced Materials* **2018,** *30* (15), 1706790.

[3] Fan, F.-R.; Tian, Z.-Q.; Wang, Z. L., Flexible triboelectric generator. *Nano Energy* **2012,** *1* (2), 328-334.

[4] Wu, C.; Wang, A. C.; Ding, W.; Guo, H.; Wang, Z. L., Triboelectric nanogenerator: a foundation of the energy for the new era. *Adv Energy Mater* **2019,** *9* (1), 1802906.

[5] Wang, Z. L., On Maxwell's displacement current for energy and sensors: the origin of nanogenerators. *Materials today* **2017,** *20* (2), 74-82.

[6] Niu, S.; Wang, S.; Lin, L.; Liu, Y.; Zhou, Y. S.; Hu, Y.; Wang, Z. L., Theoretical study of contact-mode triboelectric nanogenerators as an effective power source. *Energ Environ Sci* **2013,** *6* (12), 3576-3583.

[7] Niu, S.; Liu, Y.; Wang, S.; Lin, L.; Zhou, Y. S.; Hu, Y.; Wang, Z. L., Theory of sliding-mode triboelectric nanogenerators. *Advanced materials* **2013,** *25* (43), 6184-6193.

[8] Niu, S.; Wang, S.; Liu, Y.; Zhou, Y. S.; Lin, L.; Hu, Y.; Pradel, K. C.; Wang, Z. L., A theoretical study of grating structured triboelectric nanogenerators. *Energ Environ Sci* **2014,** *7* (7), 2339-2349.

[9] Niu, S.; Liu, Y.; Chen, X.; Wang, S.; Zhou, Y. S.; Lin, L.; Xie, Y.; Wang, Z. L., Theory of freestanding triboelectric-layer-based nanogenerators. *Nano Energy* **2015,** *12*, 760-774.

[10] Niu, S.; Liu, Y.; Zhou, Y. S.; Wang, S.; Lin, L.; Wang, Z. L., Optimization of triboelectric nanogenerator charging systems for efficient energy harvesting and storage. *IEEE Transactions on Electron Devices* **2014,** *62* (2), 641-647.

[11] Jiang, T.; Chen, X.; Han, C. B.; Tang, W.; Wang, Z. L., Theoretical study of rotary freestanding triboelectric nanogenerators. *Adv Funct Mater* **2015,** *25* (19), 2928-2938.

[12] Niu, S.; Wang, Z. L., Theoretical systems of triboelectric nanogenerators. *Nano Energy* **2015,** *14*, 161-192.

[13] Niu, S.; Liu, Y.; Wang, S.; Lin, L.; Zhou, Y. S.; Hu, Y.; Wang, Z. L., Theoretical investigation and structural optimization of single-electrode triboelectric nanogenerators. *Adv Funct Mater* **2014,** *24* (22), 3332-3340.

[14] Bill W. Lee, D. E. O. The TriboElectric Series. https://www.alphalabinc.com/triboelectric-series.

[15] Zou, H.; Zhang, Y.; Guo, L.; Wang, P.; He, X.; Dai, G.; Zheng, H.; Chen, C.; Wang, A. C.; Xu, C., Quantifying the triboelectric series. *Nat Commun* **2019,** *10* (1), 1427.

[16] Lee, J. P.; Lee, J. W.; Baik, J. M., The progress of PVDF as a functional material for triboelectric nanogenerators and self-powered sensors. *Micromachines* **2018,** *9* (10), 532.

[17] Lee, B.-Y.; Kim, D. H.; Park, J.; Park, K.-I.; Lee, K. J.; Jeong, C. K., Modulation of surface physics and chemistry in triboelectric energy harvesting technologies. *Science and technology of advanced materials* **2019,** *20* (1), 758-773.

[18] Vijayendran, B., Effect of fluorinated compounds on the triboelectric-charging property of iron surface. *Journal of Colloid and Interface Science* **1978,** *64* (3), 514-521.

[19] Diaz, A.; Felix-Navarro, R., A semi-quantitative tribo-electric series for polymeric materials: the influence of chemical structure and properties. *J Electrostat* **2004,** *62* (4), 277-290.

[20] Li, S.; Fan, Y.; Chen, H.; Nie, J.; Liang, Y.; Tao, X.; Zhang, J.; Chen, X.; Fu, E.; Wang, Z. L., Manipulating the triboelectric surface charge density of polymers by low-energy helium ion irradiation/implantation. *Energ Environ Sci* **2020,** *13* (3), 896-907.

[21] Wang, S.; Xie, Y.; Niu, S.; Lin, L.; Liu, C.; Zhou, Y. S.; Wang, Z. L., Maximum surface charge density for triboelectric nanogenerators achieved by ionized-air injection: methodology and theoretical understanding. *Advanced Materials* **2014,** *26* (39), 6720-6728.

[22] Zhang, X.-S.; Han, M.-D.; Wang, R.-X.; Meng, B.; Zhu, F.-Y.; Sun, X.-M.; Hu, W.; Wang, W.; Li, Z.-H.; Zhang, H.-X., High-performance triboelectric nanogenerator with enhanced energy density based on single-step fluorocarbon plasma treatment. *Nano Energy* **2014,** *4*, 123-131.

[23] Li, H. Y.; Su, L.; Kuang, S. Y.; Pan, C. F.; Zhu, G.; Wang, Z. L., Significant enhancement of triboelectric charge density by fluorinated surface modification in nanoscale for converting mechanical energy. *Adv Funct Mater* **2015,** *25* (35), 5691-5697.

[24] Yun, B. K.; Kim, J. W.; Kim, H. S.; Jung, K. W.; Yi, Y.; Jeong, M.-S.; Ko, J.-H.; Jung, J. H., Base-treated polydimethylsiloxane surfaces as enhanced triboelectric nanogenerators. *Nano Energy* **2015,** *15*, 523-529.

[25] Byun, K.-E.; Cho, Y.; Seol, M.; Kim, S.; Kim, S.-W.; Shin, H.-J.; Park, S.; Hwang, S., Control of triboelectrification by engineering surface dipole and surface electronic state. *Acs Appl Mater Inter* **2016,** *8* (28), 18519-18525.

[26] Wang, S.; Zi, Y.; Zhou, Y. S.; Li, S.; Fan, F.; Lin, L.; Wang, Z. L., Molecular surface functionalization to enhance the power output of triboelectric nanogenerators. *J Mater Chem A* **2016,** *4* (10), 3728-3734.

[27] Lee, J. H.; Yu, I.; Hyun, S.; Kim, J. K.; Jeong, U., Remarkable increase in triboelectrification by enhancing the conformable contact and adhesion energy with a film-covered pillar structure. *Nano Energy* **2017,** *34*, 233-241.

[28] Jang, D.; Kim, Y.; Kim, T. Y.; Koh, K.; Jeong, U.; Cho, J., Force-assembled triboelectric nanogenerator with high-humidity-resistant electricity generation using hierarchical surface morphology. *Nano Energy* **2016,** *20*, 283-293.

[29] Seol, M. L.; Woo, J. H.; Lee, D. I.; Im, H.; Hur, J.; Choi, Y. K., Nature-replicated nano-in-micro structures for triboelectric energy harvesting. *Small* **2014,** *10* (19), 3887-3894.

[30] Zhu, G.; Pan, C.; Guo, W.; Chen, C.-Y.; Zhou, Y.; Yu, R.; Wang, Z. L., Triboelectric-generator-driven pulse electrodeposition for micropatterning. *Nano Lett* **2012,** *12* (9), 4960-4965.

[31] Yang, Y.; Zhang, H.; Lin, Z.-H.; Zhou, Y. S.; Jing, Q.; Su, Y.; Yang, J.; Chen, J.; Hu, C.; Wang, Z. L., Human skin based triboelectric nanogenerators for harvesting biomechanical energy and as self-powered active tactile sensor system. *Acs Nano* **2013,** *7* (10), 9213-9222.

[32] Wang, Z. L., Triboelectric nanogenerators as new energy technology and self-powered sensors–Principles, problems and perspectives. *Faraday Discuss* **2015,** *176*, 447-458.

[33] Meng, B.; Tang, W.; Too, Z.-h.; Zhang, X.; Han, M.; Liu, W.; Zhang, H., A transparent single-friction-surface triboelectric generator and self-powered touch sensor. *Energ Environ Sci* **2013,** *6* (11), 3235-3240.

[34] Han, C. B.; Zhang, C.; Li, X. H.; Zhang, L.; Zhou, T.; Hu, W.; Wang, Z. L., Self-powered velocity and trajectory tracking sensor array made of planar triboelectric nanogenerator pixels. *Nano Energy* **2014,** *9*, 325-333.

[35] Yang, J.; Chen, J.; Liu, Y.; Yang, W.; Su, Y.; Wang, Z. L., Triboelectrification-based organic film nanogenerator for acoustic energy harvesting and self-powered active acoustic sensing. *Acs Nano* **2014,** *8* (3), 2649-2657.

[36] Ouyang, H.; Tian, J.; Sun, G.; Zou, Y.; Liu, Z.; Li, H.; Zhao, L.; Shi, B.; Fan, Y.; Fan, Y., Self-Powered Pulse Sensor for Antidiastole of Cardiovascular Disease. *Advanced Materials* **2017,** *29* (40), 1703456.

[37] Yang, P. K.; Lin, L.; Yi, F.; Li, X.; Pradel, K. C.; Zi, Y.; Wu, C. I.; He, J. H.; Zhang, Y.; Wang, Z. L., A flexible, stretchable and shape-adaptive approach for versatile energy conversion and self-powered biomedical monitoring. *Advanced Materials* **2015,** *27* (25), 3817-3824.

[38] Wang, J.; Li, S.; Yi, F.; Zi, Y.; Lin, J.; Wang, X.; Xu, Y.; Wang, Z. L., Sustainably powering wearable electronics solely by biomechanical energy. *Nat Commun* **2016,** *7*, 12744.

[39] Guo, H.; Yeh, M.-H.; Lai, Y.-C.; Zi, Y.; Wu, C.; Wen, Z.; Hu, C.; Wang, Z. L., All-in-one shape-adaptive self-charging power package for wearable electronics. *Acs Nano* **2016,** *10* (11), 10580-10588.

[40] Lai, Y. C.; Deng, J.; Niu, S.; Peng, W.; Wu, C.; Liu, R.; Wen, Z.; Wang, Z. L., Electric eel-skin-inspired mechanically durable and super-stretchable nanogenerator for deformable power source and fully autonomous conformable electronic-skin applications. *Advanced Materials* **2016,** *28* (45), 10024-10032.

[41] Khan, U.; Kim, S.-W., Triboelectric nanogenerators for blue energy harvesting. *Acs Nano* **2016,** *10* (7), 6429-6432.

[42] Chen, J.; Yang, J.; Li, Z.; Fan, X.; Zi, Y.; Jing, Q.; Guo, H.; Wen, Z.; Pradel, K. C.; Niu, S., Networks of triboelectric nanogenerators for harvesting water wave energy: a potential approach toward blue energy. *Acs Nano* **2015,** *9* (3), 3324-3331.

[43] Wang, Z. L., Catch wave power in floating nets. *Nature News* **2017,** *542* (7640), 159.

[44] Xu, M.; Wang, P.; Wang, Y. C.; Zhang, S. L.; Wang, A. C.; Zhang, C.; Wang, Z.; Pan, X.; Wang, Z. L., A soft and robust spring based triboelectric nanogenerator for harvesting arbitrary directional vibration energy and self-powered vibration sensing. *Adv Energy Mater* **2018,** *8* (9), 1702432.

[45] Yang, W.; Chen, J.; Zhu, G.; Wen, X.; Bai, P.; Su, Y.; Lin, Y.; Wang, Z., Harvesting vibration energy by a triple-cantilever based triboelectric nanogenerator. *Nano Research* **2013,** *6* (12), 880-886.

[46] Yang, W.; Chen, J.; Jing, Q.; Yang, J.; Wen, X.; Su, Y.; Zhu, G.; Bai, P.; Wang, Z. L., 3D stack integrated triboelectric nanogenerator for harvesting vibration energy. *Adv Funct Mater* **2014,** *24* (26), 4090-4096.

[47] Chen, B.; Yang, Y.; Wang, Z. L., Scavenging wind energy by triboelectric nanogenerators. *Adv Energy Mater* **2018,** *8* (10), 1702649.

[48] Zhang, L.; Zhang, B.; Chen, J.; Jin, L.; Deng, W.; Tang, J.; Zhang, H.; Pan, H.; Zhu, M.; Yang, W., Lawn structured triboelectric nanogenerators for scavenging sweeping wind energy on rooftops. *Advanced Materials* **2016,** *28* (8), 1650-1656.

[49] Yang, Y.; Zhu, G.; Zhang, H.; Chen, J.; Zhong, X.; Lin, Z.-H.; Su, Y.; Bai, P.; Wen, X.; Wang, Z. L., Triboelectric nanogenerator for harvesting wind energy and as self-powered wind vector sensor system. *Acs Nano* **2013,** *7* (10), 9461-9468.

[50] Xu, M.; Wang, Y.-C.; Zhang, S. L.; Ding, W.; Cheng, J.; He, X.; Zhang, P.; Wang, Z.; Pan, X.; Wang, Z. L., An aeroelastic flutter based triboelectric nanogenerator as a self-powered active wind speed sensor in harsh environment. *Extreme Mechanics Letters* **2017,** *15*, 122-129.

[51] Zi, Y.; Guo, H.; Wen, Z.; Yeh, M.-H.; Hu, C.; Wang, Z. L., Harvesting low-frequency (< 5 Hz) irregular mechanical energy: a possible killer application of triboelectric nanogenerator. *Acs Nano* **2016,** *10* (4), 4797-4805.

[52] Bernier, M. C.; Li, A.; Winalski, L.; Zi, Y.; Li, Y.; Caillet, C.; Newton, P.; Wang, Z. L.; Fernández, F. M., Triboelectric nanogenerator (TENG) mass spectrometry of falsified antimalarials. *Rapid Communications in Mass Spectrometry* **2018,** *32* (18), 1585-1590.

[53] Nie, J.; Chen, X.; Wang, Z. L., Electrically responsive materials and devices directly driven by the high voltage of triboelectric nanogenerators. *Adv Funct Mater* **2018**, 1806351.

[54] Bouza, M.; Li, A.; Forsythe, J. G.; Petrov, A.; Wang, Z. L.; Fernández, F. M., Compositional Characterization of Complex Protopeptide Libraries via Triboelectric Nanogenerator Orbitrap Mass Spectrometry. *Rapid Communications in Mass Spectrometry* **2019**.

[55] Zi, Y.; Wu, C.; Ding, W.; Wang, X.; Dai, Y.; Cheng, J.; Wang, J.; Wang, Z.; Wang, Z. L., Field Emission of electrons powered by a triboelectric nanogenerator. *Adv Funct Mater* **2018,** *28* (21), 1800610.

[56] Cheng, J.; Ding, W.; Zi, Y.; Lu, Y.; Ji, L.; Liu, F.; Wu, C.; Wang, Z. L., Triboelectric microplasma powered by mechanical stimuli. *Nat Commun* **2018,** *9* (1), 3733.

[57] Li, A.; Zi, Y.; Guo, H.; Wang, Z. L.; Fernández, F. M., Triboelectric nanogenerators for sensitive nano-coulomb molecular mass spectrometry. *Nature nanotechnology* **2017,** *12* (5), 481.

[58] Chen, S.; Gao, C.; Tang, W.; Zhu, H.; Han, Y.; Jiang, Q.; Li, T.; Cao, X.; Wang, Z., Self-powered cleaning of air pollution by wind driven triboelectric nanogenerator. *Nano Energy* **2015,** *14*, 217-225.

[59] Bai, Y.; Han, C. B.; He, C.; Gu, G. Q.; Nie, J. H.; Shao, J. J.; Xiao, T. X.; Deng, C. R.; Wang, Z. L., Washable multilayer triboelectric air filter for efficient particulate matter PM2. 5 removal. *Adv Funct Mater* **2018,** *28* (15), 1706680.

[60] Chen, S. W.; Cao, X.; Wang, N.; Ma, L.; Zhu, H. R.; Willander, M.; Jie, Y.; Wang, Z. L., An ultrathin flexible single-electrode triboelectric-nanogenerator for mechanical energy harvesting and instantaneous force sensing. *Adv Energy Mater* **2017,** *7* (1), 1601255.

[61] Fan, F.-R.; Lin, L.; Zhu, G.; Wu, W.; Zhang, R.; Wang, Z. L., Transparent triboelectric nanogenerators and self-powered pressure sensors based on micropatterned plastic films. *Nano Lett* **2012,** *12* (6), 3109-3114.

[62] Lin, L.; Xie, Y.; Wang, S.; Wu, W.; Niu, S.; Wen, X.; Wang, Z. L., Triboelectric active sensor array for self-powered static and dynamic pressure detection and tactile imaging. *Acs Nano* **2013,** *7* (9), 8266-8274.

[63] Yi, F.; Lin, L.; Niu, S.; Yang, J.; Wu, W.; Wang, S.; Liao, Q.; Zhang, Y.; Wang, Z. L., Self-powered trajectory, velocity, and acceleration tracking of a moving object/body using a triboelectric sensor. *Adv Funct Mater* **2014,** *24* (47), 7488-7494.

[64] Zhou, Y. S.; Zhu, G.; Niu, S.; Liu, Y.; Bai, P.; Jing, Q.; Wang, Z. L., Nanometer Resolution Self-Powered Static and Dynamic Motion Sensor Based on Micro-Grated Triboelectrification. *Advanced Materials* **2014,** *26* (11), 1719-1724.

[65] Dhakar, L.; Pitchappa, P.; Tay, F. E. H.; Lee, C., An intelligent skin based self-powered finger motion sensor integrated with triboelectric nanogenerator. *Nano Energy* **2016,** *19*, 532-540.

[66] Lin, Z. H.; Zhu, G.; Zhou, Y. S.; Yang, Y.; Bai, P.; Chen, J.; Wang, Z. L., A self-powered triboelectric nanosensor for mercury ion detection. *Angewandte Chemie International Edition* **2013,** *52* (19), 5065-5069.

[67] Li, Z.; Chen, J.; Yang, J.; Su, Y.; Fan, X.; Wu, Y.; Yu, C.; Wang, Z. L., β-cyclodextrin enhanced triboelectrification for self-powered phenol detection and electrochemical degradation. *Energ Environ Sci* **2015,** *8* (3), 887-896.

[68] Wen, Z.; Chen, J.; Yeh, M.-H.; Guo, H.; Li, Z.; Fan, X.; Zhang, T.; Zhu, L.; Wang, Z. L., Blow-driven triboelectric nanogenerator as an active alcohol breath analyzer. *Nano Energy* **2015,** *16*, 38-46.

[69] Wen, Z.; Shen, Q.; Sun, X., Nanogenerators for self-powered gas sensing. *Nano-micro letters* **2017,** *9* (4), 45.

[70] Zhang, S. L.; Lai, Y. C.; He, X.; Liu, R.; Zi, Y.; Wang, Z. L., Auxetic foam-based contact-mode triboelectric nanogenerator with highly sensitive self-powered strain sensing capabilities to monitor human body movement. *Adv Funct Mater* **2017,** *27* (25), 1606695.

[71] Yamada, T.; Hayamizu, Y.; Yamamoto, Y.; Yomogida, Y.; Izadi-Najafabadi, A.; Futaba, D. N.; Hata, K., A stretchable carbon nanotube strain sensor for human-motion detection. *Nature nanotechnology* **2011,** *6* (5), 296-301.

[72] Ryu, S.; Lee, P.; Chou, J. B.; Xu, R.; Zhao, R.; Hart, A. J.; Kim, S. G., Extremely Elastic Wearable Carbon Nanotube Fiber Strain Sensor for Monitoring of Human Motion. *ACS nano* **2015,** *9* (6), 5929-36.

[73] Pang, C.; Lee, G. Y.; Kim, T. I.; Kim, S. M.; Kim, H. N.; Ahn, S. H.; Suh, K. Y., A flexible and highly sensitive strain-gauge sensor using reversible interlocking of nanofibres. *Nature materials* **2012,** *11* (9), 795-801.

[74] Wang, C.; Li, X.; Gao, E.; Jian, M.; Xia, K.; Wang, Q.; Xu, Z.; Ren, T.; Zhang, Y., Wearable Strain Sensors: Carbonized Silk Fabric for Ultrastretchable, Highly Sensitive, and Wearable Strain Sensors (Adv. Mater. 31/2016). *Advanced materials* **2016,** *28* (31), 6639.

[75] Trung, T. Q.; Lee, N. E., Recent Progress on Stretchable Electronic Devices with Intrinsically Stretchable Components. *Advanced materials* **2016**.

[76] Bauer, S.; Bauer-Gogonea, S.; Graz, I.; Kaltenbrunner, M.; Keplinger, C.; Schwodiauer, R., 25th anniversary article: A soft future: from robots and sensor skin to energy harvesters. *Advanced materials* **2014,** *26* (1), 149-61.

[77] Wu, J. M.; Chen, C.-Y.; Zhang, Y.; Chen, K.-H.; Yang, Y.; Hu, Y.; He, J.-H.; Wang, Z. L., Ultrahigh sensitive piezotronic strain sensors based on a ZnSnO3 nanowire/microwire. *Acs Nano* **2012,** *6* (5), 4369-4374.

[78] Wu, J. M.; Chen, K.-H.; Zhang, Y.; Wang, Z. L., A self-powered piezotronic strain sensor based on single ZnSnO3 microbelts. *Rsc Advances* **2013,** *3* (47), 25184-25189.

[79] Wu, C. S.; Wang, X.; Lin, L.; Guo, H. Y.; Wang, Z. L., Paper-Based Triboelectric Nanogenerators Made of Stretchable Interlocking Kirigami Patterns. *Acs Nano* **2016,** *10* (4), 4652-4659.

[80] Yi, F.; Wang, J.; Wang, X. F.; Niu, S. M.; Li, S. M.; Liao, Q. L.; Xu, Y. L.; You, Z.; Zhang, Y.; Wang, Z. L., Stretchable and Waterproof Self-Charging Power System for Harvesting Energy from Diverse Deformation and Powering Wearable Electronics. *ACS nano* **2016,** *10* (7), 6519-6525.

[81] Yang, B.; Zeng, W.; Peng, Z. H.; Liu, S. R.; Chen, K.; Tao, X. M., A fully verified theoretical analysis of contact-mode triboelectric nanogenerators as a wearable power source. *Adv Energy Mater* **2016,** *6* (16), 1600505.

[82] Lakes, R., Foam Structures with a Negative Poissons Ratio. *Science* **1987,** *235* (4792), 1038-1040.

[83] Lakes, R., Foam structures with a negative Poisson's ratio. *Science* **1987,** *235*, 1038-1041.

[84] Yi, F.; Wang, X.; Niu, S.; Li, S.; Yin, Y.; Dai, K.; Zhang, G.; Lin, L.; Wen, Z.; Guo, H., A highly shape-adaptive, stretchable design based on conductive liquid for energy harvesting and self-powered biomechanical monitoring. *Sci Adv* **2016,** *2* (6), e1501624.

[85] Wu, C.; Wang, X.; Lin, L.; Guo, H.; Wang, Z. L., Based triboelectric nanogenerators made of stretchable interlocking kirigami patterns. *Acs Nano* **2016,** *10* (4), 4652-4659.

[86] Li, X.; Tian, J.; Garnier, G.; Shen, W., Fabrication of paper-based microfluidic sensors by printing. *Colloids and surfaces B: Biointerfaces* **2010,** *76* (2), 564-570.

[87] Eder, F.; Klauk, H.; Halik, M.; Zschieschang, U.; Schmid, G.; Dehm, C., Organic electronics on paper. *Applied Physics Letters* **2004,** *84* (14), 2673-2675.

[88] Jung, Y. H.; Chang, T.-H.; Zhang, H.; Yao, C.; Zheng, Q.; Yang, V. W.; Mi, H.; Kim, M.; Cho, S. J.; Park, D.-W., High-performance green flexible electronics based on biodegradable cellulose nanofibril paper. *Nat Commun* **2015,** *6*, 7170.

[89] Liu, J.; Yang, C.; Wu, H.; Lin, Z.; Zhang, Z.; Wang, R.; Li, B.; Kang, F.; Shi, L.; Wong, C. P., Future paper based printed circuit boards for green electronics: fabrication and life cycle assessment. *Energ Environ Sci* **2014,** *7* (11), 3674-3682.

[90] Fan, X.; Chen, J.; Yang, J.; Bai, P.; Li, Z.; Wang, Z. L., Ultrathin, rollable, paper-based triboelectric nanogenerator for acoustic energy harvesting and self-powered sound recording. *Acs Nano* **2015,** *9* (4), 4236-4243.

[91] Guo, H.; Yeh, M.-H.; Zi, Y.; Wen, Z.; Chen, J.; Liu, G.; Hu, C.; Wang, Z. L., Ultralight cut-paper-based self-charging power unit for self-powered portable electronic and medical systems. *Acs Nano* **2017,** *11* (5), 4475-4482.

[92] Chandrasekhar, A.; Alluri, N. R.; Saravanakumar, B.; Selvarajan, S.; Kim, S.-J., Human interactive triboelectric nanogenerator as a self-powered smart seat. *Acs Appl Mater Inter* **2016,** *8* (15), 9692-9699.

[93] Zhong, Q.; Zhong, J.; Hu, B.; Hu, Q.; Zhou, J.; Wang, Z. L., A paper-based nanogenerator as a power source and active sensor. *Energ Environ Sci* **2013,** *6* (6), 1779-1784.

[94] Arora, N.; Zhang, S. L.; Shahmiri, F.; Osorio, D.; Wang, Y.-C.; Gupta, M.; Wang, Z.; Starner, T.; Wang, Z. L.; Abowd, G. D., SATURN: A thin and flexible self-powered microphone leveraging triboelectric nanogenerator. *Proceedings of the ACM on Interactive, Mobile, Wearable and Ubiquitous Technologies* **2018,** *2* (2), 60.

[95] Pillai, M. A.; Deenadayalan, E., A review of acoustic energy harvesting. *International journal of precision engineering and manufacturing* **2014,** *15* (5), 949-965.

[96] Seltzer, M. L. In *Bridging the gap: Towards a unified framework for hands-free speech recognition using microphone arrays*, 2008 Hands-Free Speech Communication and Microphone Arrays, IEEE: 2008; pp 104-107.

[97] Cord, M. T.; Surr, R. K.; Walden, B. E.; Olson, L., Performance of directional microphone hearing aids in everyday life. *Journal of the American Academy of Audiology* **2002,** *13* (6), 295-307.

[98] Giurgiutiu, V., *Structural health monitoring: with piezoelectric wafer active sensors*. Elsevier: 2007.

[99] Microphones, C.; Halls, S.; by Noise, A., Acoustics Today. **2009**.

[100] Eargle, J., *The Microphone Book: From mono to stereo to surround-a guide to microphone design and application*. CRC Press: 2012.

[101] Ko, S. C.; Kim, Y. C.; Lee, S. S.; Choi, S. H.; Kim, S. R., Micromachined piezoelectric membrane acoustic device. *Sensors and Actuators A: Physical* **2003,** *103* (1-2), 130-134.

[102] Seol, W.-H.; Lee, Y. M.; Park, J.-K., Enhancement of the mechanical properties of PVDF membranes by non-solvent aided morphology control. *Journal of Power Sources* **2007,** *170* (1), 191-195.

[103] Sterman, Y.; Demaine, E. D.; Oxman, N., PCB origami: A material-based design approach to computer-aided foldable electronic devices. *Journal of Mechanical Design* **2013,** *135* (11).

[104] Chen, C.; Howard, D.; Zhang, S. L.; Do, Y.; Sun, S.; Cheng, T.; Wang, Z. L.; Abowd, G. D.; Oh, H. In *SPIN (Self-powered Paper Interfaces) Bridging Triboelectric Nanogenerator with Folding Paper Creases*, Proceedings of the Fourteenth International Conference on Tangible, Embedded, and Embodied Interaction, 2020; pp 431-442.

[105] He, X.; Zi, Y.; Yu, H.; Zhang, S. L.; Wang, J.; Ding, W.; Zou, H.; Zhang, W.; Lu, C.; Wang, Z. L., An ultrathin paper-based self-powered system for portable electronics and wireless human-machine interaction. *Nano Energy* **2017,** *39*, 328-336.

[106] Ding, W.; Wu, C.; Zi, Y.; Zou, H.; Wang, J.; Cheng, J.; Wang, A. C.; Wang, Z. L., Self-powered wireless optical transmission of mechanical agitation signals. *Nano Energy* **2018,** *47*, 566-572.

[107] Bae, J.; Lee, J.; Kim, S.; Ha, J.; Lee, B.-S.; Park, Y.; Choong, C.; Kim, J.-B.; Wang, Z. L.; Kim, H.-Y., Flutter-driven triboelectrification for harvesting wind energy. *Nat Commun* **2014,** *5* (1), 1-9.

[108] Zhao, Z.; Pu, X.; Du, C.; Li, L.; Jiang, C.; Hu, W.; Wang, Z. L., Freestanding flag-type triboelectric nanogenerator for harvesting high-altitude wind energy from arbitrary directions. *Acs Nano* **2016,** *10* (2), 1780-1787.

[109] Quan, Z.; Han, C. B.; Jiang, T.; Wang, Z. L., Robust thin films-based triboelectric nanogenerator arrays for harvesting bidirectional wind energy. *Adv Energy Mater* **2016,** *6* (5), 1501799.

[110] Phan, H.; Shin, D.-M.; Jeon, S. H.; Kang, T. Y.; Han, P.; Kim, G. H.; Kim, H. K.; Kim, K.; Hwang, Y.-H.; Hong, S. W., Aerodynamic and aeroelastic flutters driven triboelectric nanogenerators for harvesting broadband airflow energy. *Nano Energy* **2017,** *33*, 476-484.

[111] Wang, J.; Zhang, H.; Xie, Y.; Yan, Z.; Yuan, Y.; Huang, L.; Cui, X.; Gao, M.; Su, Y.; Yang, W., Smart network node based on hybrid nanogenerator for self-powered multifunctional sensing. *Nano Energy* **2017,** *33*, 418-426.

[112] Perez, M.; Boisseau, S.; Gasnier, P.; Willemin, J.; Reboud, J., An electret-based aeroelastic flutter energy harvester. *Smart materials and structures* **2015,** *24* (3), 035004.

[113] Li, S.; Nie, J.; Shi, Y.; Tao, X.; Wang, F.; Tian, J.; Lin, S.; Chen, X.; Wang, Z. L., Contributions of Different Functional Groups to Contact Electrification of Polymers. *Advanced Materials* **2020**, 2001307.

[114] Pandian, P. K.; Emmanuel, O.; Ruscoe, J.; Side, J.; Harris, R.; Kerr, S.; Bullen, C., An overview of recent technologies on wave and current measurement in coastal and marine applications. *Journal of Oceanography and Marine Science* **2010,** *1* (1), 001-010.

[115] Marimon, M. C.; Tangonan, G.; Libatique, N. J.; Sugimoto, K., Development and evaluation of wave sensor nodes for ocean wave monitoring. *IEEE Systems Journal* **2013,** *9* (1), 292-302.

[116] Babanin, A.; Verkeev, P.; Krivinsky, B.; Proshchenko, V., Measurement of wind waves by means of a buoy accelerometer wave gauge. *Physical Oceanography* **1993,** *4* (5), 399-407.

[117] Xu, M.; Wang, S.; Zhang, S. L.; Ding, W.; Kien, P. T.; Wang, C.; Li, Z.; Pan, X.; Wang, Z. L., A highly-sensitive wave sensor based on liquid-solid interfacing triboelectric nanogenerator for smart marine equipment. *Nano Energy* **2019,** *57*, 574-580.

[118] Wen, Z.; Guo, H.; Zi, Y.; Yeh, M.-H.; Wang, X.; Deng, J.; Wang, J.; Li, S.; Hu, C.; Zhu, L., Harvesting broad frequency band blue energy by a triboelectric–electromagnetic hybrid nanogenerator. *Acs Nano* **2016,** *10* (7), 6526-6534.

[119] Bhuyan, G. S. In *World-wide status for harnessing ocean renewable resources*, IEEE PES General Meeting, IEEE: 2010; pp 1-3.

[120] Ellabban, O.; Abu-Rub, H.; Blaabjerg, F., Renewable energy resources: Current status, future prospects and their enabling technology. *Renewable and Sustainable Energy Reviews* **2014,** *39*, 748-764.

[121] Salter, S. H., Wave power. *Nature* **1974,** *249* (5459), 720-724.

[122] Kofoed, J. P.; Frigaard, P.; Friis-Madsen, E.; Sørensen, H. C., Prototype testing of the wave energy converter wave dragon. *Renewable Energy* **2006,** *31* (2), 181-189.

[123] Tollefson, J., Blue energy. *Nature* **2014,** *508* (7496), 302-304.

[124] Yang, Y.; Zhang, H.; Liu, R.; Wen, X.; Hou, T. C.; Wang, Z. L., Fully enclosed triboelectric nanogenerators for applications in water and harsh environments. *Adv Energy Mater* **2013,** *3* (12), 1563-1568.

[125] Ahmed, A.; Hassan, I.; Ibn-Mohammed, T.; Mostafa, H.; Reaney, I. M.; Koh, L. S.; Zu, J.; Wang, Z. L., Environmental life cycle assessment and techno-economic analysis of triboelectric nanogenerators. *Energ Environ Sci* **2017,** *10* (3), 653-671.

[126] Zhang, S. L.; Xu, M.; Zhang, C.; Wang, Y.-C.; Zou, H.; He, X.; Wang, Z.; Wang, Z. L., Rationally designed sea snake structure based triboelectric nanogenerators for effectively and efficiently harvesting ocean wave energy with minimized water screening effect. *Nano Energy* **2018,** *48*, 421-429.

[127] Kong, C., A general maximum power transfer theorem. *IEEE Transactions on Education* **1995,** *38* (3), 296-298.

[128] Xu, M.; Zhao, T.; Wang, C.; Zhang, S. L.; Li, Z.; Pan, X.; Wang, Z. L., High power density tower-like triboelectric nanogenerator for harvesting arbitrary directional water wave energy. *Acs Nano* **2019,** *13* (2), 1932-1939.

[129] Jiang, Q.; Wu, C.; Wang, Z.; Wang, A. C.; He, J.-H.; Wang, Z. L.; Alshareef, H. N., MXene electrochemical microsupercapacitor integrated with triboelectric nanogenerator as a wearable self-charging power unit. *Nano Energy* **2018,** *45*, 266-272.

[130] Zhong, X.; Yang, Y.; Wang, X.; Wang, Z. L., Rotating-disk-based hybridized electromagnetic-triboelectric nanogenerator for scavenging biomechanical energy as a mobile power source. *Nano Energy* **2015,** *13*, 771-780.

[131] Zhang, B.; Chen, J.; Jin, L.; Deng, W.; Zhang, L.; Zhang, H.; Zhu, M.; Yang, W.; Wang, Z. L., Rotating-disk-based hybridized electromagnetic–triboelectric nanogenerator for sustainably powering wireless traffic volume sensors. *Acs Nano* **2016,** *10* (6), 6241-6247.

[132] Zhang, S. L.; Jiang, Q.; Wu, Z.; Ding, W.; Zhang, L.; Alshareef, H. N.; Wang, Z. L., Energy Harvesting-Storage Bracelet Incorporating Electrochemical Microsupercapacitors Self-Charged from a Single Hand Gesture. *Adv Energy Mater* **2019,** *9* (18), 1900152.

[133] Pech, D.; Brunet, M.; Taberna, P.-L.; Simon, P.; Fabre, N.; Mesnilgrente, F.; Conédéra, V.; Durou, H., Elaboration of a microstructured inkjet-printed carbon electrochemical capacitor. *Journal of Power Sources* **2010,** *195* (4), 1266-1269.

[134] Chmiola, J.; Largeot, C.; Taberna, P.-L.; Simon, P.; Gogotsi, Y., Monolithic carbide-derived carbon films for micro-supercapacitors. *Science* **2010,** *328* (5977), 480-483.

[135] Pech, D.; Brunet, M.; Durou, H.; Huang, P.; Mochalin, V.; Gogotsi, Y.; Taberna, P.-L.; Simon, P., Ultrahigh-power micrometre-sized supercapacitors based on onion-like carbon. *Nature nanotechnology* **2010,** *5* (9), 651.

[136] Lin, J.; Zhang, C.; Yan, Z.; Zhu, Y.; Peng, Z.; Hauge, R. H.; Natelson, D.; Tour, J. M., 3-dimensional graphene carbon nanotube carpet-based microsupercapacitors with high electrochemical performance. *Nano Lett* **2012,** *13* (1), 72-78.

[137] Hota, M. K.; Jiang, Q.; Mashraei, Y.; Salama, K. N.; Alshareef, H. N., Fractal electrochemical microsupercapacitors. *Advanced Electronic Materials* **2017,** *3* (10), 1700185.

[138] Gu, G. Q.; Han, C. B.; Lu, C. X.; He, C.; Jiang, T.; Gao, Z. L.; Li, C. J.; Wang, Z. L., Triboelectric nanogenerator enhanced nanofiber air filters for efficient particulate matter removal. *Acs Nano* **2017,** *11* (6), 6211-6217.

[139] Han, C. B.; Jiang, T.; Zhang, C.; Li, X.; Zhang, C.; Cao, X.; Wang, Z. L., Removal of particulate matter emissions from a vehicle using a self-powered triboelectric filter. *Acs Nano* **2015,** *9* (12), 12552-12561.

[140] Chen, X.; Wu, Y.; Yu, A.; Xu, L.; Zheng, L.; Liu, Y.; Li, H.; Wang, Z. L., Self-powered modulation of elastomeric optical grating by using triboelectric nanogenerator. *Nano Energy* **2017,** *38*, 91-100.

[141] Li, C.; Yin, Y.; Wang, B.; Zhou, T.; Wang, J.; Luo, J.; Tang, W.; Cao, R.; Yuan, Z.; Li, N., Self-powered electrospinning system driven by a triboelectric nanogenerator. *Acs Nano* **2017,** *11* (10), 10439-10445.

[142] Li, S.; Zhang, D.; Meng, X.; Huang, Q.-A.; Sun, C.; Wang, Z. L., A flexible lithium-ion battery with quasi-solid gel electrolyte for storing pulsed energy generated by triboelectric nanogenerator. *Energy Storage Materials* **2018,** *12*, 17-22.

[143] He, X.; Zou, H.; Geng, Z.; Wang, X.; Ding, W.; Hu, F.; Zi, Y.; Xu, C.; Zhang, S. L.; Yu, H., A Hierarchically Nanostructured Cellulose Fiber-Based Triboelectric Nanogenerator for Self-Powered Healthcare Products. *Adv Funct Mater* **2018,** *28* (45), 1805540.

[144] Liu, D.; Yin, X.; Guo, H.; Zhou, L.; Li, X.; Zhang, C.; Wang, J.; Wang, Z. L., A constant current triboelectric nanogenerator arising from electrostatic breakdown. *Sci Adv* **2019,** *5* (4), eaav6437.

[145] Niu, S.; Wang, X.; Yi, F.; Zhou, Y. S.; Wang, Z. L., A universal self-charging system driven by random biomechanical energy for sustainable operation of mobile electronics. *Nat Commun* **2015,** *6* (1), 1-8.

[146] Zhang, S. L. R., Devin J; Xu, Sixing; Wang, Peng; Zhang, Weiqiang; Qi, H. Jerry; Wang, Zhong Lin Electromagnetic Pulse Powered by a Triboelectric Nanogenerator with Applications in Accurate Self-Powered Sensing and Security. *Advanced Materials Technologies* **2020,** *(accepted)* DOI: 10.1002/admt.202000368.

[147] Hwang, K.-M.; Park, J.-Y.; Bae, H.; Lee, S.-W.; Kim, C.-K.; Seo, M.; Im, H.; Kim, D.-H.; Kim, S.-Y.; Lee, G.-B., Nano-electromechanical switch based on a physical unclonable function for highly robust and stable performance in harsh environments. *Acs Nano* **2017,** *11* (12), 12547-12552.

[148] Ebrard, E.; Allard, B.; Candelier, P.; Waltz, P., Review of fuse and antifuse solutions for advanced standard CMOS technologies. *Microelectronics Journal* **2009,** *40* (12), 1755-1765.

[149] Robson, N.; Safran, J.; Kothandaraman, C.; Cestero, A.; Chen, X.; Rajeevakumar, R.; Leslie, A.; Moy, D.; Kirihata, T.; Iyer, S. In *Electrically programmable fuse (efuse): From memory redundancy to autonomic chips*, 2007 IEEE Custom Integrated Circuits Conference, IEEE: 2007; pp 799-804.

[150] MacDonald, E.; Wicker, R., Multiprocess 3D printing for increasing component functionality. *Science* **2016,** *353* (6307), aaf2093.

[151] Mu, Q.; Lei, M.; Roach, D. J.; Dunn, C. K.; Kuang, X.; Yuan, C.; Wang, T.; Qi, H. J., Intense pulsed light sintering of thick conductive wires on elastomeric dark substrate for hybrid 3D printing applications. *Smart Materials and Structures* **2018,** *27* (11), 115007.

[152] Xi, Y.; Guo, H.; Zi, Y.; Li, X.; Wang, J.; Deng, J.; Li, S.; Hu, C.; Cao, X.; Wang, Z. L., Multifunctional TENG for blue energy scavenging and self-powered wind-speed sensor. *Adv Energy Mater* **2017,** *7* (12), 1602397.

[153] Tcho, I.-W.; Jeon, S.-B.; Park, S.-J.; Kim, W.-G.; Jin, I. K.; Han, J.-K.; Kim, D.; Choi, Y.-K., Disk-based triboelectric nanogenerator operated by rotational force converted from linear force by a gear system. *Nano Energy* **2018,** *50*, 489-496.

[154] Lin, L.; Wang, S.; Xie, Y.; Jing, Q.; Niu, S.; Hu, Y.; Wang, Z. L., Segmentally structured disk triboelectric nanogenerator for harvesting rotational mechanical energy. *Nano Lett* **2013,** *13* (6), 2916-2923.

[155] Wang, P.; Pan, L.; Wang, J.; Xu, M.; Dai, G.; Zou, H.; Dong, K.; Wang, Z. L., An ultra-low-friction triboelectric–electromagnetic hybrid nanogenerator for rotation energy harvesting and self-powered wind speed sensor. *Acs Nano* **2018,** *12* (9), 9433-9440.

[156] Guo, T.; Liu, G.; Pang, Y.; Wu, B.; Xi, F.; Zhao, J.; Bu, T.; Fu, X.; Li, X.; Zhang, C., Compressible hexagonal-structured triboelectric nanogenerators for harvesting tire rotation energy. *Extreme Mechanics Letters* **2018,** *18*, 1-8.

[157] Cheng, G.; Lin, Z.-H.; Lin, L.; Du, Z.-l.; Wang, Z. L., Pulsed nanogenerator with huge instantaneous output power density. *Acs Nano* **2013,** *7* (8), 7383-7391.

[158] Qin, H.; Cheng, G.; Zi, Y.; Gu, G.; Zhang, B.; Shang, W.; Yang, F.; Yang, J.; Du, Z.; Wang, Z. L., High energy storage efficiency triboelectric nanogenerators with unidirectional switches and passive power management circuits. *Adv Funct Mater* **2018,** *28* (51), 1805216.

[159] Li, Y.; Cheng, G.; Lin, Z.-H.; Yang, J.; Lin, L.; Wang, Z. L., Single-electrode-based rotationary triboelectric nanogenerator and its applications as self-powered contact area and eccentric angle sensors. *Nano Energy* **2015,** *11*, 323-332.

[160] Cheng, G.; Zheng, L.; Lin, Z. H.; Yang, J.; Du, Z.; Wang, Z. L., Multilayered-electrode-based triboelectric nanogenerators with managed output voltage and multifold enhanced charge transport. *Adv Energy Mater* **2015,** *5* (5), 1401452.

[161] Cheng, G.; Lin, Z. H.; Du, Z.; Wang, Z. L., Increase output energy and operation frequency of a triboelectric nanogenerator by two grounded electrodes approach. *Adv Funct Mater* **2014,** *24* (19), 2892-2898.

[162] Zi, Y.; Wang, J.; Wang, S.; Li, S.; Wen, Z.; Guo, H.; Wang, Z. L., Effective energy storage from a triboelectric nanogenerator. *Nat Commun* **2016,** *7*, 10987.

[163] Yang, J.; Yang, F.; Zhao, L.; Shang, W.; Qin, H.; Wang, S.; Jiang, X.; Cheng, G.; Du, Z., Managing and optimizing the output performances of a triboelectric nanogenerator by a self-powered electrostatic vibrator switch. *Nano Energy* **2018,** *46*, 220-228.

[164] Cheng, G.; Zheng, H.; Yang, F.; Zhao, L.; Zheng, M.; Yang, J.; Qin, H.; Du, Z.; Wang, Z. L., Managing and maximizing the output power of a triboelectric nanogenerator by controlled tip–electrode air-discharging and application for UV sensing. *Nano Energy* **2018,** *44*, 208-216.

[165] Zhang, C.; Wang, Z. L., Tribotronics—A new field by coupling triboelectricity and semiconductor. *Nano Today* **2016,** *11* (4), 521-536.

[166] Zhang, C.; Zhang, L. M.; Tang, W.; Han, C. B.; Wang, Z. L., Tribotronic logic circuits and basic operations. *Advanced Materials* **2015,** *27* (23), 3533-3540.

[167] Xue, F.; Chen, L.; Wang, L.; Pang, Y.; Chen, J.; Zhang, C.; Wang, Z. L., MoS2 tribotronic transistor for smart tactile switch. *Adv Funct Mater* **2016,** *26* (13), 2104-2109.

[168] Liu, Y.; Niu, S.; Wang, Z. L., Theory of tribotronics. *Advanced Electronic Materials* **2015,** *1* (9), 1500124.

[169] Yang, Z. W.; Pang, Y.; Zhang, L.; Lu, C.; Chen, J.; Zhou, T.; Zhang, C.; Wang, Z. L., Tribotronic transistor array as an active tactile sensing system. *Acs Nano* **2016,** *10* (12), 10912-10920.

[170] Gibson, A. S.; Riousset, J. A.; Pasko, V. P., Minimum breakdown voltages for corona discharge in cylindrical and spherical geometries. *NSF EE REU Penn State Annual Research Journal* **2009,** *7*, 1-17.

[171] Raizer, Y., *Spark discharge*. Routledge: 2017.

[172] Xu, S. G., Hengyu; Zhang, Steven L.; Jin, Long; Ding, Wenbo; Wang, Xiaohong; Wang, Zhong Lin, Theoretical investigation of air breakdown direct current triboelectric nanogenerator. *Applied Physics Letters* **2020,** *116*, 263901.